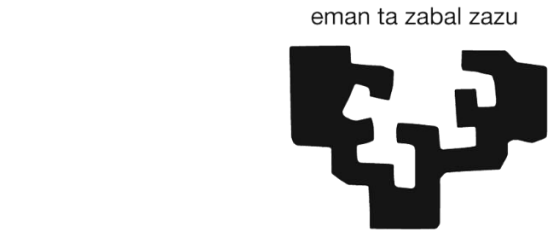

Universidad del País Vasco

Euskal Herriko Unibertsitatea

Valorization of agro-industrial wastes for the production of biodegradable products based on collagen

Mireia Andonegi San Martin

Supervisors:

Koro de la Caba & Pedro Guerrero

Department of Chemical and Environmental Engineering

Donostia-San Sebastian, 2022

Esker onak / Agradecimientos / Acknowledgements

Lerro hauek idaztean ohartzen zara, lau urte iraun duen etapa hau amaitzear dela eta bide honetan zehar bizitako esperientziez zein ezaguturiko pertsonez oroitzen zara. Horrengatik, eskerrak eman nahi dizkiet ikerkuntza ibilbide hau nirekin konpartitu dutenei baita nire ondoan egon diren pertsona guztiei ere.

Para empezar, me gustaría agradecer a mis directores, Koro de la Caba y Pedro Guerrero. Gracias por ofrecerme la oportunidad de realizar el proyecto fin de carrera, el trabajo fin de grado y master con vosotros. Gracias también por la confianza depositada en mí y por todo lo que me habéis enseñado, tanto en lo profesional como en lo personal, a lo largo de toda la tesis doctoral. Vuestra constante dedicación, seguimiento, supervisión ha sido imprescindible para conseguir este trabajo.

I would also like to thank Carlos Miguel Costa and Daniela Correia for having directed me during my both scientific stays in the University of Minho. Their teachings on ionic liquids and electricity have contribute enormously to advance in my research. Muito obrigada a todos vocês do grupo, pela agradavel acolhida na vossa pequeña-grande familia. Foi um prazer trabalhar com vocês.

Bestalde, doktorego-tesi honetan, nire ondoan egon diren lankideei, beraien laguntza sostengua eta pazientzia eskertu nahi dizkiet. Mila esker laguntza emateko prest egon zareten guztioi eta ibilbidea nirekin burutu duzuenoi. Aldi berean, etxekoei zein lagunei emandako babesa eta animoak eskertu nahiko nizkieke. Mila esker denoi hor egoteagatik, nigan sinesteagatik.

Amaitzeko, Eusko Jaurlaritzak doktorego-tesia burutzeko (PRE_2017_1_0025) emandako diru-laguntzagatik. Biomat ikerketa taldeari ere eskerrak emandako babes ekonomikoagatik. UPV/EHU-ko SGIker ikerkuntza zerbitzu orokorrak ere eskertu nahiko nituzke.

SUMMARY

In the last years, the research on biodegradable materials from renewable resources have become of great relevance, mostly due to the growing interest in environmentally friendly management and sustainability. In fact, the valorization of agro-industrial wastes and by-products may be a promising alternative of biopolymers sources, not only to minimize waste, but also to produce high value-added products. In this regard, collagen which may be extracted from livestock and fish processing industry residues, has been widely used in food, cosmetic, pharmaceutical and biomedical applications due to its structural and biological properties as well as its abundance and versatility in forming physical shapes. Furthermore, collagen can be combined with other components to open up new application areas.

In this context, the overall objective of this doctoral thesis was to develop products based on collagen, obtained from bovine and porcine skin wastes, with improved properties, incorporating other compounds, some of them also extracted from biowastes, and employing different processing methods. For that purpose, this study is made up of eleven chapters. **Chapter 1** gives an overall view of valorization of collagen-rich biowastes, collagen structure and properties, and applications of collagen and its derivatives. Then, in **Chapter 2**, the materials and reagents employed, the pretreatment of collagen and wool, the techniques used for the development of collagen-based products, and the characterization methods carried out in this research work have been described.

In Chapters 3-5, compression molding was used to process collagen-based materials. In **Chapter 3**, collagen was obtained from bovine skin using a tanning drum, treated with different contents of citric acid using laboratory rollers and, finally, the functional properties of the obtained sheets were investigated. In **Chapter 4**, collagen

was obtained from porcine skin by mechanical pretreatments and aloe vera, with inherent biological properties, was incorporated into collagen formulations in order to assess their suitability for biomedical applications. Additionally, in **Chapter 5**, chitosan/porcine collagen films were developed and characterized to evaluate their suitability for biomedical applications.

Considering the results of chitosan-collagen films, scaffolds with the same formulations were prepared by freeze-drying in **Chapter 6**, in which materials and environmental approaches were considered with the aim of providing a global strategy towards more sustainable biomaterials. Moreover, in **Chapter 7**, tetrahydrocurcumin (THC) -incorporated porcine collagen scaffolds were obtained using a syringe-based extrusion 3D printer and their potential as sustained THC delivery systems was analyzed. Before processing, the optimal 3D printing conditions were determined by rheological analysis.

Afterwards, electrical properties of bovine collagen-based films were analyzed. In **Chapter 8**, ZnO nanoparticles (NPs) were incorporated into collagen formulations processed by solvent casting in order to obtain films with induced electro-conductive properties, which could be of great relevance for biomedical applications. Moreover, in order to develop next generation advanced functional materials for sustainable electronics, in **Chapter 9**, wool and choline dihydrogen phosphate or choline serinate ionic liquids were incorporated into collagen formulations and films were prepared by compression molding.

Finally, **Chapter 10** summarizes the conclusions of the doctoral thesis and the references cited along this work are listed in **Chapter 11**.

OBJETIVES

The main objective of this doctoral thesis was to develop collagen-based materials obtained from bovine and porcine skin wastes with improved properties incorporating other compounds, some of them also extracted from biowastes, and employing different processing methods.

The specific aims are summarized as follows:

- Preserve the triple helix structure of native collagen during extraction and processing in order to provide final products with enhanced properties.
- Optimize collagen formulations for each processing method used.
- Optimize 3D printing parameters to obtain THC incorporated scaffolds.
- Determine the optimum temperature to process collagen films with wool and ionic liquids (ILs) by compression molding.
- Assess the behavior of collagen films with aloe vera, chitosan and tetrahydrocurcumin: bioactive release, mucoadhesion, degradation, cytotoxicity, biocompatibility and cell culture.
- Provide collagen films with electrical and dielectrical properties by incorporating ZnO NPs, ILs and wool.
- Assess the environmental aspects involved in the production of collagen products.

INDEX

Chapter 1

INTRODUCTION

1.1 SUMMARY

The continuous growth in plastic use has brought an increasing environmental awareness from the perspective of waste management, emissions released during manufacture, and resources use (Clark et al., 2016). For this reason, in the last years, the employment of renewable resources to produce biodegradable materials has been of great interest with the aim to reduce the use of petroleum-derived polymers and contribute to the development of environment friendly materials (Gandini et al., 2016). In particular, valorization of materials may be a promising solution not only to minimize waste, but also to produce high value-added products (Xiong et al., 2019). In this context, the extraction of biomaterials, such as proteins and polysaccharides from livestock and fish processing industry by-products represent a challenging valorization opportunity (Lee et al., 2020; Meena et al., 2020).

Collagen is the most abundant protein of the extracellular matrix (ECM) in vertebrates, being approximately 30% of the body total protein mass in mammals (Balaure et al., 2019; Martínez-Ortiz et al., 2015). There are at least 28 collagen types composed of 46 distinct polypeptide chains, constituting the major part of connective tissues, skin, tendons, blood vessels, cornea, cartilages and bones (Koch et al., 2001; Myllyharju & Kivirikko, 2001). Type I, II and III collagens are the classical fiber-forming collagens which consists of three parallel polypeptide-alpha chains in a right-handed triple-helical structure, which self-associates to form highly ordered crosslinked fibrils. Those fibrils, in turn, form insoluble fibers providing the extracellular matrix with a high integrity, inherent water stability and mechanical tensile strength due to its tight winding triple helix structure (An, Lin & Brodsky, 2016; Liu, Hu & Han, 2018). It should be noted that the triple helical structure repetition occurs in all types of collagen, but the length of the helix and the size and nature of non-helical portion varies from one to another type (Miller, 1984; Shoulders & Raines, 2009). In particular, type I collagen is the main collagen in skin and bones (90%) (Ding, Zhang & Li, 2014).

In addition to structural roles, collagen also plays functional roles taking part in tissue regulation, growth and repair (Ferreira et al., 2012). Those structural and biological properties, combined with ease of extraction and the physical versatility to form gels, films, meshes, scaffolds and fibers make collagen an attractive candidate for biomedical applications, such as tissue engineering and regenerative medicine (Agrawal & Ray, 2001; Di Summa et al., 2014; MacNeeil, 2007; Muthukumar et al., 2018). Additionally, collagen is widely used in pharmaceutical (Jeevithan et al., 2013), food (Wang et al., 2018) and cosmetic (Avila Rodríguez et al., 2018) industries.

This chapter provides an overview of materials based on collagen. First, biowaste valorization and the techniques used for collagen extraction will be described briefly and, hereafter, structure and properties of collagen will be reviewed. Finally, the possible application of collagen and its derivatives in food, cosmetic and biomedical industries will be described (**Figure 1.1**).

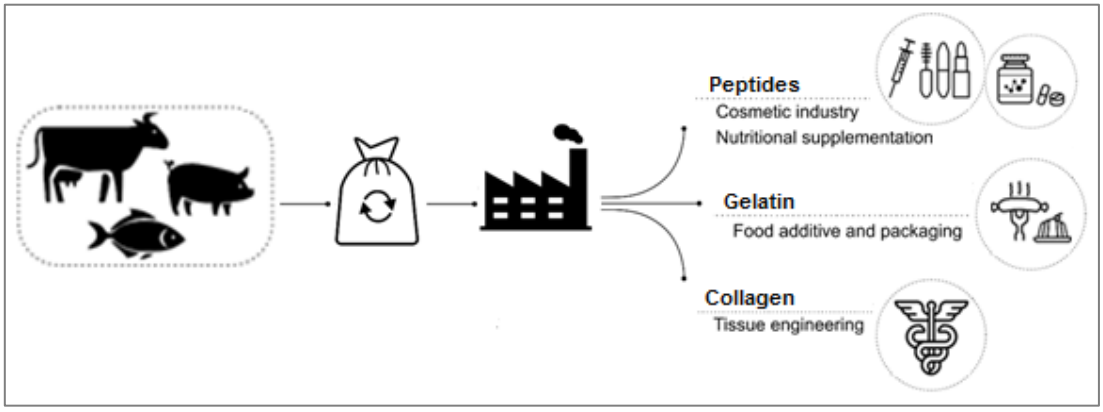

Figure 1.1. Graphical summary: collagen sources, valorization and applications.

1.2 BIOWASTE VALORIZATION

Sustainable food production has become a critical challenge due to social and environmental concerns together with the growing global population. As a consequence of processing raw materials, the production of waste is an unavoidable result. Therefore, valorization strategies may be a promising solution not only to minimize waste, but also

to produce high value-added products (Six, Velghe & Verstichel, 2016; Xiong et al., 2019).

The United Nations defined food waste as the end products of food processing industries that have not been recycled or used for other purposes. These are the non-product flows of raw materials whose economic value is less than the cost of collection and recovery for reuse and, thus, they are discarded as waste (United Nations, 2015). Several initiatives have been implemented worldwide to promote the prevention of food waste in all the life stages. In 2015, the United Nations defined the Sustainable Development Goal (SDG) 12 to ensure sustainable consumption and production patterns with the aim of reducing by half the global per capita food waste at the retail and consumption levels by 2030 and to reduce food losses along production and supply chains, including post-harvest losses (United Nations, 2015). Moreover, the European Commission committed to achieving this objective in the New Circular Economy Action Plan (European Commission, 2020), in which industrial ecology concepts, such as “from cradle to cradle” and “zero waste” have been promoted. Therefore, the exploitation of food waste as a source of proteins, polysaccharides, lipids, minerals, nutrients and flavors for the creation of a new generation of products has attracted the attention of researchers and industry, promoting the conversion of food industry wastes into value-added raw materials (Martínez-Alvarez, Chamorro & Brenes, 2015; Ong et al., 2018).

In this context, the valorization of by-products from livestock, poultry and fish-processing industries can be a worthy approach to develop sustainable products. The total global production of fish from aquaculture and marine fisheries peaked at about 171 million tons in 2016 (FAO, 2018) and about 38.5 million tons of those marine catches were considered as by-catch and discards, due to low market value of those marine fish species (Etemadian et al., 2021). Besides, livestock total production has reached more than 263 million tons annually (Aspevik et al., 2017). Furthermore, about 40-60% of fish, livestock and poultry remains as wastage after processing, generating huge amounts of

collagen-rich residues which include heads, bones, blood, skin, viscera, hooves, skin and feathers (Ferraro et al., 2017; Venkatesan et al., 2017) (**Figure 1.2**). With regard to valorization strategies, collagen can be extracted from almost every vertebrate; nonetheless, bovine, porcine and chicken skin and bones are the main sources at commercial scale (Abdollahi et al., 2018). However, due to bovine spongiform encephalopathy (BSE) and other prions diseases outbreak as well as religious considerations for the development of kosher and halal products, seafood by-products have become a promising alternative as a collagen source (Coppola et al., 2020; Pal & Suresh, 2016; Senadheera, Dave & Shahidi, 2020).

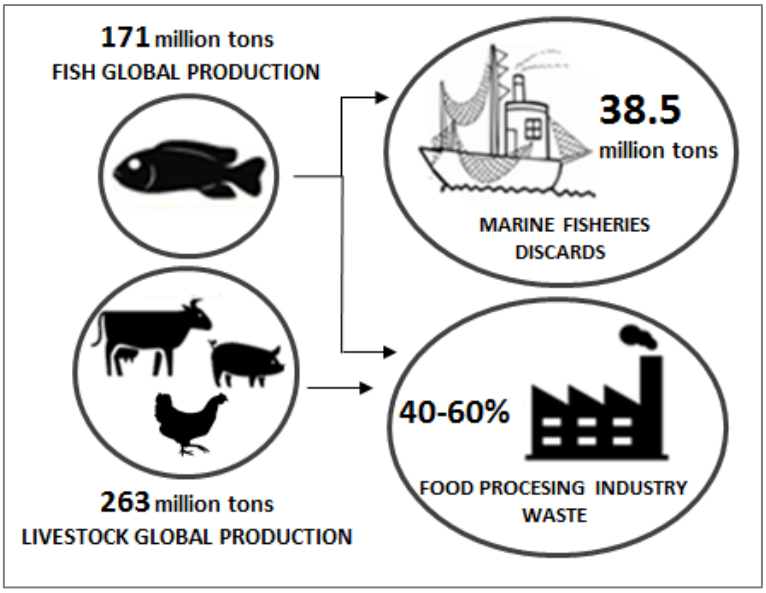

Figure 1.2. Global fishery and livestock production (2016) and wastage.

The collagen extraction process from fishery and livestock by-products consists of two main steps: pretreatment of raw materials and collagen extraction. In general, alkaline pretreatment is carried out to remove impurities like non-collagenous proteins and lipids, as well as to increase the quality of the final extracted collagen (Ahmed et al., 2018); and it can be carried out using a strong alkali, such as sodium hydroxide (Kittiphattanabawon et al., 2016; Sinthusamran et al., 2014) or calcium hydroxide (See et al., 2015). Sometimes, to remove the lipids, alcohols like ethanol (Chen et al., 2016c;

Tkaczewska et al., 2018), isopropanol (Sae-leaw et al., 2016) or butyl alcohol (Gomez et al., 2018) are used. Additionally, the demineralization of the raw materials can be carried out using ethylenediaminetetraacetic acid (EDTA); thus, calcium or other inorganic materials are removed (Chuaychan et al., 2016). After that, the extraction of collagen is usually carried out.

There are numerous methods reported for collagen extraction, based on three main extraction processes: extraction of salt-soluble collagen (SSC), acid-soluble collagen (ASC), and enzyme-soluble collagen (ESC) (**Figure 1.3**). Those extraction methods directly affect collagen properties and yield (Wang et al., 2014), and depend on factors such as fish species and age (Liao et al., 2018). It is worth noting that all procedures within collagen extraction are performed at low temperature (~4 ºC) for 24-48 h. Although an increasing extraction temperature and time can offer a higher collagen yield, it may not be desirable due to collagen degradation (Liu et al., 2015).

Regarding SSC extraction, lower yields are obtained comparing with ASC and ESC extractions (Liang et al. 2014a); hence, this method is not widely utilized and acid and/or enzymatic extractions are preferred. In terms of ASC extractions, the use of acetic acid medium for extraction and isolation of collagen from by-products such as tarpon skin (Chen et al., 2016a) and seabass scales (Chuaychan et al., 2015) has been reported. In addition to acetic acid, collagen can also be extracted using other organic acids, such as citric acid (Sae-leaw et al., 2016) or inorganic acids like hydrochloric acid (Tan & Chang, 2018) and phosphoric acid (Hanjabam et al., 2015). However, it must be considered that the solubility of collagen in acidic media is limited owing to many interchain crosslinks, covalent bonds formed via the condensation reaction of aldehydes with lysine and hydroxylysine at the telopeptide region (Pal et al., 2015). Moreover, habitat and age of animals along with the collagen source affect directly the content of keto-imine bonds and, hence, the solubility in acidic media (Thuy et al., 2014). In order to improve solubility and achieve higher yield, extraction parameters can be changed,

including acid concentration, ratio of acid solution/raw materials, extraction temperature and time; however, these parameters must be controlled in order to avoid collagen degradation (Pal & Suresh, 2016). Depending on the degree of collagen aggregation, the extraction process could also include the use of proteolytic enzymes which, together with an acidic solution, might lead to an increase in the yield by combining biological and chemical extraction (Ahmad et al., 2017; Chen et al., 2016b; Chuaychan et al., 2015; Jridi et al., 2015; Liang et al., 2014b; Sila et al., 2015). Diverse enzymes have been employed, among them, trypsin and pepsin digestive proteases (Abdollahi et al., 2018) and bacterial collagenases (Ahmed et al., 2018). Indeed, the most commonly employed enzyme is pepsin and, in this sense, the resultant pepsin extracted collagen is called pepsin-soluble collagen (PSC) (Jeevithan et al., 2013). This digestive protease can hydrolyze non-collagenous proteins and then pepsin can be removed using the salt precipitation and dialysis, increasing the purity of extracted collagen. Additionally, pepsin can also hydrolyze collagen telopeptides, contributing to the treated collagen dissolution in acid media and so, increasing the yield of acid soluble extraction (Wang et al., 2014). It is worth noting that commercial pepsin is commonly obtained from porcine gastric mucosa; however, in order to avoid some religious restrictions, a huge range of proteolytic enzymes, including pepsin, can be extracted from fish viscera (Gomez et al., 2018). Furthermore, the choice of suitable enzymes and physiochemical conditions for the enzymatic reaction, such as solution pH, temperature, hydrolysis time and enzyme concentration, must be optimized for the maximum activity. In recent years, other techniques have been used to improve SSC, ASC and ESC extraction methods, among them, ultrasonic treatments and homogenization-aided methods (**Figure 1.3**): Zou et al. (2017) worked with ultrasonic power of 200 W, having a single frequency of 24 kHz, to obtain collagen extracted from calipash of soft-shelled turtle; Tan & Chang (2018) successfully extracted collagen from catfish skin by mixing catfish skins, hydrochloric acid and pepsins at 7000 rpm for 5 min until homogenization and then, the mixture was stirred for 1 h at 4 ºC.

After extraction processes, some final steps must be carried out. Thereby, collagen is usually recovered using salt precipitation, centrifugation, dialysis, and freeze-drying. Generally, collagen solution is precipitated using NaCl. The salt concentrations employed for collagen precipitation can be adjusted to maximize the collagen recovery and removal of impurities. Then, centrifugation (around 10000-20000 rpm) is used to collect the precipitated collagen. The resultant precipitate is dissolved in acetic acid prior to dialysis against distilled water. The dialysate is finally freeze-dried and the obtained collagen powder is stored (Pal et al., 2015).

All aforementioned methods are generally time-, energy- and reactant-consuming batch type processes. Therefore, alternative methods are emerging, among them, extrusion-hydro-extraction (EHE) processes (**Figure 1.3**). Extrusion is widely used in the food industry and it offers many advantages, such as continuous production, high yield, and little waste. In that way, Huang et al. (2016) developed a novel EHE process for collagen extraction from tilapia fish scale, obtaining extruded scale samples with 2-3 times higher protein extraction yield than that of non-extruded scale samples.

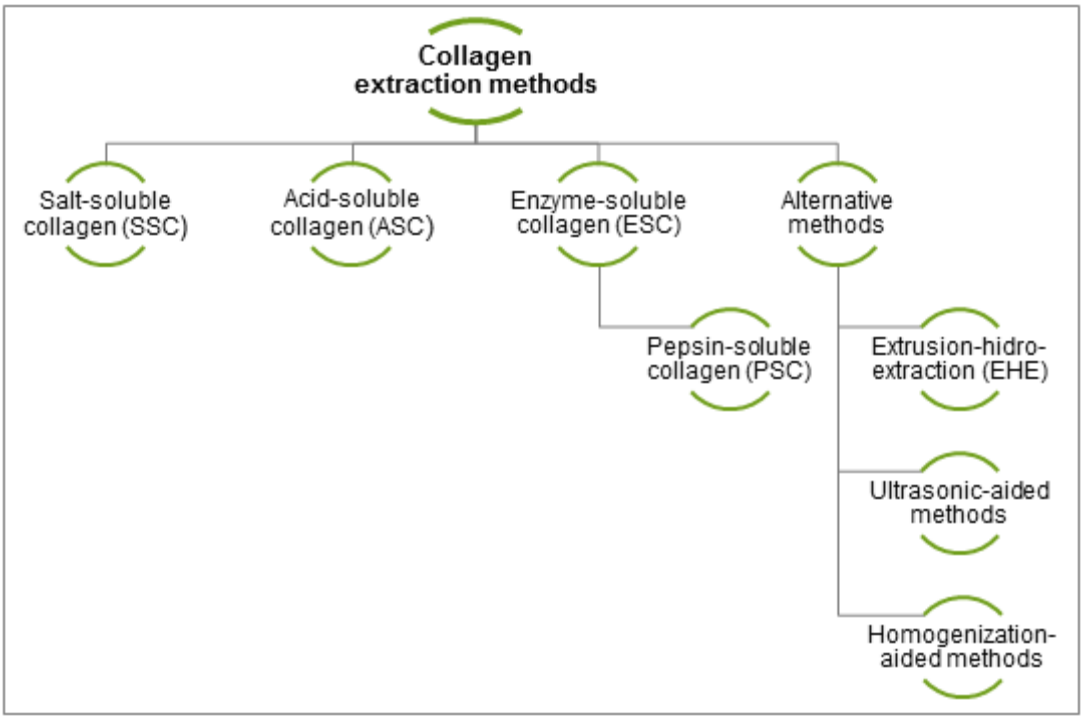

Figure 1.3. Collagen extraction methods.

1.3 COLLAGEN STRUCTURE AND PROPERTIES

The collagens represent the major family of extracellular matrix (EMC) proteins (Exposito et al., 2002). In fact, collagen is the most abundant protein in vertebrates, being approximately 30% of all proteins in mammals (Ricard-Blum, 2011). The basic structural unit of all collagens consist of three polypeptide left-handed α chains wound around one another in a characteristic right-handed triple helix (Brodsky & Ramshaw, 1997; Shoulders & Raines, 2009). Each polypeptide chain has around 1000 amino acids and contains at least one stretch of the repeating amino acid sequence Gly-X-Y, where Gly is a glycine and X or Y can be any amino acid. This motif allows the chains to form the characteristic triple helix structure, with Glycine at the core of the protein and the X and Y amino acids exposed at the surface (Van der Rest & Garrone, 1991). Moreover, proline (Pro) and hydroxyproline (Hyp) follow each other frequently and about 10% of the molecule has the sequence Gly-Pro-Hyp (Patino et al., 2002). In this sense, although all collagens showed triple helix structure, each type of collagen is unique due mainly to other regions consisting of different non-collagenous domains that fold into other kinds of three-dimensional structures (Sherman, Yang & Meyers, 2015). There are currently 28 different proteins identified as collagens, the same members known in humans. They can be grouped in two main classes based on their supramolecular structures: the fibrillar collagens and the non-fibrillar collagens (Heino, 2007).

Fibrillar collagens contain one major triple-helical domain which self-associates to form highly organized fibers and fibrils into bundles or lamellae, giving rise to tissue-specific, biomechanical, and other biological properties (Lodish et al., 2000) (**Figure 1.4**). These classical collagens include the type I, II, III, V and XI, but also the more recently characterized types XXIV and XXVII collagens (Hulmes, 2002). Type I is the most abundant structural protein found in skin, tendon, bone, cornea and lung and comprises between 80% and 99% of the total collagen (Ding, Zhang & Li, 2014). In addition, type I collagen is the mayor protein in all connective tissues, being about 90% of the entire

collagen content of skin and bones (Ding, Zhang & Li, 2014). Type II has a more specific tissue conformation, being limited essentially to cartilage and type III found in relatively elastic tissues, such as embryonic skin, lung and blood vessels. Additionally, Type V and type XI are found as quantitatively minor collagens, in association with collagen I, with particularly high amounts in cornea and in cartilage in association with collagen II (Van der Rest & Garrone, 1991). Little is known about type XXIV and XXVII collagens, except that appear to be associated with types II and I containing tissues, respectively, being their (Gly-X-Y) region relatively short (Plumb et al., 2007). It may be highlighted that most collagen fibrils are composed of two or more different collagen types (Patino et al., 2002).

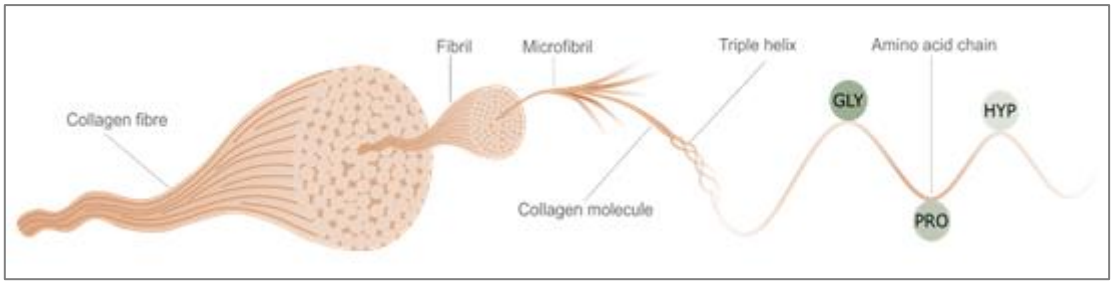

Figure 1.4. Structure of fibrous collagen.

Concerning to the non-fibrous collagens, they are classified according to their molecular characteristics, supramolecular structures and types of extracellular network in basement membrane, beaded filaments, short-chain and fibril-associated collagens (FACITs). Basement membrane collagens, underlying type IV, is found at tissue boundaries such as epithelial, endothelial, fat, muscle and nerve cells, as well as at the dermal-epidermal junction (Gelse, Pöschl & Aigner, 2003). Collagen VI, which is the main beaded filament collagen, is present in relatively all-over connective tissues to maintain their integrity (Knupp & Squire, 2005). Among the short-chain collagens, type VIII and and type X can be found in endothelial cells and in the hypertrophic zone of cartilage, respectively (Sutmuller, Bruijn & Heer, 1997). Finally, FACITs (Fibril Associated Collagens with Interrupted Triple Helices) are a large group composed by types IX, XII, XIV, XV, XIX, XX and XXII (Gelse, Pöschl & Aigner, 2003). Type IX collagen is one of

the founder member of this group and is an important component of cartilage collagen fibrils, together with collagen II and XI. The similar structure of type XII and XIV collagens has also been associated with type I collagen in skin, tendons, ligaments and cornea (Sherman, Yang & Meyers, 2015). After a brief classification of non-fibrillar collagens, this chapter will focus on fibrillar collagens.

Traditionally, the role attributed to fibrous collagens has been a structural one contributing to mechanical properties, organization, and shape of tissues. Highly organized collagen fibrils, the basic building block of collagen-rich tissues, are assembled to a variety of more complex structures with very different mechanical properties, such as mechanical stability, strength and toughness, to a range of tissue from bone, skin tendons and ligaments, to blood vessels, nerves and intestines (Fratzl et al., 1998). In addition to structural roles, collagen has been shown to be involved, either directly or indirectly, in functional roles (Ghodbane & Dunn, 2016). Due to its remarkable capacity to act as a substrate for cell adhesion and growth, collagen has been considered as a valuable candidate to design renovable medical devices. Moreover, collagen is largely non-immunogenic and poorly antigenic and, thus, biocompatible (Lynn, Yannas, & Bonfield, 2004). Besides, although collagen is resistant to common proteases having a long lifetime, it can be biodegraded in the body by some enzymes of the matrix metalloproteinase (MMP) family, leading to biodegradable collagenous biomaterials (Fu et al., 2018). Those collagen structures, their physical and biological properties, and their physical versatility to form gels, films, meshes, scaffolds and fibers make collagen an attractive candidate for several applications.

1.4 APPLICATIONS OF COLLAGEN AND ITS DERIVATIVES

Collagen, the main component of the extracellular matrix, is largely used in food and cosmetic industries (**Figure 1.5**) in its native fibrillary form, as well as after denaturation, due to its multiple functional properties and physical versatility to be

processed in a variety of products, including gels, porous scaffolds, fibers, films, meshes and micro/nanoparticles (Oliveira et al., 2021). In this context, gelatin, thermally denatured collagen with molecular weight (MW) from 15 to 250 kDa, shows unique rheological properties and is prevalently used in food industry as a food additive, microencapsulating agent, and biodegradable packaging material (Bello et al., 2020). Additionally, peptides with biological activity and MW between 300 and 8000 Da can be obtained by chemical hydrolysis, enzymatic treatment or/and proteolytic fermentation of collagen or gelatin (León-López et al., 2019). The studies about collagen-derived peptides have revealed their antioxidant and antihypertensive activity, as well as other promising health beneficial effects for cosmetic and nutraceutical applications (Nguyen, Heimann & Zhang, 2020).

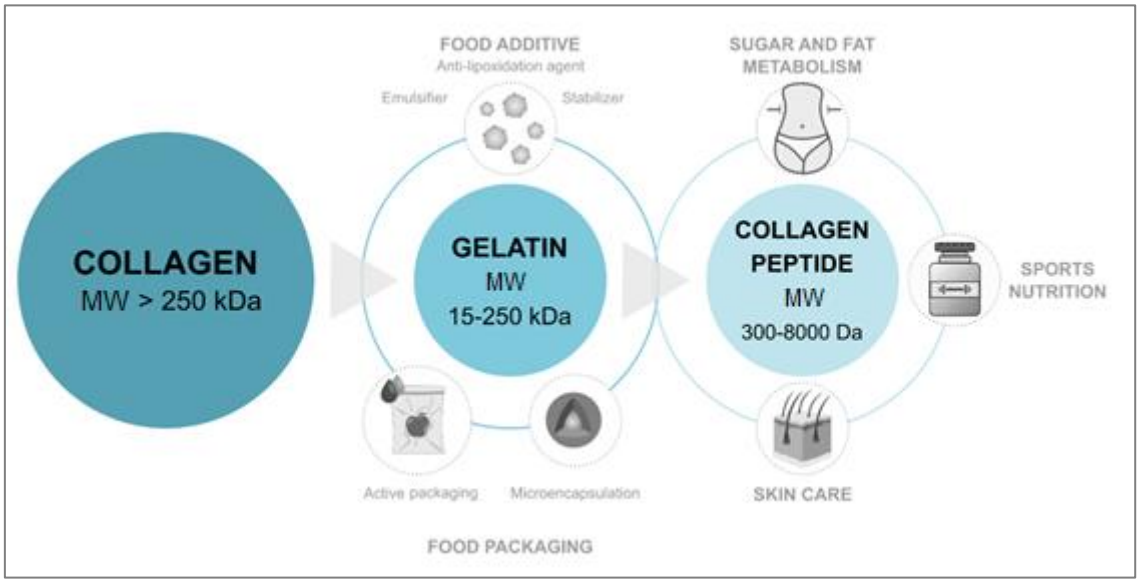

Figure 1.5. Collagen applications in food and cosmetics industries.

1.4.1 Peptides for cosmetics and nutraceutical industry

Based on the above-mentioned bioactive properties, collagen has also been increasingly utilized for the development of cosmeceutical products, such as skin anti-aging formulations with moisturizing, softening and glowing, antioxidant and UV protective properties (Abuine et al., 2019; Zamorano-Apodaca et al., 2020) (**Figure 1.5**).

It should be noted that hydrolyzed collagen is mainly applied in cosmetic formulations because it offers better effects than native collagen thanks to its superior solubility at neutral pH, water-binding properties, and easy dermis penetration (Alves et al., 2017; Skov et al., 2019). Although hydrolyzed collagen can slightly penetrate the epidermis, it cannot replace the lost collagen of the skin (Venkatesan et al., 2017). In this regard, cosmetics industries are interested in subcutaneous injections and oral supplementations. Collagen injections have been popularly used for the repair of dermatological defects, as well as subcutaneous disorders, such as acne scars, and aging symptoms, thanks to collagen biodegradability, price and facility to be produced (Cockerham & Hsu, 2009). When collagen is injected into the dermis, it seems that collagen promotes the biosynthetic capacity of fibroblasts and the formation of an optimal physiologic environment and, thus, increases cell activity, hydration, and the synthesis of collagen (Ganceviciene et al., 2012). Alternatively, the positive effect of oral collagen-based supplements on skin appearance has been recently observed (Wang et al., 2018). The fast digestibility of bioactive collagen peptides in the form of liquids, pills or functional foods seems to contribute to the increase of fibroblast density and, hence, to the production of collagen. In that way, several studies have shown the efficacy of the daily bioactive collagen peptides supplementation in the skin hydration, wrinkling, elasticity and density (Genovese, Corbo & Sibilla, 2017; Ito, Seki & Ueda, 2019; Kim et al., 2018).

Besides cosmetics applications, several recent studies have reported the potential of collagen in functional foods and health care applications in form of pills and beverages (Bilek & Bayram, 2015; Guo et al., 2015; Pal & Suresh, 2016). On the one hand, collagen peptides were found to increase the fatty acid metabolism and fats burn, and reduce hypertension and hyperlipidemia. Additionally, they can inhibit the fatty acid synthesis of the liver, decreasing hepatic fat accumulation (Ishak & Sarbon, 2018). On the other hand, they enhanced insulin sensibility and reduced blood sugar levels, which could be attributed to their antioxidant property (Lauritano & Ianora, 2016). Therefore,

bioactive collagen peptides are used to prevent and treat obesity and type 2 diabetes, inducing the weight loss and reestablishing lipid and blood glucose level (Astre et al., 2018). In this regard, other studies reported that the ingestion of food or drinks enriched with hydrolyzed collagen can help on wound healing, bone formation, mineral density and osteoarthritis (Sato, 2017; Suresh et al., 2015). Collagen is also in demand within the sport nutrition field, nutraceutical industry offers dietary supplements intended to sport nutrition field boost, since it can increase lean muscle, decrease recovery time, reconstruct damaged joint and improve cardiovascular performance (Oertzen-Hagemann et al., 2019).

1.4.2 Gelatin for food industry

Collagen and gelatin have also found wide application in food industry as food additives or packaging materials (**Figure 1.5**). Gelatin is incorporated in foods during the food processing to modify color, texture, flavor and consistence, among others food properties. However, the prevalent applications of gelatin are as food stabilizers and consistence enhancers to form stable gels, emulsions or foaming (Mardani et al., 2019; Yang et al., 2020). The most popular single use of gelatin as gelling agent may be in water gel desserts, due to its unique melt-in-the-mouth property, but it is also commonly used to form insoluble cross-linked hydrogels that maintain their shape after water uptake equilibrium (Huang et al., 2019; Li et al., 2021). Additionally, heat-treated collagen fibers have been used as emulsifiers, as natural alternatives to synthetic emulsifiers, especially in acidic products. For example, the incorporation of collagen improves the rheological properties and avoid the fat cap of the oil-in-water emulsions of sausages (Fustier et al., 2015; Huang et al., 2020). In this context, thanks to their antioxidant activity, collagen hydrolysates have been frequently used to inhibit the peroxidation of lipids whose reaction products are dangerous for human health (Bolognesi, Spier & Rocha Garcia, 2020). This antioxidant activity is generally associated to the radical scavenging capacity of the imidazole group of histidine (Pan et al., 2020).

In recent years, collagen-based films and coatings have played an important role in the development of sustainable packaging materials to protect, maintain, and extend the shelf life of foods (Moreno et al., 2018; Pellá et al., 2020). Generally, food-packaging materials are required to act as a barrier against the migration of oxygen and moisture, as well as to preserve the sensory qualities and prevent fat oxidation, discoloration, and microbial activity (Regubalan et al., 2018). In this context, gelatin has been widely studied thanks to its film-forming ability, biodegradability and good gas barrier properties. However, it has poor mechanical strength, and due to its high hygroscopic nature, it tends to swell and dissolve when it is in contact with food with high moisture content, limiting its direct application in food packaging (Jiang et al., 2020; Liu et al., 2020). Therefore, chemical or physical methods, such as crosslinking (Beghetto et al., 2019; Tonndorf, Aibibu, & Cherif, 2020; Uranga et al., 2020; Wu et al., 2019) or combination with other biopolymers (Bhuimbar, Bhagwat & Dandge, 2019; Hou et al., 2020; Zhuang et al., 2017), are carried out to improve those properties. Crosslinking reduces the mobility of gelatin chains, improving dimensional stability, water and heat resistance, barrier and mechanical properties (Huang et al., 2019).

The production of sausage casings using coextrusion process has been the best-known industrial application of collagen and gelatin films. However, the strong sensitivity of gelatin to moisture reduces the barrier and mechanical properties of the casings (Chen et al., 2019; Tosati et al., 2017), and multilayered structures can be a strategy to overcome this kind of weakness, where layers with different moisture and oxygen barrier properties are combined in order to comply the required specific package conditions (Figueroa-Lopez et al., 2018; Nilsuwan et al., 2020; Wang et al., 2020).

In recent years, gelatin has been reported to be one of the first materials used as a carrier of bioactive substances. Gelatin films and coatings can be functionalized with the incorporation of natural antioxidants and antimicrobial components, obtaining active packaging. Many bioactive components have been reported for active packaging but, in

the last years, there is a growing interest in using plant extracts like rosemary (Yeddes et al., 2020), grape (Rodrigues et al., 2020), lemon (Jiang et al., 2020), and oregano (Hernández-Nava et al., 2020). Since those extracts may be readily inactivated by exposure to light, heat, and oxygen (Molino et al., 2020), several researchers have tried to embed solid, liquid, or gaseous materials in microcapsules in order to entrap functional components in a carrier, protect them, and control their release (Mohseni & Goli, 2019). Moreover, encapsulation may be a useful solution to minimize the taste and odor of some vegetable extracts. Thus, encapsulation technology could be used to manufacture functional food formulations based on gelatin (Kuai et al., 2020; Paula et al., 2019; Rezaee et al., 2018; Yüksel & Şahin-Yeşilçubuk, 2018).

1.4.3 Collagen for biomedical use

Tissue engineering is a multidisciplinary field that combines the knowledge of engineering and biology in order to develop tissue substitutes capable of replace or improve damaged tissues or organs. The methodology of this science is based on the integration of cells, biologically active molecules and materials, recreating in that way the native structure (Langer & Vacanti, 1999). In that context, the material acts as a template to provide structural integrity, define a potential space, guide the restructuring while regeneration, permit diffusion of the nutrients and gas, and provide mechanical characteristics needed for the cell proliferation (Hollister, 2009). In other words, the material attempts to shape the cell microenvironment (**Figure 1.6**).

Originally, biomaterials used in the field of biomedicine tended to be inert, such as metals and ceramics, in order to avoid any eventual immune response. However, with the course of time and a better awareness of cellular biology, the use of new materials such as polymers, both natural and artificial, emerged. These materials not only comply with the function of a scaffold, but they are able to interact with the organism, contributing to an active regeneration. A promising approach has been the use of natural polymers,

as they have an inherent interaction with the organism, facilitating the development of new tissues while enhancing regeneration. The most widely used among them is collagen, as the major structural component of the native extracellular matrix (O'Brien, 2011). Thus, collagen presents high biocompatibility, biodegradability and malleability. However, collagen by its own forms fiber-like structure scaffolds that exhibit poor mechanical properties, making necessary the modification of the material for its optimal effectiveness (Benayahu et al., 2018, 2020; Yang, Best, & Cameron, 2016). One of the strategies employed is the combination of collagen with other natural polymers. The combination of collagen and chitosan is largely employed due to its great potential in tissue engineering applications (Shah et al., 2019). Chitosan offers high biocompatibility, moderate degradation, and antimicrobial effect, among other characteristics. By the addition of chitosan, sheet-like structures with enhanced integrity, mechanical properties and better viability are obtained (Hayashi et al., 2012; Hollister, 2009; McBane et al., 2013). According to the literature, the collagen-chitosan construct acquires suitable characteristics when higher concentrations of collagen (>50%) are employed, although a small proportion of chitosan is sufficient to achieve the desired mechanical properties while maintaining cell adhesion and proliferation (Pezeshki-Modaress, Zandi & Rajabi, 2018).

Recently, physical and chemical strategies have been implemented in order to ensure that the characteristics of the materials are satisfied. On the one hand, mechanical features can be tuned by means of physical or chemical techniques. Those are based on the creation of non-covalent interactions through the use of UV light or temperature, among other agents (Guan et al., 2017). These are inexpensive and easy-to-perform methods that prevent the introduction of possible cytotoxic chemical substances. However, the process is often hard to monitor and fails to achieve a sufficiently high level of crosslinking to meet mechanical requirements (Perez-Puyana et al., 2019). This is why the most common approach to overcome the limitations of

biomaterials, such as collagen-chitosan scaffolds, is chemical crosslinking. By this method, a chemical compound is added to the material and irreversible covalent bonds are created to interconnect molecules. This approach offers enhanced mechanical properties and an improvement in stability. However, the unreacted crosslinker inside the scaffold can lead to an increase in cytotoxicity together with subsequent processing difficulties caused by the reaction itself (Hennink & van Nostrum, 2012; Reddy, Reddy, & Jiang, 2015; Shah et al., 2019).

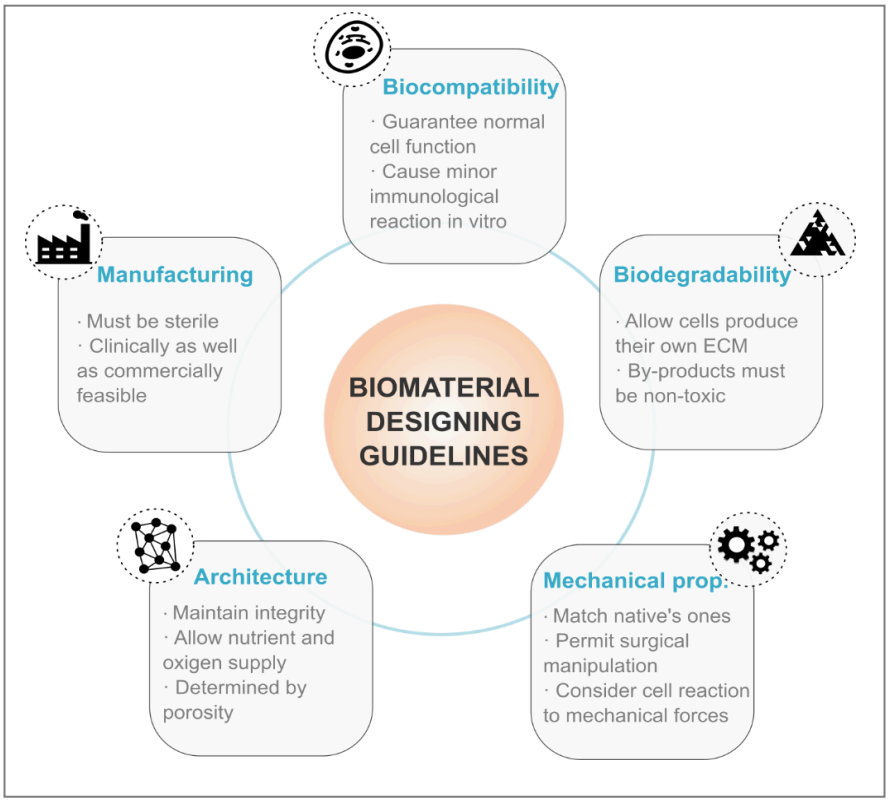

Figure 1.6. Criteria to be considered when choosing or designing biomaterials.

There is a great diversity of chemical crosslinking agents according to the degree of improvement desired. In the case of artificial tissues based on collagen and chitosan, one of the most widely used chemical compounds is glutaraldehyde due to its great effectiveness but, even at concentrations higher than 10%, produces cytotoxicity (Liu, Ma, & Gao, 2012; Reddy, Reddy, & Jiang, 2015; Reyna-Urrutia et al., 2019). Additionally, tannic acid stands out for its antimicrobial, anti-inflammatory and antioxidant properties (Shah et al., 2019; Sionkowska, Kaczmarek, & Lewandowska, 2014), the combination of

N-ethyl-N'-(3-dimethylamino propyl) carbodiimide with N-hydroxysuccinimide (EDC-NHS) enables the maintenance of the porous structure (Martínez et al., 2015; Reddy, Reddy, & Jiang, 2015), and citric acid permits the availability of the binding sites of both biomaterials making feasible further bioconjugations (Reddy, Reddy, & Jiang, 2015; Uranga et al., 2019). Finally, genipin is an aglycone present in the *Gardenia jasminoides*. This natural compound is effective at low concentrations, creating both intramolecular and intermolecular unions with primary amines of collagen and chitosan, and achieving a totally stable structure that maintains its original porosity (Perez-Puyana et al., 2019; Yan et al., 2010). The properties of collagen-chitosan scaffolds using the abovementioned crosslinking agents are summarized in **Table 1.1**.

Table 1.1. Assessment of different crosslinking agents used in collagen-chitosan scaffolds based on the crosslinking effectivity or level, cytotoxicity, improvement of the biomechanical properties and morphology of the resulting structure. Differences between techniques are shown on a scale of ---/+++, with higher crosslinking level, cytotoxicity and biomechanical improvement corresponding to +++.

AGENT		CROSSLINKING LEVEL	CYTOTOXICITY	BIOMECHANICAL PROPERTIES	REMAINING STRUCTURE
PHYSICAL	**Temperature**	-	--	++	No change
CHEMICAL	**Glutaraldehyde**	+++	+	+	Smaller pores
	Tannic acid	+	-	+	High porosity
	EDC-NHS	+	-	+	No change
	Citric acid	+	-	+	Rougher surface
	Genipin	++	-	+	No change

Because of their excellent characteristics, particularly their malleability, the combination of collagen and chitosan has been used for the regeneration of a wide variety of tissues. One of the widest applications has been the regeneration of bone. It has been demonstrated that collagen-chitosan membranes have a higher elongation to fracture and lower rate of degradability, critical factors for bone regeneration, than those scaffolds formed only by collagen (Guo et al., 2020). *In vitro*, the collagen-chitosan

combination presents osteoid differentiation capacity, even in the absence of a specific differentiation medium, indicating the capacity of induction to self-differentiation (Georgopoulou et al., 2018; Wang et al., 2016a). *In vivo*, the collagen-chitosan constructs have also demonstrated optimal properties for guided bone regeneration. In this case, electrospun collagen-chitosan membranes allow the formation of new bone in models of calvarial bone defect. By week eight, the cranial defect was completely restored by massive and mature bone tissue (Guo et al., 2020; Lotfi et al., 2016). Similarly, collagen-chitosan scaffolds, crosslinked with carbodiimide, were shown to promote cartilage regeneration in rabbit articular cartilage defects. New cartilage formation was observed as early as at 1 month, and by 6.5 months the cell number, collagen quantity, as well as compressive and storage moduli, approached to the normal cartilage (Whu et al., 2013). Recently, a porous collagen-chitosan scaffold enriched with hydroxyapatite, as a bioactive component, was developed (Campos et al., 2020).

Chitosan-collagen scaffolds approximate very closely the structural hierarchy, organization, biochemical composition, and functional features of native skin extracellular matrix. Furthermore, the combination presents hemostasis and antibacterial properties along with the potential to accelerate the synthesis of extracellular matrix compounds by fibroblast induction, thus, its potential use in skin tissue engineering. The microfiber structures may favor these properties since it has been shown that crosslinked collagen-chitosan microfiber scaffolds can control water loss by evaporation. In addition, the re-epithelization of wounds after 14 days of application of the scaffold, through guided infiltration of fibroblasts and remodeling of collagen in synchrony with the degradation of the scaffold, has been demonstrated (Sarkar et al., 2013). In skin tissue engineering, the thickness of the graft is crucial, as this influences the effectiveness of the construct implantation. Thinner scaffolds, especially 0.5 mm thick, have been shown to promote ordered fibroblast infiltration and better collagen remodeling. By week 16 after implantation in skin defects, such implants showed total degradation together with

complete replacement with new well-arranged host tissue, newly formed vessels, and 76% of the tensile strength of native skin (Haifei et al., 2014).

Recently, some attempts have been made to use collagen-chitosan combination in diseases related to the neural tissue such as spinal cord injury. In this case, 3D printed scaffolds could have significant therapeutic effects by bridging axons across the fracture and allowing the mobility of cells, partially re-establishing a microenvironment for axonal regeneration. Once implanted in rat models, nerve-fiber regeneration as well as neurological and locomotor recovery were achieved (Sun et al., 2019).

1.4.4 Future trends and opportunities

In the biomedical field, major efforts are being focused on adapting the properties of collagen and chitosan constructs to clinical demands. In this sense, the development of additive manufacturing techniques has meant a great advance in the field, as they allow the rapid and reproducible manufacture of complex 3D shapes. Recently, the emergence of a novel and innovative 4D printing has allowed the combination of traditional and smart materials. These possess features that allow to respond to external stimuli (heat, moisture, light, magnetic field or pH), adapting their properties to the microenvironment (change shape or color, produce an electrical current, become bioactive, or perform an intended function). 4D printing benefits from the property of smart materials to have dynamic responses and to control the construct spatially and temporally. Moreover, 4D printing eliminates the need for external devices or methods for post-processing. Therefore, 4D printing can cause a disruptive effect in the medical field, since it represents a great potential for non-invasive and remoted-control therapies, such as drug delivery, biosensors or regenerative medicine. Considering that each model in medicine varies from patient to patient, 4D printing could allow the achievement of effective personalized medicine (Lui et al., 2019; Mantha et al., 2019; Piedade, 2019; Shie et al. 2019; Tamay et al., 2019).

Chapter 2

MATERIALS AND METHODS

2.1 MATERIALS AND REAGENTS

Bovine and porcine collagen obtained from trimmings and the splitting-derived residues supplied by Tenerias Omega (Navarra, Spain) were used as the main component of the formulations. The amino acid composition of bovine and porcine collagen are showed in **Table 2.1**. Pure glycerol (pharmaceutical grade), provided from Panreac (Barcelona, Spain), was used as plasticizer. Acetic acid, purchased from Panreac, and distilled water were used for sample preparation.

Table 2.1. Amino acid composition of bovine and porcine skin native collagen (expressed as residues/1000 residues).

Amino acid	Bovine collagen	Porcine collagen
Aspartic acid	45.3	43.0
Threonine	16.1	15.3
Serine	37.0	33.7
Glutamic acid	72.5	71.5
Glycine	330.9	336.7
Alanine	109.7	108.2
Valine	18.7	20.4
Methionine	6.0	6.6
Isoleucine	10.3	8.2
Leucine	28.8	23.4
Tyrosine	5.7	4.4
Phenylalanine	15.6	14.8
Hydroxylysine	6.7	5.8
Lysine	25.7	29.3
Histidine	4.5	3.8
Arginine	45.4	44.7
Hydroxyproline	98.1	91.2
Proline	122.9	129.7
Imino acids	221.0	43.0

Zinc oxide nanoparticles (Ø < 100 nm, specific surface of 10–25 m^2/g), high molecular weight (HMW, batch MMBC0059, 375 kDa) and low molecular weight (LMW, batch MKBB9037, 190 kDa) chitosan with a deacetylation degree higher than 75% provided by Sigma-Aldrich (Madrid, Spain), anhydrous citric acid powder (purity of 99.5%) supplied by OPPAC (Navarra, Spain), aloe vera powder obtained from Agora Valencia (Valencia, Spain), tetrahydrocurcumin gifted by Sabinsa Corporation (New Jersey, USA), choline dihydrogen phosphate ([Ch][DHP], > 98%) and choline serinate ([Ch][Seri], > 95%, 60% in H_2O) supplied by IOLITEC GmbH (Germany), and sheep wool obtained from Landazurieta farm (Alava) were used as additives in collagen formulations.

2.2 SHEET PREPARATION

Bovine collagen was obtained through the technology described in “Process of obtaining collagen from the skin of an animal” patent (PCT/ES2011/070467, 2013). Bovine skin was pretreated in an alkaline solution at 80 ºC for 10 min in a tanning drum in order to soften it and facilitate the subsequent processing.

Then, collagen, 25 wt % glycerol (based on dry collagen) and different amounts of citric acid (2.5, 5.0, 7.5, and 10.0 wt % based on dry collagen) were mixed for 15 min in laboratory rollers, previously heated at 55 ºC, until total homogenization of the mixture. After that, the mixtures were pressed by compression at 80 ºC and 300 bar, obtaining rectangular sheets with an average thickness of 1.30 mm. Sheet systems were designated as CA2.5, CA5.0, CA7.5 and CA10.0 as a function of citric acid content. Sheets without citric acid were produced and designated as control sample.

The sheets were conditioned in a controlled environment chamber (ACS SU700V) at 25 ºC and 50% relative humidity before testing. The sheets thickness was measured to the nearest 0.001 mm with a hand-held QuantuMike digimatic micrometer (Mitutoyo Spain, Elgoibar, Spain) and the obtained values were 1.42 ± 0.13 mm.

2.3 FILMS AND SCAFFOLDS PREPARATION

2.3.1 Treatments

Bovine and porcine skins were treated with NaOH 1 M at room temperature for 12 h. Afterwards, these samples were neutralized with phosphate buffer saline (PBS) at pH 7.4 for 3 h. These samples were designated as native collagen. Finally, native collagen was grinded and freeze-dried in order to facilitate the subsequent processing.

In order to remove impurities, wool fibers h were washed twice with tap water and soap, and dry in an oven at 30 °C for 48 h before being used.

2.3.2 Films by solution casting

Bovine collagen films with different ZnO nanoparticles (NPs) contents (0, 2, 4, 6 and 8 wt % based on dry collagen) were prepared by solution casting. Hence, native collagen, 20 wt % glycerol (based on dry collagen) and ZnO NPs were incorporated into 0.5 M acetic acid (1:20 collagen/acetic acid ratio). The blends were maintained at room temperature under mechanical stirring at 150 rpm for 3 h and then, poured into Petri dishes and left dry at room temperature to obtain the films. Film were designated as 2ZnO, 4ZnO, 6ZnO and 8ZnO as a function of ZnO NPs content. Films without ZnO were produced and designated as control films.

Bovine collagen films with 30 wt % (based on dry collagen) LMW chitosan or HMW chitosan were prepared by solution casting. Firstly, chitosan was dissolved in 0.5 M acetic acid (1:20 collagen/acetic acid ratio) under continuous stirring for 30 min and then, native collagen and 20 wt % glycerol (based on dry collagen) were added. The blend was maintained under mechanical stirring for 3 h and then, poured into petri dishes and left drying at room temperature to obtain the films. Films were designated as HMW and LMW, as a function of chitosan. Films without chitosan were prepared and designated as control films.

All films were conditioned in a controlled environment chamber (ACS SU700V) at 25 ºC and 50% relative humidity for 48 h before testing. The film thickness was measured to the nearest 0.001 mm with a hand-held QuantuMike digimatic micrometer (Mitutoyo Spain, Elgoibar, Spain) and the obtained values were 42 ± 16 μm in collagen-ZnO NPs films and 265 ± 55 μm in collagen-chitosan films.

2.3.3 Films by compression molding

Aloe vera containing porcine collagen films were prepared by compression molding. Native collagen, aloe vera (0, 10, 20 and 30 wt % based on dry collagen), 20

wt % glycerol (based on dry collagen) and 0.05 M acetic acid (1:1 collagen/acetic acid ratio) were manually mixed and pastes were stored in a plastic bag for 24 h at room temperature for dough hydration. Then, the hydrated dough was thermally molded using a Specac laboratory press. The dough was placed between two aluminum plates, put into the press, previously heated up to 90 ºC for 30 s, and then pressed at 0.5 MPa for 1 min to obtain the films. It is worth noting that those temperature and pressure conditions were selected since no film could be obtained at lower temperatures and pressures. Three film systems were produced and designated as AV10, AV20 and AV30, as a function of aloe vera content. Films without aloe vera were prepared and designated as control films.

Bovine collagen films with 0.1 wt % [Ch][DHP], 0.1 wt % [Ch][Seri] or 5 and 10 wt % wool (all additives on dry collagen basis) were prepared by compression molding. Collagen, additives, 20 wt % glycerol (based on dry collagen) and 0.5 M acetic acid (1:2 collagen/acetic acid ratio) were mixed using a T25 ultra-turrax (IKA, Germany) until homogeneous pastes were achieved (2000 rpm, 2 min). Then, hydrated doughs were molded by hot-pressing (Specac press). The dough was placed between two aluminum plates, previously heated up to 50 °C for 30 s, and then pressed at 0.5 MPa for 1 min to obtain the films. It is worth noting that the compression temperature was determined by rheological analysis. Films were designated as 5wool (sample with 5 wt % wool), 10wool (sample with 10 wt % wool), CDHP (sample with 0.1 wt % [Ch][DHP]) and CS (sample with 0.1 wt % [Ch][Seri]). Films without ILs or wool were prepared and designated as control films.

All films were conditioned in a controlled environment chamber (ACS SU700V) at 25 ºC and 50% relative humidity for 48 h before testing. The film thickness was measured to the nearest 0.001 mm with a hand-held QuantuMike digimatic micrometer (Mitutoyo Spain, Elgoibar, Spain) and the obtained values were 59 ± 13 μm in AV containing films and 20-30 μm in ILs and wool containing films.

2.3.4 Freeze-drying

Bovine collagen scaffolds with 30 wt % (based on dry collagen) HMW or LMW chitosan were prepared by freeze-drying. Hence, chitosan was dissolved in 0.5 M acetic acid (1:20 collagen/acetic acid ratio) under continuous stirring. Then, collagen and 20 wt % glycerol (based on dry collagen) were added and the blends were maintained under mechanical stirring for 3 h at 125 rpm. Then, the blends were poured into each well of a 12 multiwell plate (Costar 3513, Corning Incorporated), and the plate was frozen for 24 h at -23 ºC and then freeze-dried (Alpha 1-4 LDplus freeze-dryer, CHRIST) for 48 h. Finally, cylinder-shaped chitosan-collagen samples (2.26 cm diameter and 1 cm height) were taken out from the wells and neutralized by immersion into 0.4 M NaOH solution for 15 min and subsequently rinsed in water. In that way, amino groups of chitosan were deprotonated, leading to the disappearance of ionic repulsions and favoring physical crosslinking with collagen. The scaffolds were designated as HMW and LMW as a function of chitosan. Scaffolds without chitosan were prepared and designated as control scaffolds. All scaffolds were conditioned in a controlled environment chamber (ACS SU700V) at 25 ºC and 50% relative humidity for 48 h before testing.

2.3.5 3D Printing

Tetrahydrocurcumin (THC) containing porcine collagen scaffolds were prepared by 3D printing. Native collagen, THC (0, 2, 4, 6 wt % based on dry collagen) and 0.5 M acetic acid (1:5 collagen/acetic acid ratio) were mixed by using ultra-turrax T25 (IKA, Germany) until homogeneous pastes were achieved. The mixing process (2000 rpm, 2 min) was carried out in a cold bath to prevent the dough from heating up. Finally, the mixtures were stored in light-protected syringes at 4 ºC ± 1 until use. Scaffolds were designated as THC2, THC4, and THC6, as a function of THC content. Films without THC were prepared and designated as control sample.

In the 3D printing process, Cura (Ultimaker Cura 4.6.1 Software, Utrecht, The Netherlands) was used to design the scaffolds as cylindrical mesh (21 mm diameter; 0.9 mm height) with infill of 75% (340 μm pore diameter). Collagen scaffolds were fabricated at a printing temperature of 35 ºC using a syringe-based extrusion 3D DomoBIO printer (Domotek, Tolosa, Spain). The 3D printing speed was set at 3 mm/s through a G18 nozzle with an inner diameter of 0.84 mm. The temperature of the 3D-printer bed was fixed at 25 ºC with a layer height of 0.3 mm. No post-processing treatment was carried out. All scaffolds were conditioned in a controlled environment chamber (ACS SU700V) at 25 ºC and 50% relative humidity for 48 h before testing.

2.4 THERMAL CHARACTERIZATION

2.4.1 Thermo-gravimetric analysis (TGA)

The thermal stability of samples was measured by using the Mettler Toledo TGA/SDTA 851 thermo-balance. Dynamic scans from 25 to 750 °C were carried out at a constant rate of 10 °C/min under inert atmosphere (10 mL N_2/min) to avoid thermo-oxidative reactions.

2.4.2 Differential scanning calorimetry (DSC)

DSC measurements were performed by a Mettler Toledo DSC 822. Samples (3.0 ± 0.2 mg) were subjected to a heating ramp from 25 to 250 °C at a rate of 10 °C/min under inert atmosphere (10 mL N_2/min) to avoid oxidative reactions. In the case of aloe vera containing samples, -50 - 250 ºC was the temperature range used. In the case of aloe vera and ZnO NPs containing collagen samples, those were subjected to a two-heating ramp at the same conditions, firstly from 25 to 125 ºC and then from 25 to 250 ºC. Sealed aluminum pans were used to prevent mass loss during the experiments.

2.4.3 Dynamic mechanical analysis (DMA)

Thermo-mechanical measurements of ZnO NPs containing collagen films were performed using a DMA Explexor 100 N, Gabo Qualimeter (JM Toneu, Spain). Experiments were performed in a temperature range from −100 °C to 250 °C at a heating rate of 2 °C/min. The measurements were carried out under tension at a constant frequency of 1 Hz and the strain applied was fixed at 0.05%.

2.5 RHEOLOGICAL EVALUATION

The viscoelastic properties of THC, ILs and wool containing collagen mixtures were studied at 35 ºC by a Thermo Scientific Haake Rheostress1 Rheometer (IFI S.L., Vigo, Spain), equipped with serrated plate-plate geometry (diameter of 35 mm). The gap between plates was 1 mm. Firstly, strain sweep tests were carried out at a constant frequency of 1 Hz and between 0.01% and 100% strain to determine the linear viscoelastic range (LVR) and the critical strain of the LVR.

In collagen-THC mixtures, frequency sweep test at a strain within the LVR was carried out between 0.01 and 50 Hz to obtain loss tangent (tag δ), elastic (G') and viscous (G'') moduli. Finally, the shear flow test was carried out in the shear rate ($\dot{\gamma}$) range from 0.1-50 s^{-1} using the same probe and gap. Samples were left running for 5 min before the test started to stabilize temperature and allow residual stress to relax.

The obtained flow data were fitted to the Williamson model for shear-thinning materials:

$$\eta = \frac{\eta_0}{1 + (k \cdot \dot{\gamma})^{(1-n)}}$$

where η is the viscosity, η_0 is the limiting viscosity at low shear rate, k is the consistency coefficient and n is a shear-thinning index (Williamson, 1929).

Additionally, a master curve of flow rate was obtained in order to describe the flow behavior of the doughs. A time-concentration superposition was made; first, using a vertical shift, given by a normalization with the η_0 of each dough; then, a horizontal shift specified by a time-concentration factor, a_c (Álvarez-Castillo et al., 2021). Finally, the master curve was fitted to Williamson's model:

$$\eta = \frac{\eta_0}{1 + (k\, a_c \cdot \dot{\gamma})^{(1-n)}}$$

Moreover, the flow behavior of collagen doughs at 3D printing processing conditions can be assessed by the Weissenberg-Rabinowitsch equation:

$$\dot{\gamma}_w = \dot{\gamma}_{wN} \frac{(3n+1)}{4n}$$

where n is the flow index, $\dot{\gamma}_w$ is the shear rate at the wall, $\dot{\gamma}_{wN}$ = (8V/D) is the nominal shear rate, D is nozzle diameter, and V is the average inlet velocity of the fluid (Chhabra & Richardson, 1999).

Additionally, in ILs and wool containing collagen mixtures, temperature sweep was carried out from 35 ºC to 70 ºC to obtain elastic (G') and viscous (G") moduli, as well as the complex viscosity (η^*), with the frequency fixed at 1.0 Hz and the strain at 1%.

2.6 PHYSICOCHEMICAL CHARACTERIZATION

2.6.1 Fourier transform infrared (FTIR) spectroscopy

Fourier transform infrared (FTIR) spectra were recorded on a Nicolet 380 FTIR spectrometer equipped with horizontal attenuated total reflectance (ATR) crystal (ZnSe). A total of 32 scans were made at 4 cm^{-1} resolution. All spectra were smoothed using the Savitzky–Golay function. Second-derivative spectra of the amide region were used at peak position guides for the curve fitting procedure of CA sheets, and ZnO NPs and chitosan containing films, using OriginPro 2019b software.

2.6.2 Moisture content (MC) and mass loss (ML)

To determine MC, samples were weighed (w_0) and then freeze-dried. After that, samples were reweighed (w_1) and MC was calculated as:

$$MC\ (\%) = \frac{w_0 - w_1}{w_0} \times 100$$

Mass loss values were calculated using dried specimens. Samples were immersed into 200 mL of PBS for 5 days and then, samples were reweighed (w_2). Mass loss for three specimens of each sample was calculated as:

$$ML(\%) = \frac{w_1 - w_2}{w_1} \times 100$$

2.6.3 Water uptake (WU) measurements

In order to study the water uptake of films or scaffolds, first, three rectangular pieces (1 cm x 2 cm) of films or scaffolds were weighed (w_i) and submerged into PBS. Then, samples were reweighed at specific times (w_t), until getting constant values. The water uptake (WU) was calculated by the following equation:

$$WU\ (\%) = \frac{w_t - w_i}{w_t} \times 100$$

2.7 MORPHOLOGICAL CHARACTERIZATION

2.7.1 Scanning electron microscopy (SEM)

The morphology of the samples was visualized using an S-4800 scanning electron microscope. Samples were mounted on a metal stub with double-side adhesive tape and coated under vacuum with gold, using a JEOL fine-coat ion sputter JFC-1100 (Izasa, Spain) in an argon atmosphere prior to observation. All samples were examined using an accelerating voltage of 10 kV.

2.7.2 X-ray diffraction (XRD)

XRD analysis of the samples was performed with a diffraction unit PANalytical Xpert PRO, operating at 40 kV and 40 mA. The radiation was generated from a Cu-K_α (λ= 1.5418 Å) source. The diffraction data were collected from 2θ values from 2 to 50º, where θ is the angle of incidence of the X-ray beam on the sample.

2.7.3 X-ray photoelectron spectroscopy (XPS)

XPS of chitosan-collagen scaffolds was performed in a SPECS spectrometer using a monochromatic radiation equipped with Al Kα (1486.6 eV). The binding energy was calibrated by Ag 3d5/2 peak at 368.28 eV. All spectra were recorded at 90º take-off angle. Survey spectra were recorded with 1.0 eV step and 40 eV analyzer pass energy and the high-resolution regions with 0.1 eV step and 20 eV pass energy. All core level spectra were referenced to the C 1s neutral carbon peak at 284.6 eV. Spectra were analyzed using the CasaXPS 2.3.19 PR1.0 software, and peak areas were quantified with a Gaussian-Lorentzian fitting procedure.

2.8 BARRIER PROPERTIES

2.8.1 Water contact angle (WCA)

Water contact angle measurements of chitosan and aloe vera containing films were performed using a DataPhysics OCA 20 contact angle system. A 3 µL droplet of distilled water was placed on film surface to estimate its hydrophobic or hydrophilic character. The image of the drop was captured using SCA20 software.

2.8.2 Water vapor permeability (WVP) and water vapor transmission rate (WVTR)

WVP of ZnO containing collagen samples and WVTR of chitosan containing collagen samples was determined in a controlled humidity environment chamber

PERME™ W3/0120 (Labthink Instruments Co. Ltd., China), according to ASTM E96-00 (ASTM, 2000). Circles of 7.40 cm diameter, with a test area of 33 cm^2, were cut. The setup was subjected to a temperature of 38 °C and a relative humidity of 90%. Water vapor transmission rate (WVTR) was calculated by the following expression:

$$\text{WVTR}\left(\frac{g}{s\ cm^2}\right) = \frac{G}{t \times A}$$

where G is the change in weight (g), t is time (s), and A is the test area (cm^2). WVP was calculated as:

$$\text{WVP}\left(\frac{g}{cm\ s\ Pa}\right) = \frac{\text{WVTR} \times L}{\Delta P}$$

where L is the thickness of the test specimen (cm) and ΔP is the partial pressure difference of the water vapor across the film (Pa). WVP was calculated and reported for three specimens of each sample.

2.8.3 Ultraviolet-visible (UV-vis) spectroscopy

The light-barrier properties of films were determined by measuring their light absorption at wavelengths ranging from 200 nm to 800 nm, using a UV-Jasco spectrophotometer (Model V-630).

2.9 MECHANICAL PROPERTIES

2.9.1 Tensile test

Tensile strength (TS) and elongation at break (EB) of films were measured according to ASTM D 638-03 standard (ASTM, 2003) using a MTS Insight 10 electromechanical testing system (MTS, Spain) at room temperature. Five specimens for each sample were cut into bone-shaped samples of 4.75 mm × 22.25 mm and tensile tests were performed at a constant deformation of 5 mm/min for citric acid containing collagen sheets and 1 mm/min for aloe vera, ZnO NPs and chitosan containing films.

Tensile strength (TS) and elongation at break (EB) of ILs and wool containing collagen films were measured at room temperature, using a Linkam Scientific Instruments TST 360. 10 specimens for each sample were cut into rectangular-shaped samples of 30 mm × 10 mm and tensile tests were performed at a constant deformation of 50 μm s^{-1} with a load cell of 20 N.

2.9.2 Compression test

Compression tests of chitosan-collagen scaffolds were performed using a TA.XT plusC Texture Analyzer (Stable Micro Systems) equipped with a 50 kg load cell. The analysis was carried out using a 50 mm Dia Aluminium Radiused AACC probe. The crosshead speed was set at 1 mm/s and the activation force was 0,05 N. All samples were tested at room temperature and load was applied until the specimen was compressed to 80% of its original height. The software used for the analysis was Exponent 7,0,7,0. For the tests with hydrated scaffolds, samples were immersed into PBS until water uptake equilibrium (120 min). The compression test of hydrated scaffolds was carried out 4-fold since scaffolds recovered their initial size at the end of each compression.

2.10 ELECTRICAL AND DIELECTRICAL PROPERTIES

Electrical properties of ZnO containing collagen films were analyzed by a Keithley 4200-SCS equipment for semiconductors analysis in a Faraday cage at room temperature. Two point measurements were carried out with a homebuilt dispositive, performing linear scans from −20 to 20 V in order to obtain intensity vs voltage curves. The films were placed in contact with two copper sheets, adhered in turn to polycarbonate plates; two copper wires, which came up from the copper plates, were put in contact with the electrodes of the equipment to close the electric circuit. The distance between the two electrodes was 2 mm. The dimensions of the samples were 1.0 cm^2 section and 0.25 mm height.

The DC volume electrical conductivity (σ, S/cm) of ILs and wool containing films was obtained after measuring the characteristic I-V curves at room temperature with an applied voltage between ± 10 V using a Keithley 487 picoammeter/voltage source (Barcelona, Spain). Previous to the measurements, the samples were coated on both sides with 5 mm circular diameter electrodes and σ was calculated as:

$$\sigma = \frac{d}{R.A}$$

where *d* is thickness, *R* is the resistance of the sample, and *A* is the electrode area.

Dielectric measurements of ILs and wool containing films were also performed using a Quadtech 1920 LCR precision meter. The capacity and tan δ were obtained at room temperature in the frequency range of 1 kHz to 1 MHz with an applied voltage of 0.5 V. Then, the real part (ε') of the dielectric function was obtained:

$$\varepsilon' = \frac{C.d}{\varepsilon_0.A}$$

$$tan\,\delta = \frac{\varepsilon''}{\varepsilon'}$$

where C is the capacitance (F), ε_o is the permittivity of free space (8.85×10^{-12} F·m^{-1}), A is the electrode area (m^2) and d is the thickness of the sample (m).

The AC electrical conductivity was calculated as:

$$\sigma'(\omega) = \varepsilon_0 \omega \varepsilon''(\omega)$$

where ε_0 is the permittivity of free space, $\omega = 2\pi f$ is the angular frequency and $\varepsilon''(\omega) = \varepsilon' tan\,\delta$ is the frequency dependent imaginary part of the dielectric permittivity.

2.11 BIOACTIVE RELEASE

UV-vis spectroscopy (V-630 UV-Jasco spectrophotometer) was used to determine the THC release of collagen scaffolds in PBS solution (pH = 7.4). Firstly, the

wavelength of maximum absorbance for THC in PBS was measured (λ_{max} 280 nm) and then, standard solutions of THC were prepared over a concentration range (3.906-1000 ppm) to establish a calibration curve (y = 0.0004x + 0.0683; R^2= 0.9635).

THC release was determined by immersing the scaffolds in PBS solution (10 mL) at room temperature for 2 d. Aliquots (3 mL) were withdrawn at specific times (4, 6, 8, 24, 30 and 48 h), replaced with fresh buffer and analyzed by UV-Vis spectroscopy at 280 nm. All tests were carried out in triplicate for the evaluation of each composition.

The THC release data were kinetically evaluated by Korsmeyer-Peppas models:

$$\frac{M_t}{M_\infty} = kt^n$$

where M_t/M_∞ is the fraction of drug released at time t and *k* is Korsmeyer-Peppas related to the properties of the delivery system, such as its structural and geometric properties, *n* is the release exponent that shows the release mechanism: from $n < 0.45$, a pseudo-Fickian diffusion mechanism; $n = 0.45$ a Fickian mechanism; $0.45 < n < 0.89$, an anomalous diffusion mechanism; and $n = 0.89$, a non-Fickian diffusion mechanism (Costa & Lobo, 2001).

2.12 IN VITRO MUCOADHESION STUDY

Mucoadhesive properties of collagen-THC scaffolds were determined using TA.XT.Plus C Texture Analyzer (Aname Instrumentación científica, Spain) equipped with a 5 kg load cell and a 3.5 mm diameter cylinder probe. Type II mucin from porcine stomach (Sigma-Aldrich, Madrid, Spain) was used as biological substrate. Before testing, a filter paper was hydrated by immersion into a PBS solution of type II mucin (1.0 wt %) for 5 min at 37 ºC.

The excess surface liquid was withdrawn and then, the substrate was horizontally kept on the cylinder probe. Samples of each formulation were packed into cylindrical

vessels (15 mm diameter) and placed on an upper cylinder probe lowered at a constant speed of 1 mm/s until the mucoadhesive surface was reached. After keeping the contact time of 30 s under a force of 0.2 N, the probe with the attached sample was removed at a constant rate (1 mm/s). Texture Exponent 32 software was used to determine the maximum detachment force (F_{max}), and the work of adhesion (W_{adh}). All measurements were performed with at least five replicates.

2.13 DEGRADATION STUDIES

Degradation studies of chitosan-collagen films and scaffolds were conducted in order to determine the weight loss due to the hydrolytic and enzymatic degradation. To this end, 8 mm diameter samples were cut and weight (w_0). Scaffolds were then washed with 70% ethanol for 30 min and irradiated with UV for 30 min to be sterilized. Following this, samples were exposed to the degradation agents and incubated at 37 ºC. At determined time points, films were freeze-dried and reweighed (w_t). In the case of the scaffold, a single measurement was taken after 4 days. The degradation degree (DD) was calculated with the following equation:

$$DD\ (\%) = \frac{w_0 - w_t}{w_0} x\ 100$$

The hydrolytic degradation (HDD) was performed submerging the samples in PBS. To assess the enzymatic degradation (EDD), a collagenase P (Sigma-Aldrich, Spain) solution (0.5 mg/mL) in culture medium was used for films and collagenase D (Roche, Basel, Switzerland) solution (1 mg/mL) in culture medium for scaffolds. Every test was performed in three-fold.

Degradation studies of aloe vera containing collagen films were also performed in order to determine the weight loss due to the hydrolytic, cell-mediated and “simulated body fluid” degradation. Following this, samples (8 mm diameter) were exposed to the degradation agents and incubated at 37 ºC. At different time-points, the samples were

removed, freeze-dried and reweighed. The hydrolytic degradation (HDD) was performed submerging the samples in PBS. For cell-degradation (CDD) 30,000 cells of HS27 fibroblasts scaffold were seeded per scaffold. To assess the “simulated body fluid” degradation (BFDD) of collagen, body fluid simulant (BFS) was added into the well. Every test was performed in triplicate. Every test was performed in five-fold.

2.14 CYTOTOXICITY ASSAY

The cytotoxicity analysis of chitosan-collagen films was performed by direct contact of the films with L-929 fibroblasts (ATCC® 30-2003™), in accordance with the ISO 10993-5:2009 guidelines for biological evaluation of medical devices (ISO 10993-5, 2009). Briefly, 35,000 cells/well were seeded in a 24-well plate with 500 µL of EMEM complete medium and incubated for 24 h at 37 °C. Then, the culture medium was aspirated and 600 µL of fresh medium were added, placing films of 8 mm diameter in contact with the seeded fibroblasts at the bottom of the well. After 48 h of incubation, the films were removed and the medium was replaced by 370 µL/well of CCK-8 (Sigma-Aldrich, Spain) solution in medium (1:11). After 4 h of incubation, the absorbance was read with a plate reader (Infinite® 200 PRO series, Tecan Trading AG, Männedorf, Switzerland) at 450 nm using 650 nm as the reference wavelength. Cells without film exposure were used as 100 % viability group (blank).

2.15 BIOCOMPATIBILITY ASSAY

The biocompatibility of aloe vera containing collagen films was determined. 10,000 cells/cm^2 were seeded into a 24 well plate in 200 µL of complete medium. After 24 h of culture at 37 ºC and 5% CO_2 atmosphere, samples were placed in contact with the cells. In accordance with the ISO 10993-5:2009 standard, a distinction was made between indirect and direct exposure to the material, by placing the samples on transwells or immediately on top of the cells, respectively. The scaffolds were previously sterilized by submerging in 70% ethanol for 10 min, UV for 30 min, and washed by

dialysis in PBS for 72 h. Additionally, some wells were left without biomaterial to be included subsequently as positive and negative controls. All wells were supplemented with 300 µL of culture medium. The following assays were performed in order to evaluate the biocompatibility of HS27 cells under the exposure of the film based on porcine collagen and 20% aloe vera.

On the one hand, cell mortality was assessed according to plasma membrane integrity. The Cell-Tox Green Cytotoxicity Assay (Promega #G8742) was used for this purpose. To this end, the protocol recommended by the manufacturer was followed. Briefly, the dye was added to the different wells by diluting it with the medium in a ratio of 1:1000 and incubated for 15 min protected from light, after which the fluorescence was measured.

On the other hand, metabolic activity was measured based on the reductive capacity of the cells. In this case, the Cell Counting Kit-8 colorimetric assay (Merck #96992) was used. Following the manufacturer's recommendations, and after several washes with PBS to remove the products from the previous assay, the compound was added and the absorbance was measured after 2 h of incubation.

In addition to the study conditions, positive and negative controls were included. For the first ones (CTR+), cells seeded in the same conditions but without biomaterial were used. For the negative controls (CTR-), cells treated with the lysis buffer provided by Promega's kit were used to cause cell death. Assays were conducted at exposure days 1, 2, 4, and 7, with each condition being analyzed in triplicate. Once the results were obtained, they were relativized to the controls. In the case of mortality, the CTR- was considered as 100% of mortality, and 0% the CTR+; while in the assay of metabolic activity they were considered inversely.

2.16 CELL CULTURE

The cell culture of aloe vera containing films was analyzed. Following the

recommendations of the ISO 10993-5:2009 guidelines for biological evaluation of medical devices, HS27 (ECACC) cells were cultured on complete medium that was composed of Dulbecco's modified Eagle's medium (Sigma) supplemented with 10% (v/v) inactive FBS (Sigma), 1% (v/v) penicillin-streptomycin (Lonza) and 1% (v/v) L-glutamine (Gibco) at 37 ºC in a humidified incubator with a 5% CO_2 atmosphere. All the biological assays were carried out in aseptic conditions and the cell passages were performed weekly depending on the cell confluence. At the fifth passage HS27 cells were collected by 0.05% trypsin (Sigma, Darmstadt, Germany) and centrifuged at 1500 rpm for 5 min at room temperature. The obtained pellet was resuspended in the previously described medium to obtain a homogeneous cell suspension, after which the experimental plates of the degradation and biocompatibility studies were carried out.

2.17 ENVIRONMENTAL ASSESSMENT

The environmental analysis of chitosan-collagen scaffolds was carried out according to ISO 14040 guidelines and recommendations (ISO 14040, 2006). The software used was SimaPro 9.0.0.30 (PRé Consultants, The Netherlands). The inventory analysis was carried out considering the materials used in the laboratory and the energy consumption regarding the pretreatments and the preparation steps, as well as the transportation of skins (Bergara-Donostia). Data were obtained from Ecoinvent database. The functional unit considered in this study was 5 g of collagen. Based on the inventory data, environmental impacts were evaluated according to the Hierarchist version of ReCiPe 2016, midpoint. The impact categories analyzed were global warming, stratospheric ozone depletion, ionizing radiation, ozone formation (human health), fine particulate matter formation, ozone formation (terrestrial ecosystems), terrestrial acidification, freshwater eutrophication, marine eutrophication, terrestrial ecotoxicity, freshwater ecotoxicity, marine ecotoxicity, human carcinogenic toxicity, human non-carcinogenic toxicity, land use, mineral resource scarcity, fossil resource scarcity, and water consumption.

2.18 STATISTICAL ANALYSIS

In order to determine significant differences between samples, analysis of variance (ANOVA) was done with SPSS software (SPSS Statistic 25). Tukey's test with a statistically significance at the $P < 0.05$ level was considered for multiple comparisons among different systems.

Chapter 3

CITRIC ACID CONTAINING COLLAGEN SHEETS

Effect of citric acid on compression-molded collagen sheets

3.1 SUMMARY

In this work, bovine collagen was treated with different contents of citric acid and the functional properties of the sheets prepared by compression molding were investigated. Fourier transform infrared (FTIR) spectroscopy and mechanical properties gave indirect evidence that citric acid-incorporated collagen sheets preserved the triple-helix structure of the native collagen. Although citric acid did not react with collagen through covalent linkages, collagen structure was stabilized by hydrogen bonding between citric acid and collagen, as shown by FTIR results. These interactions enhanced mechanical properties, both tensile strength and elongation at break. Moreover, water uptake capacity increased with the addition of citric acid as a result of the formation of some microvoids in the internal structure of collagen, as observed by SEM analysis.

3.2 RESULTS AND DISCUSSION

3.2.1 Thermal properties

In order to study the thermal behavior of collagen with different contents of citric acid, TGA was performed. TGA and DTG curves are displayed in **Figure 3.1**. All blends showed similar behavior with three main stages. For temperatures below 150 ºC, the weight loss was ascribed to the loss of absorbed moisture, which was around 5 %. The second stage, at 240-250 ºC, was attributed to the glycerol evaporation (Leceta et al., 2015) and the citric acid decomposition (Guerrero et al., 2019). The temperature of the peak maximum was higher than the boiling temperature of pure glycerol (182 °C) and the decomposition temperature of citric acid (175 ºC). Therefore, this increase suggested the existence of interactions, such as hydrogen bonding, among the components of the blends. The third stage above 250 ºC is associated to the degradation of the collagen, in accordance with other authors who observed the bovine collagen decomposition in the range of 250-400 ºC (Labastida-Pólito et al., 2009). More specifically, a value of 283 ºC was observed for pure bovine collagen, which increased up to 330 ºC for collagen

composites due to the interactions between collagen and inorganic particles (Wei et al., 2015). A similar finding was observed in this work, since thermal degradation happened at temperatures above 315 ºC, indicating the interactions of collagen with the additives incorporated in the formulation.

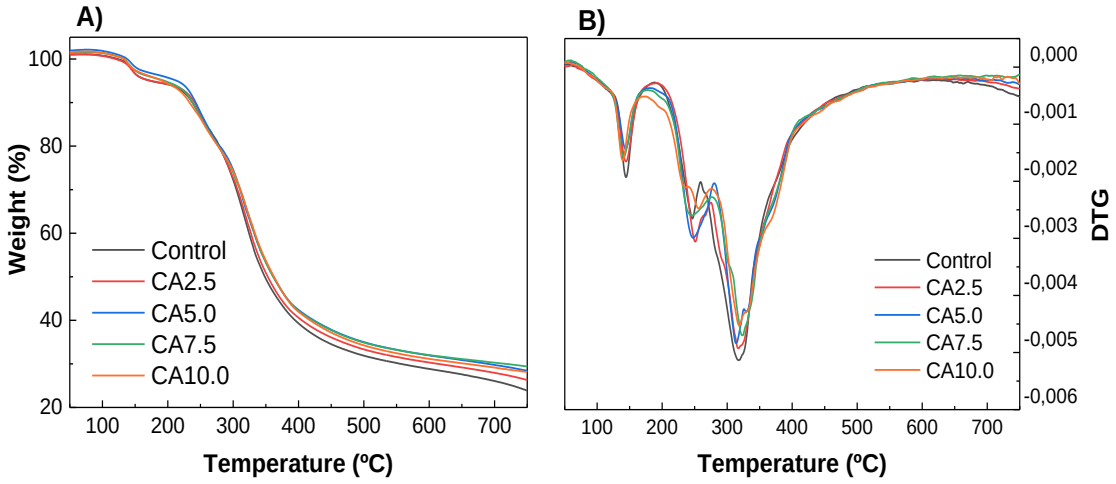

Figure 3.1. A) TGA and B) DTG thermograms of collagen sheets with different citric acid (CA) contents.

Concerning DSC measurements, all samples exhibited two endothermic peaks, as shown in **Figure 3.2**. The peak in the temperature range of 65-70 ºC was related to the free and bound water release (Miles & Gelashvili, 1999). This temperature range, associated to the interfibrillar fraction of water, is in accordance with the values shown for native fibers; furthermore, the constant value of the temperature associated to this peak indicates that fibers remained unchanged (Miles et al., 2005). The denaturation temperature was associated to the endothermic peak above 125 ºC (Chakrapani et al., 2012). It is worth noting that the height of this peak decreased and its width increased when citric acid content increased, which might be related to the interactions among collagen and citric acid.

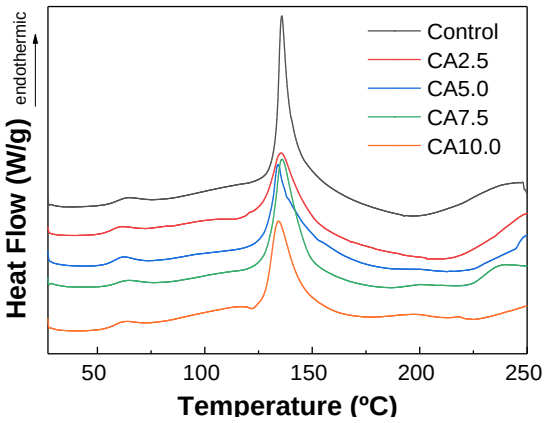

Figure 3.2. DSC thermograms of collagen sheets with different citric acid (CA) contents.

3.2.2 Physicochemical properties

In order to assess the interactions among the components of the blends, FTIR analysis was carried out and FTIR spectra are exhibited in **Figure 3.3**. All the spectra showed the characteristic absorption bands assigned to the peptide bonds in collagen. Specifically, the absorptions related to the amide A, amide I, amide II and amide III are commonly observed in the wavenumbers of 3400-3440, 1600-1700, 1540, and 1239 cm^{-1}, respectively (Barth & Zscherp, 2002; Riaz et al., 2018; Yu et al., 2014). The amide A band, corresponding to the N-H stretching vibration, appeared at 3287 cm^{-1} which means shifting to lower wavenumbers. When N-H groups in collagen are involved in hydrogen-bonding, the band position is shifted to a lower frequency, leading to stability in the collagen triple-helical structure (Duan et al., 2009; Li et al., 2004; Liao et al., 2018).Additionally, when citric acid was incorporated, the band shifted to 3277 cm^{-1} (**Figure 3.3A**), corroborating the hydrogen bonding of collagen with glycerol and citric acid.

Regarding the amide I band, which shows a strong absorption in the range of 1600-1700 cm^{-1} (**Figure 3.3B**), this is associated to the C=O stretching vibration along the protein backbone; this band absorption was measured at 1630 cm^{-1}, regardless of citric acid content (**Table 3.1**). Both the position of this band and its intensity did not vary

after citric acid incorporation and, thus, these results revealed that collagen maintained the high structural order related to the triple-helical structure in native collagen (de Campos Vidal & Mello, 2011) since the amide I band intensity is dependent on the protein chain conformation (Bryan et al., 2007). For a quantitative analysis, the wavenumber difference between amide I (ν_I) and amide II (ν_{II}) bands was calculated and data are summarized in **Table 3.1**. As can be seen, the values were lower than 100 cm^{-1}, indicating that the triple helix structure was maintained (Sizeland et al., 2018).

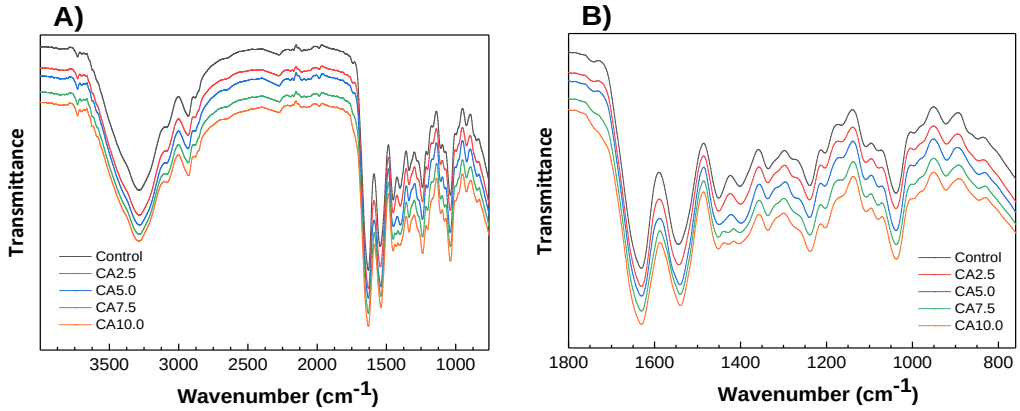

Figure 3.3. FTIR spectra of collagen sheets with different citric acid (CA) contents: A) from 4000 to 800 cm^{-1} and B) from 1800 to 800 cm^{-1}.

These slight changes in the amide area indicated physical crosslinking since chemical crosslinking would have led to noticeable changes in this area, as reported in previous works (Uranga et al., 2016; Wu et al., 2017). Additionally, the relative intensity between the band at 1450 cm^{-1}, attributed to CH_2 bending vibrations (Chakrapani et al., 2012; Plepis, Goissis, & Das-Gupta, 1996;), and the band at 1400 cm^{-1}, corresponding to C=O stretching vibrations changed (Wu et al., 2017). This may confirm that hydrogen bonds were involved in the structure of collagen. In particular, the difference in the relative intensity between those two bands became smaller when 2.5 wt % citric acid was added and the relative intensity became similar for the sample with 5.0 wt %. Furthermore, a third band appeared between those two bands for the samples with 7.5 and 10.0 wt % citric acid, indicating that citric acid formed physical interactions with collagen.

Table 3.1. Wavenumber of amide I (ν_I) and amide II (ν_{II}) bands, as well as the wavenumber difference between them (ν_I - ν_{II}).

Samples	ν_I	ν_{II}	ν_I - ν_{II}
Control	1630.42	1544.26	86.16
CA2.5	1630.27	1543.12	87.15
CA5.0	1630.08	1540.89	89.19
CA7.5	1630.15	1540.17	89.98
CA10.0	1630.15	1539.92	90.23

Since interactions within proteins lead to conformational changes, the secondary structure of collagen was assessed by analyzing the amide I profile. Amide I contains three major components: a band at 1650 cm^{-1}, associated to the α-helix/random coil conformation; a band corresponding to the β-sheet conformation, which appeared at 1615-1630 cm^{-1}; and a band corresponding to the β-turn at 1660-1670 cm^{-1} (Etxabide et al., 2016; Guerrero, Kerry & de la Caba, 2014; Wu et al., 2017). As shown in **Table 3.2**, α- helix/β-sheet ratio increased with the incorporation of citric acid into the formulation. Therefore, the addition of citric acid increased the content of α- helix conformation, indicating that the protein structure changed as a result of citric acid-collagen physical crosslinking, as previously shown by the slight changes in the amide area.

Table 3.2. Area (%) of the curve fitting of amide I as a function of citric acid content and α-helix/β-sheet ratio.

Samples	β-Sheet (%)	α-helix/random coil (%)	β-Turn (%)	α-helix/β-sheet ratio
Control	35.6	49.3	15.1	0.97
CA2.5	36.9	52.8	10.3	1.12
CA5.0	37.6	53.1	9.3	1.13
CA7.5	38.0	54.9	7.1	1.22
CA10.0	38.1	55.0	6.9	1.22

Additionally, water uptake tests were carried out and results are shown in **Figure 3.4**. It is worth noting that all samples maintained their structural integrity after immersion

for 600 min. Water uptake increased rapidly above 100% in the first 60 min; after that, water uptake rate slowed down up to 500 min and then, water uptake values remained constant, with values lower than 300%. Water uptake reached the equilibrium at the same time irrespective of the citric acid content, but the water uptake values for the samples with citric acid contents from 5.0 to 10.0 wt % were slightly higher than those for the sheets without CA and with 2.5 wt % CA.

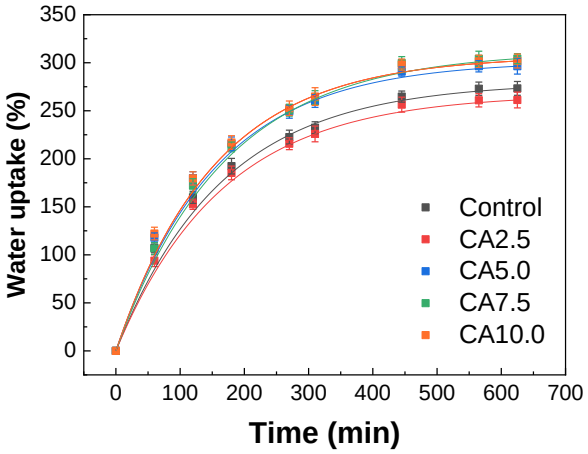

Figure 3.4. Water uptake curves of collagen sheets prepared with different citric acid (CA) contents.

This behavior is in accordance with FTIR results that suggested the existence of physical interactions between citric acid and collagen since chemical crosslinking would have caused the decrease of the water uptake values. As the water holding capacity depends on the material structure, the morphology of the sheets as a function of citric acid content was assessed and related to the physicochemical properties observed for the collagen sheets.

3.2.3 Morphological and mechanical properties

In order to determine the sheets microstructure and relate it to the properties measured, XRD and SEM analyses were carried out. Regarding XRD analysis, a small peak around 7º in collagen is indicative of the intermolecular lateral packing distance between collagen chains, so the disappearance of this peak, as is the case in **Figure**

3.5, can be considered as an increase of the inter-chain space, as reported by Valencia et al. (2019). This fact would indicate that a more loosen fibril structure was obtained as a consequence of the treatment carried out. Additionally, the broad band around 20º in **Figure 3.5**, associated to the diffuse scattering of collagen fibers (Zou et al., 2017), indicated the amorphous structure of collagen. Collagen sheets without citric acid and with 2.5 wt % citric acid showed similar XRD patterns, in accordance with the similar physicochemical properties observed for these samples by FTIR and water uptake analyses. Therefore, 2.5 wt % citric acid did not seem to be enough amount to change the structure of collagen. However, when higher contents of citric acid were added, the structural order of the sheets increased.

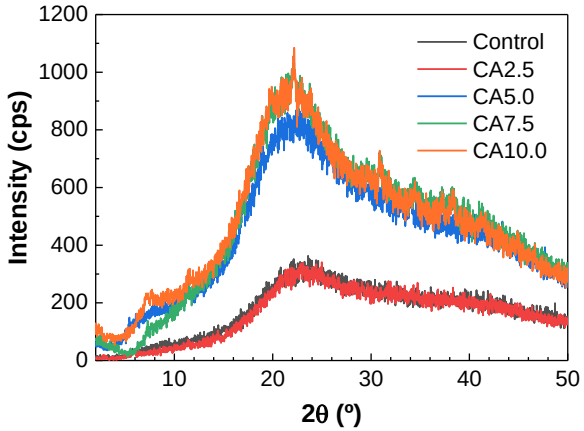

Figure 3.5. XRD patterns of collagen sheets prepared with different CA contents.

In order to assess the effect of citric acid on collagen structure, SEM analysis was carried out and the images of cross-sections are shown in **Figure 3.6**. SEM micrographs showed that the collagen sheets without citric acid (**Figure 3.6A**) and with 2.5 wt % citric acid (**Figure 3.6B**) had a similar structure, in accordance with XRD and physicochemical analyses; both of them showed a rough structure. When citric acid increased from 5.0 (**Figure 3.6C**) to 10.0 wt % (**Figure 3.6D**), some holes were observed, and the number of holes increased with citric acid content, which allowed a higher water holding capacity in accordance with the higher water uptake values observed for the sheets with citric acid content from 5.0 to 10.0 wt %.

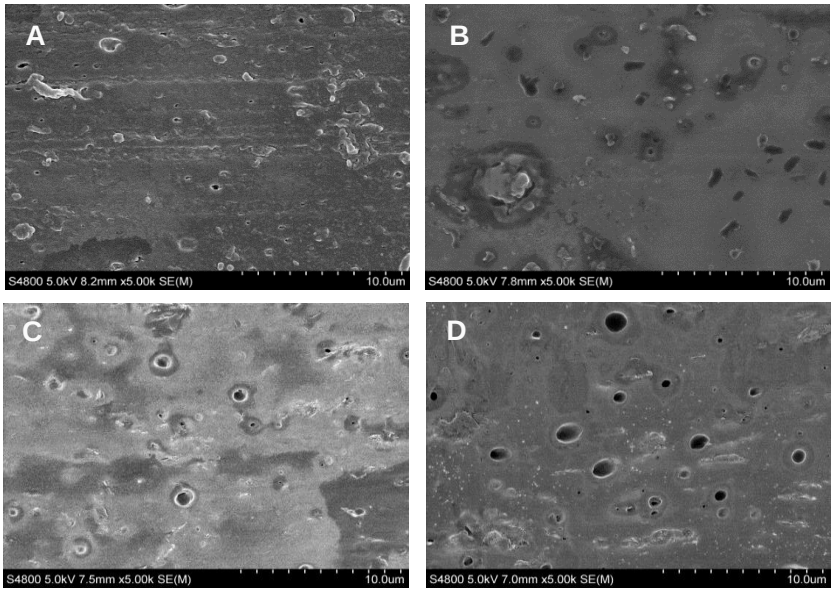

Figure 3.6. SEM images of the cross-sections for A) control, B) CA2.5, C) CA5.0, and D) CA10.0 samples.

The structure of the sheets can also be related to the mechanical properties of the citric acid-incorporated collagen sheets. It is worth noting that all sheets were easy to handle and mechanically resistant, as shown in **Figure 3.7A**. This behavior is associated to the fibril structure of collagen (Sherman, Yang & Meyers, 2015). As the elongation increased, the fibers of collagen were orientated, increasing tensile resistance up to the point of break, as shown in **Figure 3.7B**.

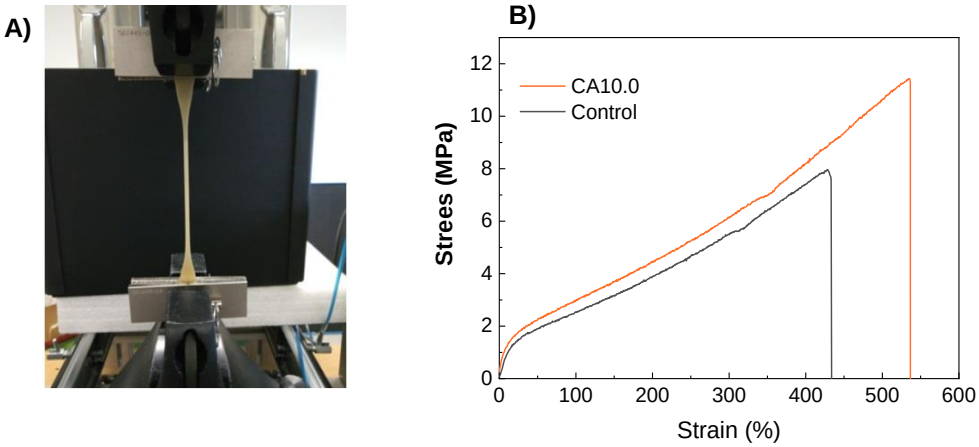

Figure 3.7. A) Tensile test and B) stress-strain curves of collagen sheets without citric acid (control) and with 10 wt % citric acid (CA10.0).

The values of tensile strength and elongation at break are shown in **Table 3.3**. Tensile strength significantly ($P < 0.05$) increased with the addition of citric acid, regardless of citric acid content ($P > 0.05$), due to the interactions formed between collagen and citric acid, as shown by FTIR analysis. Additionally, elongation at break significantly ($P < 0.05$) increased as the citric acid content increased. As the glycerol content was the same for all the formulations, the higher elongation values for the films with citric acid were attributed to the role of free citric acid as plasticizer. This dual role of citric acid as crosslinking agent and plasticizer has been previously reported in the literature (Shi et al., 2008; Yoon, Chough & Park, 2007). An enhanced chain mobility and, thus, film flexibility could also be provoked by water molecules, due to the higher water holding capacity of the sheets with citric acid, which has one hydroxyl and three carboxyl groups.

Table 3.3. Tensile strength (TS) and elongation at break (EB) of collagen sheets with different citric acid (CA) contents.

Samples	TS (MPa)	EB (%)
Control	8.0 ± 0.7^{a}	414 ± 17^{a}
CA2.5	11.7 ± 0.9^{b}	$434 \pm 18^{a,b}$
CA5.0	12.3 ± 0.7^{b}	459 ± 19^{b}
CA7.5	12.4 ± 1.1^{b}	510 ± 25^{c}
CA10.0	10.7 ± 1.0^{b}	568 ± 7^{d}

$^{a\text{-}d}$Two means followed by the same letter in the same column are not significantly ($P > 0.05$) different through the Turkey's multiple range test. N = 5 was the minimum number of replications.

Since collagen treatments, processing methods and conditions, as well as the resulting sheet thickness are very different among the works reported in the literature, comparison of tensile strength and elongation at break values of collagen sheets is not easy. A recent work has been published regarding collagen sheets (0.057-0.127 mm thickness) obtained from bovine dermal fibroblasts with TS values from 8.7 to 28.4 MPa and EB values from 0.1 to 13.6% (Jakab et al., 2019). Also recently, nanosilver loaded

mineralized collagen films were mechanically analyzed and average TS values of 15.0 MPa and EB of 8.9 % were obtained (Socrates et al., 2019). It is worth noting that the minimum values of TS and EB required for 1 mm-thick leather are 10 MPa and 30-80%, respectively (Jakab et al., 2019), values reached in this work.

3.3 CONCLUSIONS

Collagen sheets were prepared by compression molding after a pretreatment with citric acid to facilitate processing. Thermal analysis of the resulting sheets suggested the interaction between collagen and citric acid, which was confirmed by FTIR results. Although chemical crosslinking did not occur due to the absence of relevant changes in the amide region, physical crosslinking was evidenced by changes in the relative intensities of FTIR bands. However, the wavenumber difference between amide I was lower than 100 cm^{-1}, indicating that the triple helix structure was maintained. Further analysis of amide region showed the predominance of the helical structure of collagen after citric acid incorporation. This resulted in the improvement of the mechanical properties of collagen sheets, indicating that the incorporation of citric acid and the compression molding process did not affect the fibril structure of collagen. Furthermore, the formation of the voids observed in the collagen microstructure increased the water uptake capacity of the sheets, which can be taken in advantage for the use of these sheets as delivery systems for active packaging or pharmaceutics.

Chapter 4

ALOE VERA CONTAINING COLLAGEN FILMS

Compression-molded aloe vera/collagen films suitable for biomedical applications

4.1 SUMMARY

Collagen was obtained from porcine skin by mechanical pretreatments with the aim of preserving the triple helix structure of native collagen, which was indirectly corroborated by differential scanning calorimetry (DSC) and Fourier transform infrared spectroscopy (FTIR) results. Moreover, aloe vera (AV), with inherent biological properties, was incorporated into collagen film formulations, and films were prepared by compression and characterized to assess their suitability for biomedical applications. SEM images showed that the fibrillar structure of collagen changed to a rougher structure with the addition of AV, in accordance with the decrease of the lateral packaging of collagen chains observed by XRD analysis. These results suggested interactions between collagen and AV, as observed by FTIR. Considering that AV content higher than 20 wt % did not promote further interactions, this formulation was employed for biological assays and the suitability of AV/collagen films developed for biomedical applications was confirmed.

4.2 RESULTS AND DISCUSSION

4.2.1 Physicochemical properties

In order to assess the interactions among the components of the film forming formulation, FTIR analysis was carried out and the resultant spectra of collagen films are shown in **Figure 4.1**. The broad band at around 3000-3600 cm^{-1} (**Figure 4.1A**) can be attributed to the stretching of hydroxyl groups of uronic acid, mannose, and galacturonic acid, and to phenolic groups in antraquinones present in AV, as well as to amide A (N-H stretching) in collagen (Bajer, Janczak & Bajer, 2020; Kapashi et al., 2019). Additionally, all the spectra showed the characteristic absorption bands assigned to the peptide bonds in collagen (**Figure 4.1B**): 1630 cm^{-1} for amide I (C=O stretching), 1542 cm^{-1} for amide II (N-H bending), and 1240 cm^{-1} for amide III (C-N stretching). The band around 1630 cm^{-1} can also be assigned to the stretching vibrations of carbonyl groups in aloe vera

(Bajer, Janczak, & Bajer, 2020) and the shoulder at 1245 cm^{-1} could be due to the C-O-C stretches of acetyl groups, which may indicate the presence of storage bioactive polysaccharides, such as acemannan and glucamannans (Kiran & Rao, 2016). The spectral region between 1200 cm^{-1} and 900 cm^{-1} is attributed to the stretching vibrations of C-O bonds in collagen, those related to hydroxyl groups in glycerol, as well as those associated to polysaccharides and sugars in aloe vera (Andonegi, de la Caba & Guerrero, 2020). The changes in the relative intensity between bands in this area suggest that the interactions among the components of the film forming formulation are physical bonds, mainly among carboxyl, amino, and hydroxyl groups present in collagen, glycerol, and aloe vera. In particular, the band at 992 cm^{-1} corresponds to the stretching of C-O bonds of hemicellulose, pectin, and lignin present in AV, and the band at 1037 cm^{-1} is associated to C-O vibrations in collagen. With the addition of AV, the band corresponding to C-O bonds shifted to 1034 cm^{-1} for 10AV, to 1026 cm^{-1} for 20AV, and to 1025 cm^{-1} for 30AV. Therefore, it can be said that AV contents higher than 20 wt % did not cause further shifting and did not promote further interactions with collagen and glycerol.

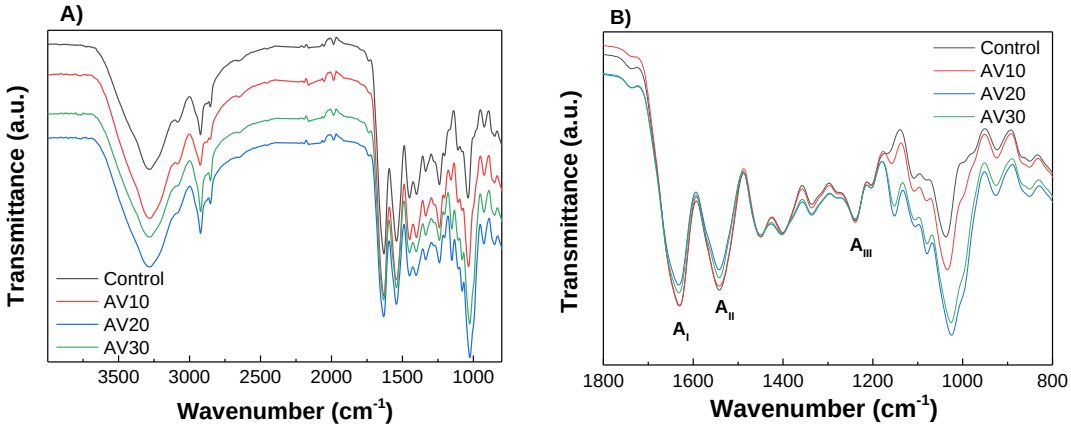

Figure 4.1. FTIR spectra of aloe vera (AV)/collagen films: A) from 4000 to 800 cm^{-1} and B) from 1800 to 800 cm^{-1}.

The moisture content (MC) and the mass loss (ML) of the films were measured and values are shown in **Table 4.1**. As can be seen, MC values decreased from 12.2% in control films to 5.8% in AV30 due to the interactions among polar groups, reducing the

affinity of the films for moisture. In contrast, ML values increased for AV-incorporated films. In particular, the ML value around 20% in control films is related to glycerol and the increase of this value for the films with AV can be related to the dissolution of AV (Ahlawat & Khatkar, 2011).

Table 4.1. Moisture content (MC) and mass loss (ML) of aloe vera (AV)/collagen films.

Film	MC (%)	ML (%)
Control	12.2 ± 0.7[a]	21.9 ± 0.7[a]
AV10	9.8 ± 0.4[b]	31.1 ± 0.8[b]
AV20	7.3 ± 0.4[c]	31.7 ± 0.5[b]
AV30	5.8 ± 0.6[c]	35.6 ± 0.8[c]

[a-c]Two means followed by the same letter in the same column are not significantly (P > 0.05) different through the Tukey's multiple range test.

Considering the potential application of these composite films as wound dressings, water uptake tests were carried out to determine the capacity of the films to absorb exudates from wounds. As can be seen in **Figure 4.2**, all films present a rapid absorption of water along the first 20 min of immersion in PBS (pH 7.4), reaching the equilibrium in approximately 40 min with WU values around 300%, regardless of AV content. These results indicated that the addition of AV did not affect the water uptake capacity of collagen films, a required property for wound dressing purposes.

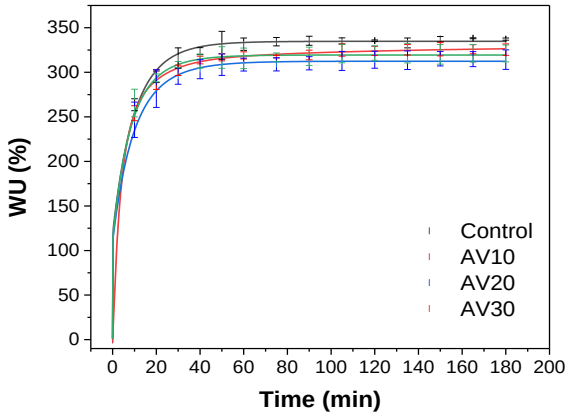

Figure 4.2. Water uptake (WU) capacity of aloe vera (AV)/collagen films.

4.2.2 Thermal properties

The thermal behavior of the films was tested by TGA and DSC analyses. TGA and DTG curves of collagen films are displayed in **Figure 4.3**. All films showed similar behavior with three main stages. For temperatures below 150 ºC, the weight loss was attributed to the loss of adsorbed and bound water, which was around 10%. The second stage, at 240-250ºC, was ascribed to the glycerol evaporation which is higher than the boiling temperature of glycerol (182ºC), indicating the interactions of the hydroxyl groups of glycerol with the polar groups of collagen and AV, in accordance with FTIR results. When AV content increased, DTG curve became broader and this second stage can also be related to the degradation of the hemicellulose and sugars present in AV (El Azazy et al., 2019; Rethinam et al., 2020). The third stage, for temperatures above 270 ºC, was referred to the thermal degradation of collagen (Ma et al., 2018) and aloe vera (El Azazy et al., 2019). Finally, the slight weight loss at 453 ºC in the films with AV is attributed to the thermal degradation of cellulose and lignin present in AV (Shadangi & Mohanty, 2014).

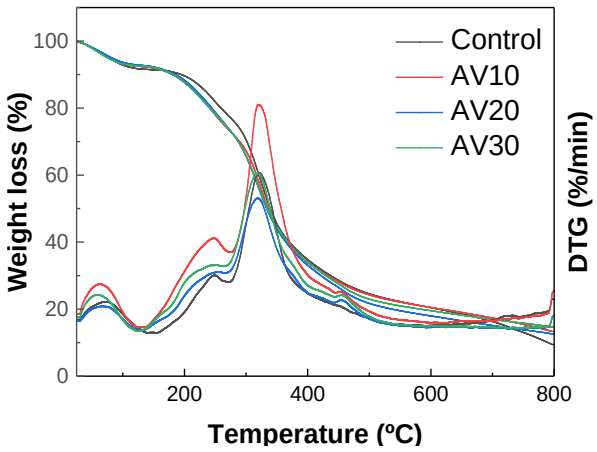

Figure 4.3. TGA and DTG curves of aloe vera (AV)/collagen films

The effect of compression temperature and AV addition on the denaturation of collagen was analyzed by DSC and the results are shown in **Figure 4.4A**. All samples exhibited two endothermic peaks: the first peak, around 80 ºC, was related to free water

release, and the second peak at around 150 ºC was associated to denaturation of the collagen triple helix (Bozec & Odlyha, 2011). These values are in accordance with those obtained for bovine skin collagen (Shi et al., 2019). It is worth nothing that denaturation peak also appeared when AV was added, indicating maintenance of the triple helix structure after AV addition and compression molding. Additionally, for a better analysis of the collagen denaturation peak, the possible interferences caused by the evaporation of water were avoided subjecting selected samples to a heating ramp to eliminate moisture. As can be seen in **Figure 4.4B**, no difference was observed in the denaturation peak with the addition of AV, confirming the prevalence of the triple helix structure when AV was added.

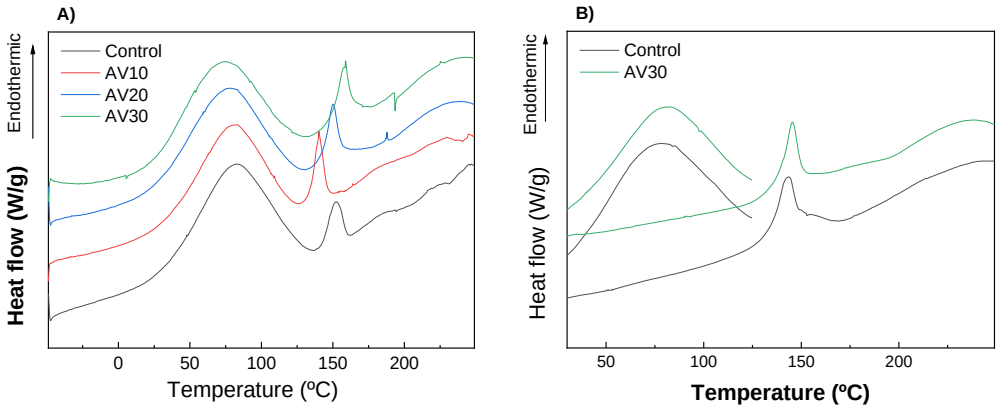

Figure 4.4. DSC curves of aloe vera (AV)/collagen films A) for a single scan and B) for two scans.

4.2.3 Barrier and mechanical properties

Light barrier properties of the films were analyzed and UV-vis spectra are shown in **Figure 4.5**. Films exhibited a small absorbance peak between 250 and 280 nm associated to aromatic amino acids residues on collagen, such as phenylalanine and tyrosine, and a maximum absorbance peak from 200 to 240 nm related to carbonyl groups present in collagen (Abdollahi et al., 2018; Duan et al., 2009). Similar values, around 230 nm, were found for type I fish collagen (Chen et al., 2016b). The addition of aloe vera increased the absorbance in 250-290 nm range, attributed to the flavonoids present in AV (Dey, Bera & Chakrabarty, 2015). Therefore, considering that one potential

application of collagen films could be as wound dressing, the addition of AV may provide higher UV light resistance during wound care.

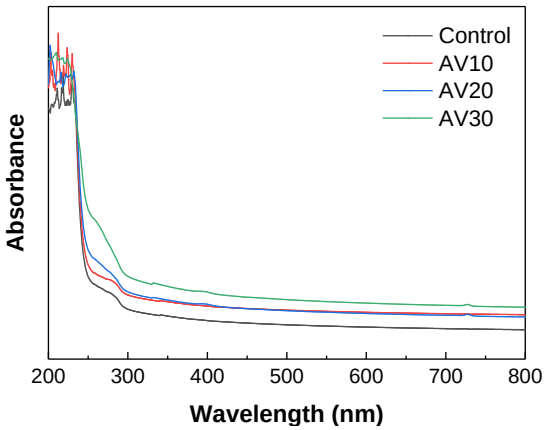

Figure 4.5. UV-vis spectra of aloe vera (AV)/collagen films.

Furthermore, the film hydrophilic character was analyzed by the measurement of water contact angles. As shown in **Table 4.2**, WCA values significantly ($P < 0.05$) decreased from 107º to 86º by the incorporation of aloe vera, leading to hydrophilic surfaces. These values are in agreement with WCA values observed for collagen films for regenerative applications (Perumal et al.,2018). This increase in hydrophilic character of the films can allow better draining of excess secretions in wounds.

Table 4.2. Water contact angle (WCA), Young modulus (YM), tensile strength (TS), and elongation at break (EB) of aloe vera (AV)/collagen films.

Samples	WCA (º)	YM (MPa)	TS (MPa)	EB (%)
Control	107 ± 5^{a}	805 ± 25^{a}	13.8 ± 1.1^{a}	13.5 ± 1.0^{a}
AV10	106 ± 3^{a}	$840 \pm 11^{a,b}$	11.5 ± 0.8^{b}	11.5 ± 1.2^{b}
AV20	97 ± 3^{b}	$867 \pm 11^{a,b}$	11.3 ± 1.3^{b}	11.2 ± 0.8^{b}
AV30	86 ± 5^{c}	$879 \pm 52^{a,b}$	10.2 ± 0.7^{b}	8.6 ± 0.8^{c}

$^{a\text{-}c}$Two means followed by the same letter in the same column are not significantly ($P > 0.05$) different through the Tukey's multiple range test.

As also displayed in **Table 4.2**, mechanical properties were also influenced by the addition of aloe vera. It was found that tensile strength slightly decreased when aloe vera was added, regardless of AV concentration. In the same manner, Young modulus

was not significantly ($P < 0.05$) affected by the concentration of AV. Regarding elongation at break, EB values decreased, especially for the films with the highest content of AV, probably due to the rigid structure of AV, which limits the chain mobility.

4.2.4 Morphological properties

In order to investigate the film structure and relate it to the properties measured, XRD and SEM analyses were carried out. As can be seen in **Figure 4.6**, films exhibited a XRD pattern characteristic of partially crystalline materials, with a small peak around $2\theta = 7^{o}$, indicating an intermolecular lateral packing distance between the molecular collagen chains, and a broad diffuse peak at about $2\theta = 20^{o}$ due to the diffuse scattering of collagen fibers, representing the amorphous structure of the films (Zou et al., 2017). These peaks were also found for fish skin collagen (Liao et al., 2018). The intensity of the peaks at 7^{o} and 20^{o} slightly decreased with the addition of aloe vera, suggesting the decrease in the structural order.

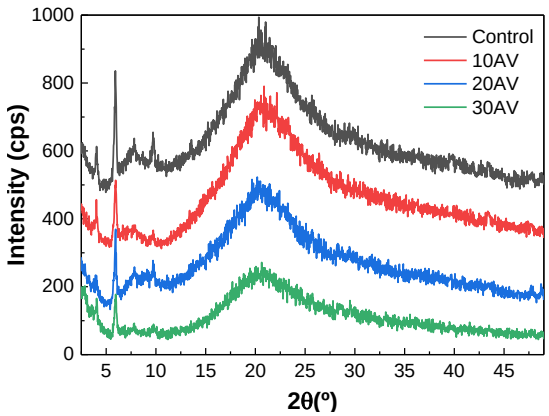

Figure 4.6. XRD patterns of aloe vera (AV)/collagen films.

To further assess the effect of aloe vera on collagen structure, SEM analysis was carried out and the images of cross-sections are shown in **Figure 4.7**. All films showed a compact and homogeneous structure. Control films exhibited a dense fibrillar structure and this structure changed to a rougher structure with the addition of aloe vera, in accordance with the decrease of the lateral packaging of collagen chains observed by XRD analysis.

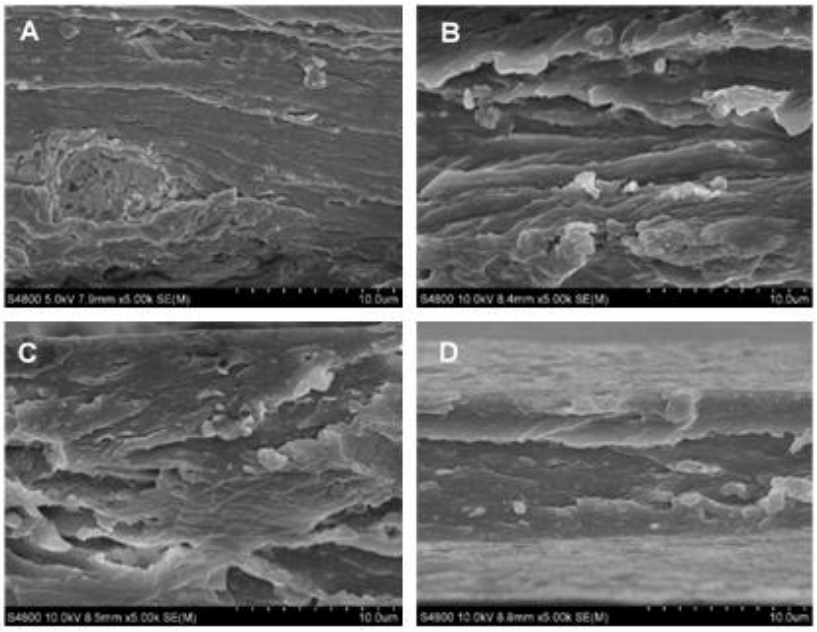

Figure 4.7. SEM images for the cross-sections of A) control, B) AV10, C) AV20 and D) AV30 films.

4.2.5 Degradation and biocompatibility

Degradation studies were conducted to evaluate the behavior of biomaterials exposed to PBS (pH 7.4), "simulated body fluid", and cell suspension (**Figure 4.8**). With respect to hydrolytic degradation degree (HDD), films suffered a degradation of 13.29 % ± 0.86 on the first day, rising until day 7 when complete degradation was achieved. Similarly, cell-related degradation (CDD) began with a DD of 8.05 % ± 1.05 by day 1, increased to 36.10 % ± 1.96 by day 7, and peaked at day 14. Finally, the films under the exposure of BFS as "body fluid simulant" underwent a slight degradation (BFDD = 9.90 % ± 1.30) after 24 h, and then suffered a drastic degradation at day 4. These results are consistent with the literature as collagen biomaterials are known for their high biodegradation ability (Shekhter et al., 2019).

Concerning the biocompatibility assessment (**Figure 4.9**), after 24 h from the placement of the material, the cells showed a behavior related to the exposure to the sample and the release of possible excipients (Hu et al., 2008). A statistically significant, transient mortality was observed with respect to the positive control in both the indirect

and direct assays (16.1±4.4 and 29.5±10.0%, respectively). After 48 h, cell mortality decreased considerably, reaching acceptable values for a cell culture to the last day of study. With regard to metabolic activity, cells showed optimal values from the first day (102.6±5.8 and 94.6±13.6%, respectively), reaching the maximum activity at 2 days in case of the indirect exposure and 4 days of culture in case of the direct one. By day 7, a decrease in cellular metabolic activity (64.7±10.9 and 73.7±15.6, respectively) was observed and attributed to the confluence of the culture and the shortage of nutrients (media were not changed through the duration of the experiments).

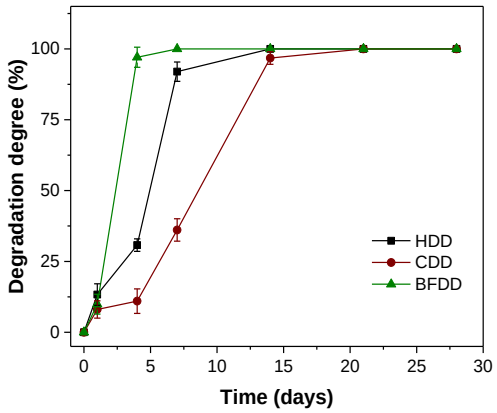

Figure 4.8. Hydrolytic (HDD), cell-mediated (CDD) and "simulated body fluid" (BFDD) degradation degrees for AV20 films.

In summary, the biomaterial composed of porcine collagen and aloe vera could be considered biocompatible for the cells studied. According to ISO 10993-5: 2009, the biomaterial reaches 70% viability in both indirect and direct tests, at all study times, (except for indirect exposure on day 7) with no remarkable mortality data once the culture is established. These results were expected since collagen biocompatibility is well established (Shekhter et al., 2019).

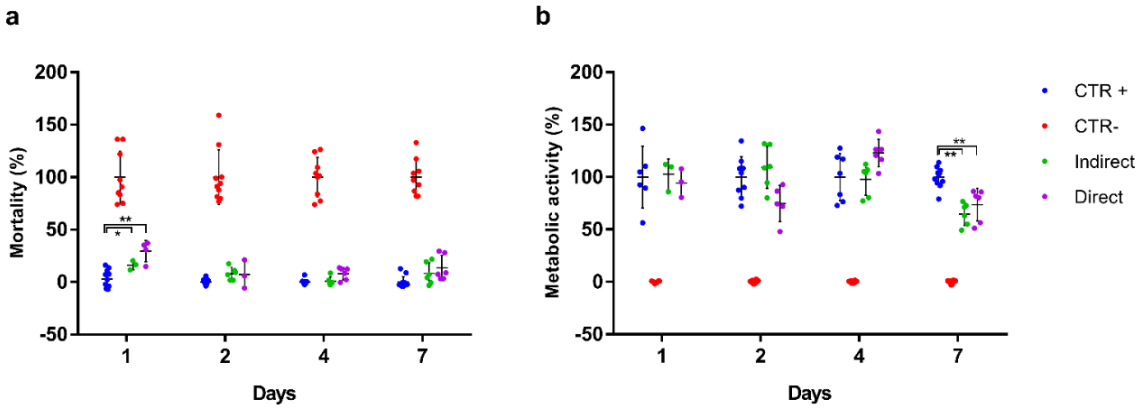

Figure 4.9. Biocompatibility assesment of the collagen and aloe vera films on HS27 cells. a) Cell mortality. b) Metabolic activity. Asterisks indicate significant differences between the samples and the positive control ($P < 0.05$).

4.3 CONCLUSIONS

Collagen films were prepared with aloe vera by compression molding with the aim of enhancing functional properties for biomedical applications. The addition of AV increased the hydrophilic character of the surface, which allows a better fibroblast adhesion during wound healing, thus promoting tissue regeneration. Furthermore, the water uptake behavior of collagen films was not modified and the film integrity was preserved after immersion. This performance was explained by XRD and SEM results, which showed the prevalence of the triple helix structure of native collagen with a slight decrease of the structural order with the addition of AV. Additionally, collagen films were easy to handle and showed good mechanical properties, with a slight decrease of tensile strength when AV content increased, probably due to the decrease of the structural order observed by XRD analysis. Furthermore, FTIR analysis indicated that AV contents higher than 20 wt % did not promote further physical interactions between collagen and aloe vera and, thus, this was the composition selected to confirm the suitability of aloe vera-incorporated collagen films for biomedical applications.

Chapter 5

CHITOSAN-COLLAGEN FILMS

Compression-molded chitosan-collagen films suitable for biomedical applications

.

5.1 SUMMARY

Chitosan-collagen films were developed and characterized in order to assess the suitability of these films for biomedical applications. Hence, physicochemical, thermal, barrier and mechanical properties were analyzed and related to the film structure, which showed the prevalence of the triple helix of native collagen after the addition of chitosan. Furthermore, collagen fiber diameter changed from 3.9 ± 0.6 μm, for collagen films without chitosan, to 1.8 ± 0.5 μm, for collagen films with low molecular weight chitosan. These results suggested interactions between collagen and chitosan molecules, as observed by Fourier transform infrared (FTIR) analysis. Regarding film barrier properties, chitosan-collagen films showed a water vapor transmission rate around 1174 $g \cdot m^{-2} \cdot day^{-1}$, suitable for biomedical applications such as wound healing. Additionally, biological tests confirmed that the chitosan-collagen films developed are suitable for biomedical applications.

5.2 RESULTS AND DISCUSSION

5.2.1 Physicochemical properties

The moisture content (MC) and the mass loss (ML) of the films were analyzed and values are shown in **Table 5.1**. Regarding MC, all films showed similar mean values, around 12%, lower values than those found for other collagen-polysaccharide films which showed moisture content close to 20% (Ma et al., 2020). Besides, ML values did not significantly ($P > 0.05$) change, and the value closed to 15% can be associated to the dissolution of glycerol since chitosan cannot be dissolved at pH 7.4. ML found in this work is much lower than that reported for collagen films with 50% of alginate (ML > 40%) or 50% of carboxymethylcellulose (ML > 50%) (Ma et al., 2020).

Table 5.1. Moisture content (MC) and mass loss (ML) of chitosan-collagen films.

Samples	MC (%)	ML (%)
Control	12.12 ± 0,04[a]	15.41 ± 0.73[a]
LMW	11.97 ± 0,51[a]	15.50 ± 0.58[a]
HMW	11.53 ± 0,50[a]	14.31 ± 0.58[a]

[a]Two means followed by the same letter in the same column are not significantly (P > 0.05) different through the Turkey's multiple range test. N = 3 was the minimum number of replications.

Additionally, water uptake tests were carried out and results are shown in **Figure 5.1**. Firstly, water uptake increased rapidly up to 20 min of immersion and the equilibrium values, around 110% for control films, 65% for the films with HMW chitosan, and 50% for the films with LMW chitosan, were achieved after 60 min of immersion. The different water uptake values between control films and films with chitosan suggested that the incorporation of chitosan promoted the interactions with the polar groups of collagen and glycerol. As a consequence, polar groups were less accessible to interact with water molecules and, thereby, lower water uptake degree was achieved. It is also worth noting that water uptake values were lower for the films with LMW chitosan than for those with HMW chitosan, indicating that hydrogen bonding would be favored for the films with LMW chitosan.

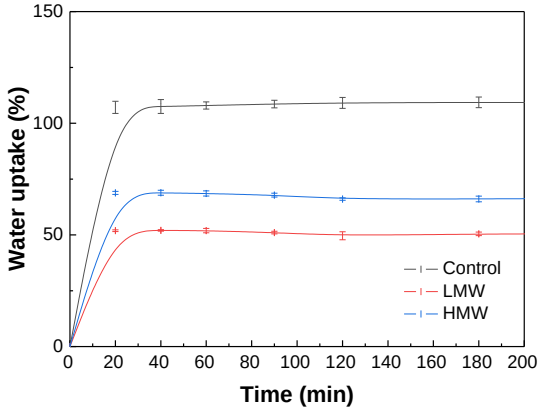

Figure 5.1. Water uptake curves of chitosan-collagen films.

In order to analyze the interactions between collagen and chitosan, FTIR analysis was carried out and FTIR spectra are shown in **Figure 5.2A** and **B**. All the spectra

showed the characteristic absorption bands assigned to the peptide bonds in collagen: 3300 cm^{-1} for amide A (N-H stretching), 1630 cm^{-1} for amide I (C=O stretching), 1545 cm^{-1} for amide II (N-H bending), and 1238 cm^{-1} for amide III (C-N stretching) (Deepthi et al., 2016; Riaz et al., 2018). It is worth noting that the relative intensity between amide I and amide II bands changed when chitosan was added. In particular, the intensity of the amide I band was slightly higher than that corresponding to amide II band for control films, while the intensity of amide I band became smaller than that of amide II band for the films with chitosan. The same trend was observed for the relative intensity between the band at 1450 cm^{-1}, attributed to CH_2 bending vibrations (Chakrapani et al., 2012; Plepis, Goissis & Das-Gupta, 1996), and the band at 1400 cm^{-1}, corresponding to C=O stretching vibrations (Wu et al., 2017). Concerning amide III, the addition of chitosan led to a displacement of this band toward higher wavenumbers. These differences in the relative intensity of FTIR bands suggest hydrogen bonding among carboxyl, amino, and hydroxyl groups present in the components of the film. Additionally, ionic interactions between oppositely charged groups occurred, especially between protonated amino groups in chitosan and anionic groups in collagen.

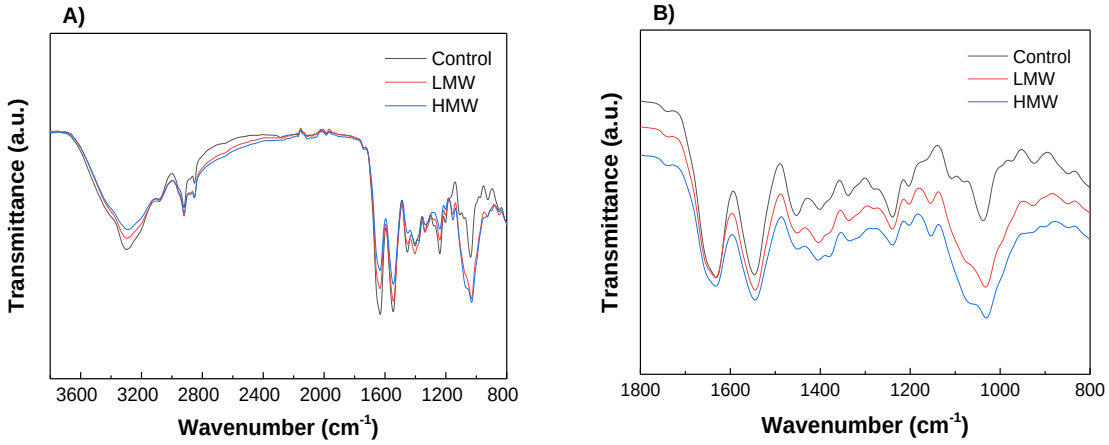

Figure 5.2. FTIR spectra of chitosan-collagen films: A) from 4000 to 800 cm^{-1} and C) from 1800 to 800 cm^{-1}.

In order to assess the effect of chitosan in the stability of collagen, the secondary structure of collagen was analyzed through the amide I profile. This absorption band

contains three major components: the α-helix conformation at 1650 cm^{-1}, and two bands that appear at 1615–1630 cm^{-1} and 1680 – 1700 cm^{-1}, corresponding to the β-sheet conformation (Wu et al., 2017). As shown in **Table 5.2**, α-helix was the main conformation in the films with chitosan, indicating that chitosan contributed to the preservation of the native collagen secondary structure. The preservation of the collagen triple helix structure was confirmed by two methods. Firstly, the absorption ratio between the amide III band and the band at 1452 cm^{-1} (A_{III}/A_{1452}) was calculated (Shi et al., 2019). As shown in **Table 5.2**, the A_{III}/A_{1452} ratio was higher than 1 in all the samples. Secondly, the wavenumber difference between amide I (ν_I) and amide II (ν_{II}) bands was calculated (Sizeland et al., 2018). As can be seen in **Table 5.2**, the difference was lower than 100 cm^{-1}. Hence, the results obtained by both methods indicated that the triple helix structure of collagen was maintained. Furthermore, those values increased with the addition of chitosan, confirming that chitosan contributed to the preservation of the native collagen structure.

Table 5.2. Area (%) of the curve fitting of amide I, absorption ratio between the amide III band and the band at 1452 cm^{-1} (A_{III}/A_{1452}), and wavenumber difference between amide I (ν_I) and amide II (ν_{II}) bands (ν_I - ν_{II}) in chitosan-collagen films.

Samples	β-Sheet (1615-1630 cm^{-1})	α-helix (1650 cm^{-1})	β-Sheet (1680-1700 cm^{-1})	A_{III}/A_{1453}	ν_I - ν_{II}
Control	35.6	49.3	15.1	1.1	85.0
LMW	36.9	52.8	10.3	1.7	88.2
HMW	38.1	55.0	6.9	1.7	87.5

5.2.2 Thermal properties

In order to study the thermal behavior of chitosan-collagen films, TGA and DSC experiments were performed. Regarding TGA, TGA and DTG curves are displayed curves are shown in **Figure 5.3**. As can be seen, there are three main weight loss steps. The first one, around 100 ºC, is related to water evaporation, as also observed by DSC (**Figure 5.4**), and its value, around 12%, was in accordance with the MC values shown

in **Table 5.1**. The maximum temperature corresponding to this first peak appeared at higher temperatures for the films prepared with chitosan, which could be related to the interactions between chitosan and water. The second weight loss step appeared around 250 ºC, and it is associated to the evaporation of glycerol (Andonegi, de la Caba & Guerrero, 2020). Finally, the main weight loss step appeared at 310-320 ºC and corresponds to collagen (Andonegi, de la Caba & Guerrero, 2020) and chitosan (Leceta et al., 2013) degradation processes. It was observed that the second and third stages changed with the addition of chitosan. This change could be related to the different structure of the network formed, as previously shown by FTIR results (**Table 5.2**), confirming the existence of interactions between collagen and chitosan, as also shown by other works carried out with collagen films modified with polysaccharides such as fucoidan (Perumal et al., 2018).

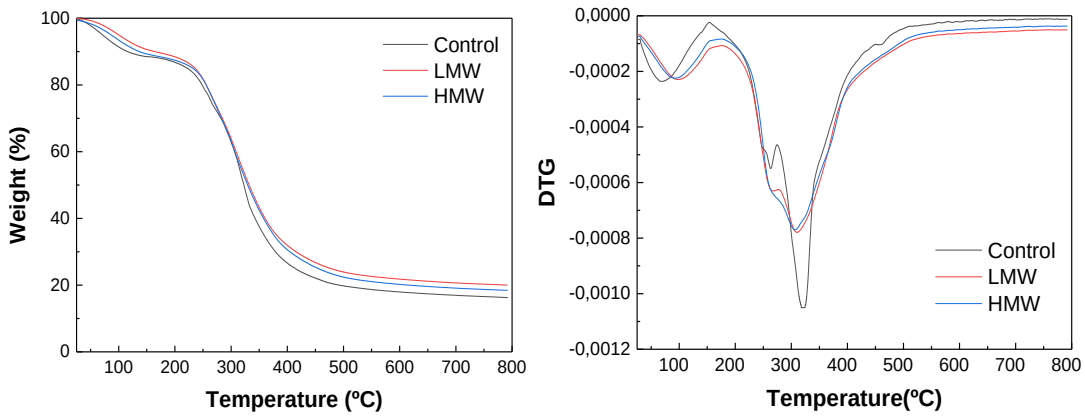

Figure 5.3. TGA and DTG thermograms of chitosan-collagen films.

Concerning DSC measurements, all samples exhibited three endothermic peaks, as shown in **Figure 5.4**. The peak around 90 ºC was related to the free and bound water release (Kaczmarek, Sionkowska & Skopinska-Wisniewska, 2018). The denaturation temperature was associated to the endothermic peak around 150 ºC (Chakrapani et al., 2012). The temperature at which the maximum of this peak appeared increased with the addition of chitosan, and the highest value was found for the films with LMW chitosan. This fact would confirm that collagen-chitosan interactions would be favored for the

chitosan with lower molecular weight, as previously shown by water uptake results. Finally, the third endothermic peak appeared between 210 and 250 ºC, and it was associated to conformational changes from the triple helix structure of collagen to random coil (Bozec & Odlyha, 2011). The temperature corresponding to the maximum of this peak increased with the addition of chitosan due to the existence of interactions between collagen and chitosan, as observed by FTIR results. In particular, DSC revealed the characteristic collagen-collagen and collagen-water interactions for control films. In the films with chitosan, these interactions are partially replaced by interactions between collagen and chitosan, indicating that the formation of hydrogen bonds between collagen and chitosan competed with hydrogen bonding between collagen chains. Similar results have been found for collagen-fucoidan films, showing the increase of thermal stability by the incorporation of polysaccharides into collagen film forming formulations (Perumal et al., 2018).

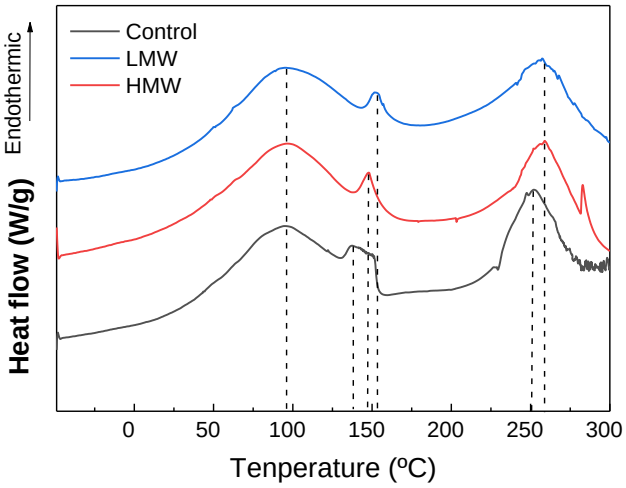

Figure 5.4. DSC thermograms of chitosan-collagen films.

5.2.3 Morphological properties

The changes showed above require information about the structure of chitosan-collagen films, thus XRD and SEM analyses were carried out. All the films exhibited XRD patterns of amorphous materials (**Figure 5.5**). The small reflection peak at 10° is

attributed to the chitosan crystal form (Leceta et al., 2015) and the peak around 7º is related to the triple helix structure of collagen (Valencia et al., 2019). Collagen molecules generally assemble into fibrils and then form collagen fibers by intermolecular crosslinking, leading to the characteristic hierarchical interwoven structure of collagen. According to XRD results, the addition of chitosan did not cause any relevant change, indicating that the helical structure of collagen was maintained after chitosan addition, in consistence with FTIR results. Additionally, a broad band appeared around 20º, associated to the diffuse scattering of collagen fibers, indicating the amorphous structure of the films (Zou et al., 2017). As can be seen, all samples showed similar XRD patterns with a slight increase in the intensity of the band at 20º for the films with HMW chitosan, indicative of the increase in the structural order.

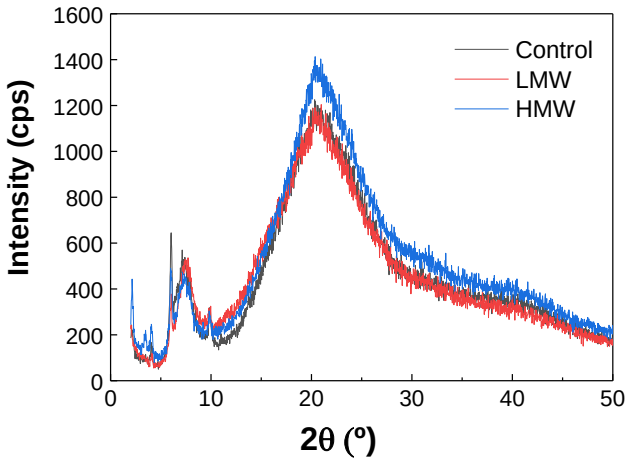

Figure 5.5. XRD patterns of chitosan-collagen films

To further asses the changes caused by the addition of chitosan in collagen films, SEM analysis was carried out and the images of film surface are shown in **Figure 5.6B**, **C** and **D**. SEM micrographs exhibited the fibril structure of collagen for all the films, showing the collagen periodicity corresponding to native collagen (Socrates et al., 2019). With the addition of chitosan, the surface was rougher and more fibers could be observed, especially for collagen films with HMW chitosan. Furthermore, a significant ($P < 0.05$) decrease of collagen fiber diameter was observed from 3.9 ± 0.6 μm for control films to 1.8 ± 0.5 μm and 1.9 ± 0.5 μm for the films with LMW and HMW chitosan.

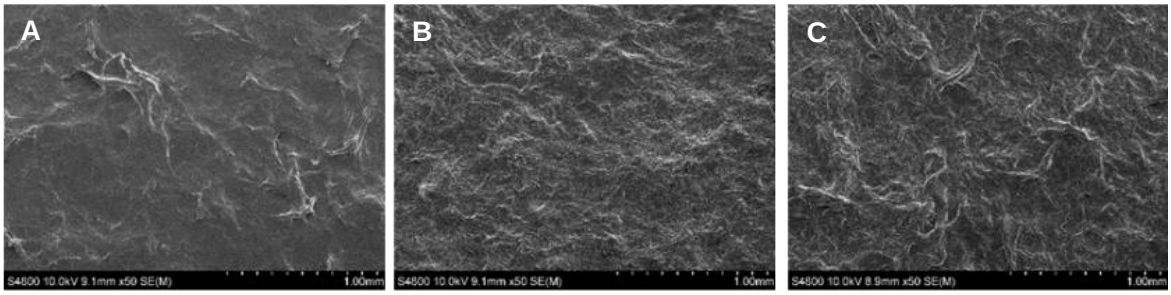

Figure 5.6. SEM images of surfaces for A) control films, B) collagen films with LMW chitosan, and C) collagen films with HMW chitosan.

5.2.4 Barrier and mechanical properties

Light barrier properties of chitosan-collagen films were analyzed and UV-vis spectra are shown in **Figure 5.7**. As can be seen, collagen films provided a maximum UV light barrier from 200 to 250 nm, associated with carbonyl, carboxyl, and amide groups in the polypeptide chains of collagen (Pal, Nidheesh & Suresh, 2015; Veeruraj, Arumugam & Balasubramanian, 2013), and a small absorption peak at 250-280 nm, associated to tyrosine and phenylalanine amino acid residues in collagen (Duan et al., 2009; Huang et al., 2011). The addition of chitosan showed a strong UV blocking capacity, increasing the absorbance at 250-280 nm due to the hydroxyl auxochrome groups of chitosan (Uranga et al., 2019).

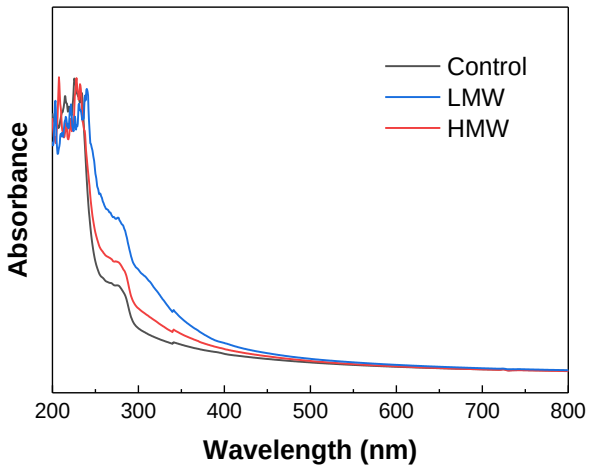

Figure 5.7. UV-vis spectra of chitosan-collagen films.

Biomaterials for wound dressing need to maintain moisture loss from the wound at an optimum rate and, thus, favor evaporation and inhibit excess fluid absorption (Singh, Gupta & Gupta, 2018). Taking the above into consideration, water vapor transmission rate was measured. For normal skin, the inherent water vapor evaporation rate is about 204 $g \cdot m^{-2} \cdot day^{-1}$, while the evaporation rate increases to 279 $g \cdot m^{-2} \cdot day^{-1}$ and 5138 $g \cdot m^{-2} \cdot day^{-1}$ for injured skin and burn skin, respectively (Lamke, Nilsson & Reithner, 1977). As can be seen in **Table 5.3**, there was no significant ($P > 0.05$) difference in WVTR values with the addition of chitosan and all samples showed a high occlusive character, appropriate for biomedical applications such as wound healing. Additionally, WCA values were measured to determine the film hydrophilic character, which is known to have a great effect on the interaction between the biomaterial and the tissue. As shown in **Table 5.3**, WCA values significantly ($P < 0.05$) decreased with the incorporation of chitosan, which would favor the adhesion of fibroblasts and endothelial cells during wound healing. This decrease of WCA values has also been reported for collagen-fucoidan films (Perumal et al., 2018).

Table 5.3. Water vapor transmission rate (WVTR), water contact angle (WCA), tensile strength (TS), and elongation at break (EB) of dry and wet chitosan-collagen films.

Samples	WVTR ($g \cdot m^{-2} \cdot day^{-1}$)	WCA (º)	TS_{dry} (MPa)	EB_{dry} (%)	TS_{wet} (MPa)	EB_{wet} (%)
Control	1172^{a}	103 ± 7^{c}	7.7 ± 0.6^{a}	13.2 ± 0.5^{a}	2.0 ± 0.1^{a}	50.6 ± 1.9^{a}
LMW	1176^{a}	90 ± 7^{a}	12.4 ± 0.8^{b}	24.1 ± 0.8^{b}	2.8 ± 0.1^{b}	34.0 ± 0.4^{b}
HMW	1174^{a}	93 ± 7^{b}	13.0 ± 0.6^{b}	21.9 ± 0.7^{c}	2.3 ± 0.1^{c}	39.3 ± 1.1^{c}

$^{a-c}$Two means followed by the same letter in the same column are not significantly ($P > 0.05$) different through the Turkey's multiple range test. N = 5 was the minimum number of replications.

Mechanical properties of films are largely associated with distribution and density of intermolecular and intramolecular interactions in the network, so the effect of chitosan on mechanical properties is shown in **Table 5.3**. For the dry films, TS and EB significantly ($P < 0.05$) increased when chitosan was added, induced by the interactions between

collagen and chitosan, as found by FTIR analysis. As previously shown in **Table 5.2**, collagen is mainly composed of α-helix chains with intense hydrogen bonds and Van der Waals forces among these chains. Due to the triple helix structure, collagen shows appropriate tensile strength, but the intense interactions among chains can prevent stretching. However, in the wet state, water can weaken these interactions among collagen chains, facilitating stretching and providing the films with a greater flexibility. Nevertheless, this effect was less noticeable for the films with chitosan due to the additional interactions among collagen and chitosan, especially for the films with LMW chitosan, since the interactions with smaller size-molecules are favored. This fact is in accordance with the water uptake behavior shown in **Figure 5.1**, where water uptake was higher for control films, followed by the films with HMW chitosan and finally, by the films with LMW chitosan. It is worth noting that all films showed a fibril structure in the fracture surface after mechanical testing, as shown in **Figure 5.8**.

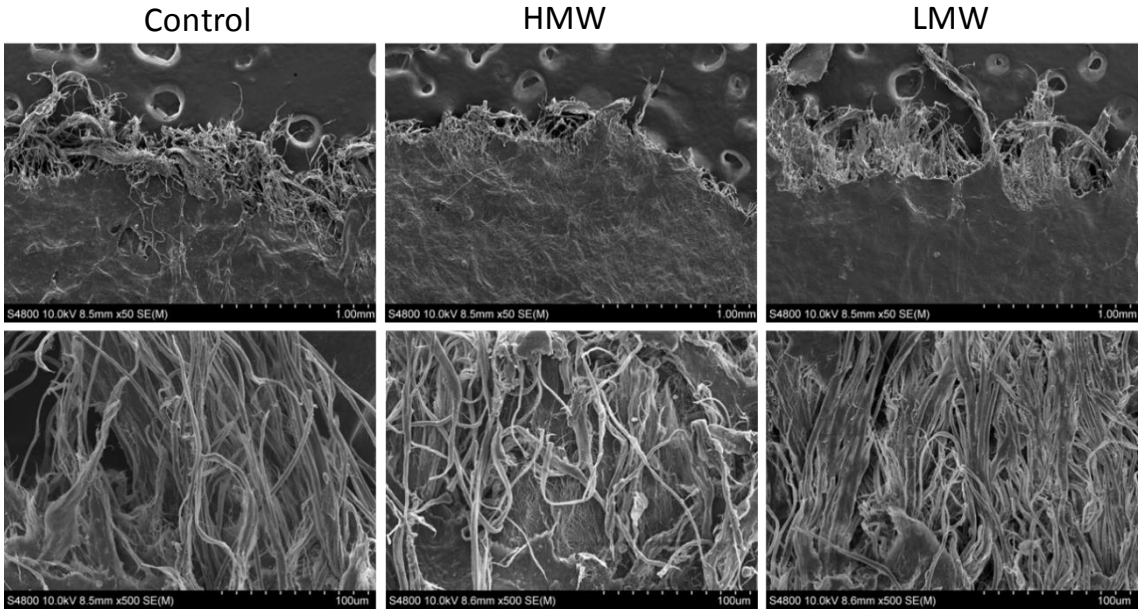

Figure 5.8. SEM images of the fracture surface in the break zone after mechanical analysis for A) control films, B) collagen films with LMW chitosan, and C) collagen films with HMW chitosan.

5.2.5 Biodegradation and cytotoxicity assessment

On the one hand, degradation studies showed that there was no progressive weight decrease due to the hydrolytic action after 21 days in any of the chitosan-collagen films. The initial loss, approximately 15% for the films with chitosan and 23% for the control films (**Figure 5.9A**), was likely due to the dissolution of glycerol. These findings also suggested that chitosan decreased the dissolved glycerol since the films with chitosan showed a lower percentage of degraded weight through the entire assay and non-significant differences were observed in any time-point between the films with LMW or HMW chitosan. The insoluble character of collagen in water explains the observed film resistance to hydrolysis. This property was improved with the addition of chitosan that formed hydrogen bonds with collagen molecules, as previously shown by FTIR analysis.

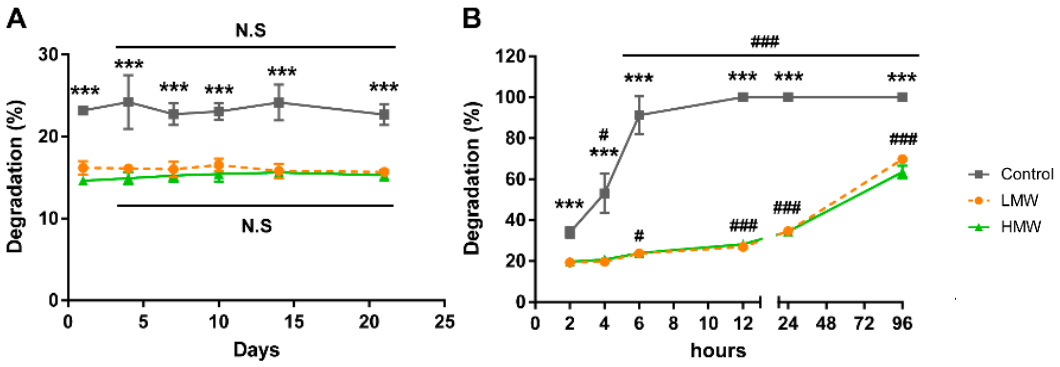

Figure 5.9. Degradation assessment: A) hydrolytic degradation with *** indicating P < 0.001 for control vs both LMW and HMW groups and N.S. indicating non-significant differences between any time-point and day 1 for each group; B) enzymatic degradation with *** indicating P < 0.001 for control vs both LMW and HMW groups, # indicating P < 0.05, and ### indicating P < 0.001 between any time-point and 2 h for each group.

On the other hand, enzymatic degradation studies showed a complete degradation of the control films in less than 12 h; however, for collagen films with chitosan, only 27-28% of the weight was lost at 12 h (**Figure 5.9B**). These values are in accordance with those found by Perumal et al. (2018), who reported 27% of degradation

after 12 h for collagen films with 40% of fucoidan. After 96 h, approximately 70% loss of the initial weight was reached, with no significant differences between the films with LMW and HMW chitosan. The 30% of the remaining weight in the films with chitosan corresponded to chitosan, which was not affected by the enzymatic action. Thus, it is demonstrated that chitosan increased the resistance of the collagen to the action of collagenase. These findings may be explained due to the fact that the enzymatic degradation depends on the number of cleavage sites in the forming polymer and on the concentration of available enzymes in the scaffold environment (Drury & Mooney, 2003). In that sense, the addition of chitosan hindered the access of the enzyme to the cleavage sites of collagen, reducing the degradation caused by the collagenase. As previously reported (Etxabide et al., 2017), films of these characteristics can be loaded with growth factors such as epidermal growth factor (EGF). The slow degradation profile allows a controlled release of bioactives, thus protecting them from the harsh microenvironment with increased metalloprotease activity present in inflammatory diseases such as chronic wounds (Barrientos et al., 2014).

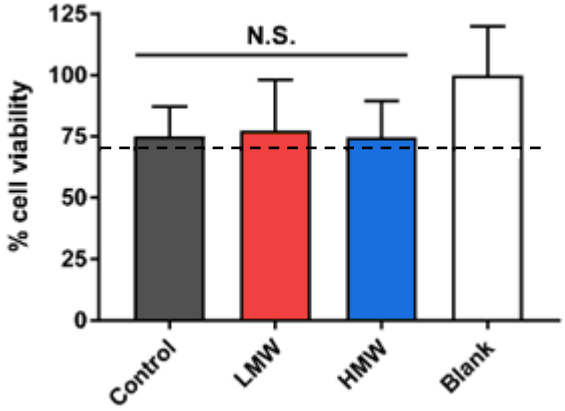

Figure 5.10. Cytotoxicity assay with N.S. indicating non-significant differences vs blank group, and dashed line marking the 70% of cell viability.

Since films for biomedical applications must fulfill additional requirements such as biocompatibility, *in vitro* cytotoxicity assay was performed following an adapted protocol from the ISO 10993-5:2009 guidelines for biological evaluation of biomedical devices. As can be seen in **Figure 5.10**, all the films showed more than 70% of cell

viability after 48 h of direct contact with the film. These results are in agreement with the biocompatibility of each component of the film forming formulation. Taking these findings into account, chitosan-collagen films are in compliance with the ISO 10993-5:2009 and may be considered as non-cytotoxic biomaterials.

5.3 CONCLUSIONS

Chitosan-collagen films with enhanced functional properties for biomedical applications such as wound healing were developed. The addition of chitosan reduced the water uptake degree of collagen films, which could allow a controlled release of epidermal growth factors, substances of interest if films were used as wound dressings. This behavior was explained by the interactions between collagen and chitosan, as found by FTIR analysis, which showed the prevalence of the triple helix structure of native collagen, as confirmed by XRD results. No significant differences were found in most of functional properties as a function of the molecular weight of chitosan, including mechanical resistance in wet state and a cell viability higher than 70% for all the films assessed.

Chapter 6

CHITOSAN-COLLAGEN SCAFFOLDS

Environmental and physicochemical assessed chitosan-collagen scaffolds processed by freeze-drying

6.1 SUMMARY

Native collagen scaffolds were prepared in this work, in which both materials and environmental approaches were considered with the aim of providing a global strategy towards more sustainable biomaterials. From the environmental perspective, it is worth mentioning that acid and enzymatic treatments have been avoided to extract collagen, allowing the reduction in the use of resources, in terms of chemicals, energy, and time, and leading to a low environmental load of this step in all the impact categories under analysis. With the incorporation of chitosan into the scaffold-forming formulations, physical interactions occurred between collagen and chitosan, but the native collagen structure was preserved, as observed by Fourier transform infrared (FTIR) and X-ray diffraction (XRD) analyses. The incorporation of chitosan also led to more homogenous porous microstructures, with higher elastic moduli and compression resistance for both dry and hydrated scaffolds. Furthermore, hydrated scaffolds preserved their size and shape after some compression cycles.

6.2 RESULTS AND DISCUSSION

6.2.1 Environmental assessment

Collagen can be obtained from different animal by-products, such as pig, bovine and chicken skin and bones, their main sources at commercial scale (Abdollahi et al., 2018; Ma et al., 2003). In this work, collagen was obtained from the trimmings and the splitting-derived by-products (Andonegi, de la Caba & Guerrero). Regarding collagen extraction, it is worth noting that there are several methods reported, which include the treatment of raw materials with chemicals, such as sodium hydroxide, butyl alcohol, and acids and/or enzymes, such as pepsin and trypsin (Vidal et al., 2020). In contrast, only sodium hydroxide and mechanical pretreatments were used in this work, reducing the use of chemicals and bringing environmental and economic benefits, since lower amounts of resources (materials, energy, time) were employed in comparison to those

works that use acid and enzymatic treatments (Martínez-Ortiz et al., 2015; Noorzai et al., 2020). In the analysis, the use of acetic acid (0.5 M) in a ratio of 1:20 (w/v) in the scaffolds preparation process, as well as the distilled water production procedure, were also considered. Taken the above into consideration, the global environmental results of collagen scaffolds production are reported in **Table 6.1** for all the impact categories under evaluation. It is worth noting that, since the impact of the pretreatment step in comparison with the scaffolds preparation was so small (**Figure 6.1**), the impact values of both processes were jointly represented in **Table 6.1**.

Table 6.1. Impact category values related to collagen scaffolds.

Impact category	Unit	Total
Global warming	kg CO_2 eq	0.7730
Stratospheric ozone depletion	kg CFC11 eq	$4.09 \cdot 10^{-7}$
Ionizing radiation	kBq Co-60 eq	0.4080
Ozone formation, human health	kg NO_x eq	0.0026
Fine particulate matter formation	kg $PM_{2.5}$ eq	0.0019
Ozone formation, terrestrial ecosystems	kg NO_x eq	0.0027
Terrestrial acidification	kg SO_2 eq	0.0048
Freshwater eutrophication	kg P eq	0.0003
Marine eutrophication	kg N eq	$3.32 \cdot 10^{-5}$
Terrestrial ecotoxicity	kg 1,4-DCB	0.8840
Freshwater ecotoxicity	kg 1,4-DCB	0.0105
Marine ecotoxicity	kg 1,4-DCB	0.0146
Human carcinogenic toxicity	kg 1,4-DCB	0.0233
Human non-carcinogenic toxicity	kg 1,4-DCB	0.3050
Land use	m^2a crop eq	0.0211
Mineral resource scarcity	kg Cu eq	0.0007
Fossil resource scarcity	kg oil eq	0.2350
Water consumption	m^3	0.0086

Results showed that terrestrial ecotoxicity, global warming, and ionizing radiation caused low environmental damage in the collagen production process, whereas the other categories minimally contributed to the overall environmental burden. Additionally, disaggregating environmental results in percentage ratios are displayed in **Figure 6.1** for each impact category. In this way, the contribution of each stage over the final product can be evaluated. In this case, contributions from the different processes and activities involved throughout the entire life cycle were determined in relation to global results. As can be seen, mechanical stirring and freeze-drying steps were the main contributors to

the impact category values, representing around 80% of the total impact. The environmental assessment identified these two processes as the most relevant indicators with higher potential of improvement for decision-making in future works. In particular, the energy used in these processes, specifically electricity consumption, had a critical role in the environmental impact, regardless the impact category considered. Therefore, the assessment indicated that those processes should be improved and optimized in order to reduce the environmental load associated to the development of collagen scaffolds. Since collagen scaffolds were developed at laboratory scale, scaling up processes could lead to achieve the goal of the reduction in the environmental impacts abovementioned.

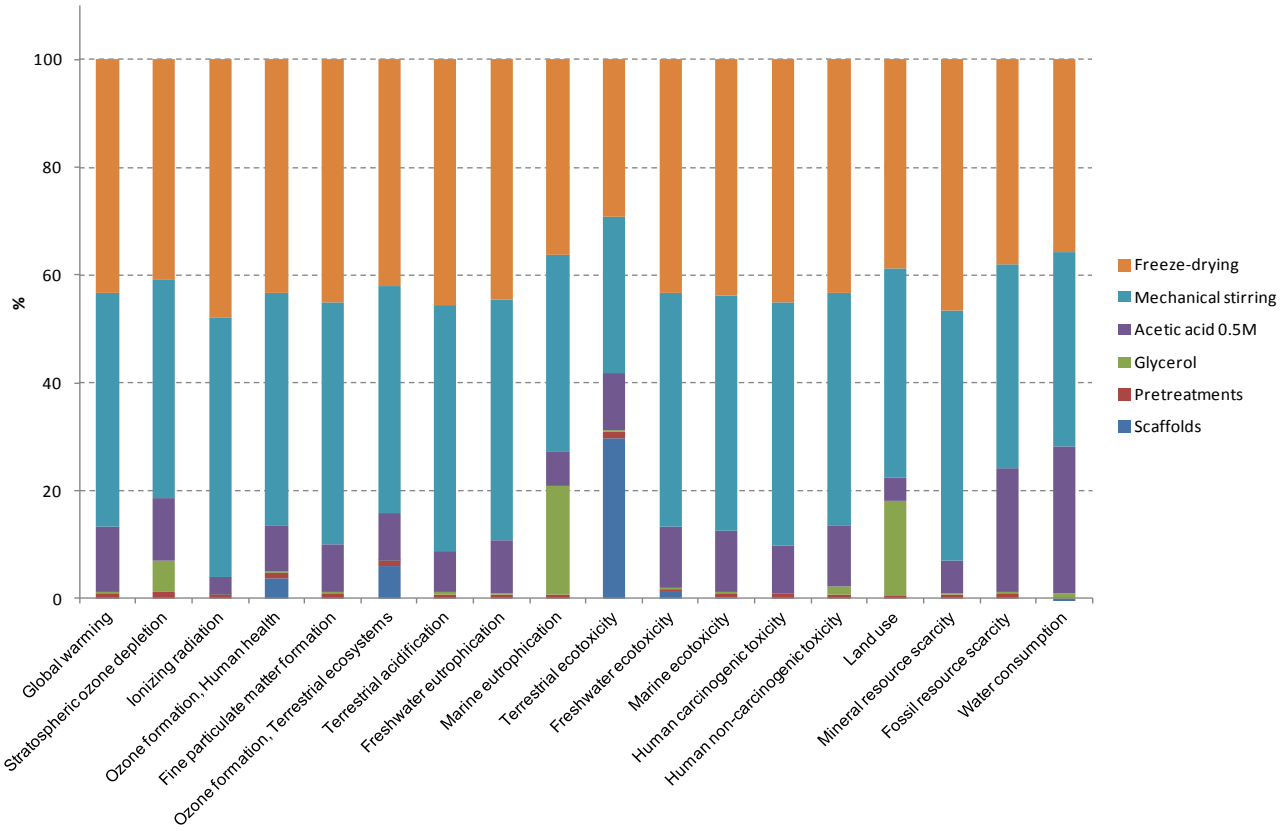

Figure 6.1. Relative contributions in each impact category for the most relevant processes involved in the entire life cycle of collagen scaffolds. Disaggregating environmental results are displayed in percentage ratios for the most relevant contributing factors: pretreatments, mechanical stirring, acetic acid solution (0.5 M), glycerol, and freeze-drying.

6.2.2 Fourier transform infrared (FTIR) spectroscopy

FTIR spectra (**Figure 6.2**) showed the characteristic absorption bands assigned to the peptide bonds in collagen (Riaz et al., 2018): 3298 cm^{-1} for amide A (stretching vibrations of N-H groups and O-H), 1631 cm^{-1} for amide I (C=O stretching), 1544 cm^{-1} for amide II (N-H bending), and 1239 cm^{-1} for amide III (C-N stretching). As can be seen in **Figure 6.2A**, the band at 3298 cm^{-1} was broadened to some degree when chitosan was incorporated into the scaffold formulation, indicating interactions between collagen and chitosan, both LMW and HMW chitosan. In the same manner, the band at 1038 cm^{-1}, associated to C-O vibrations, was notably broadened with the addition of chitosan, as shown in **Figure 2B**, supporting the interactions between collagen and chitosan. This fact is also in accordance with the change in the relative intensity of the band at 1456 cm^{-1}, attributed to CH_2 bending vibrations of aliphatic groups, which became smaller when chitosan was added. Also, a change was observed for the relative intensity between amide I and amide II bands.

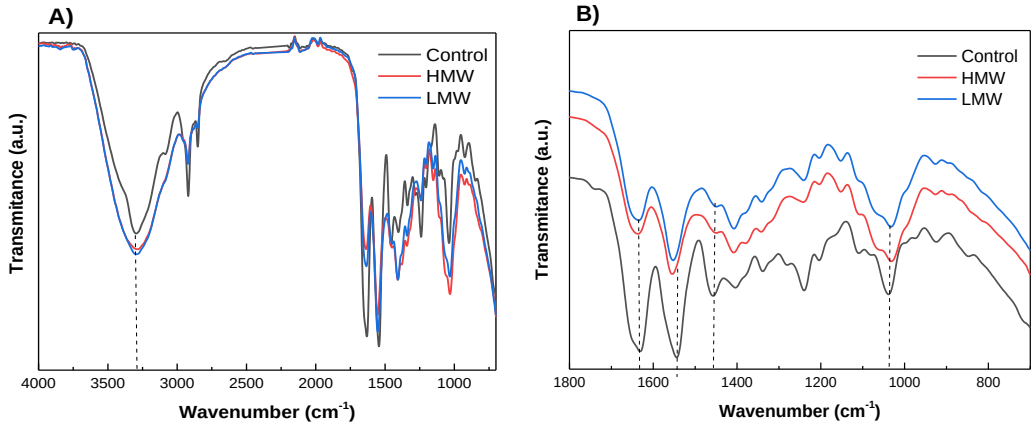

Figure 6.2. FTIR spectra of control scaffolds and collagen scaffolds with HMW and LMW chitosan A) from 4000 to 800 cm^{-1}, and B) from 1800 to 800 cm^{-1}.

Additionally, the amide II band shifted towards higher wavenumbers, although the amide I band, related to the collagen triple helix, was maintained at the same position, suggesting that the collagen triple helix could be preserved with the addition of chitosan and that the interactions involved between collagen and chitosan were hydrogen bonds.

Furthermore, the wavenumber difference between amide I (ν_I) and amide II (ν_{II}) bands was lower than 100 cm^{-1}, indicating that the triple helix structure of collagen was maintained (Sizeland et al., 2018). As can be seen in **Table 6.2**, those values decreased with the addition of chitosan, confirming that chitosan contributed to the preservation of the native collagen structure.

Table 6.2. Wavenumber of amide I (ν_I) and amide II (ν_{II}) bands, as well as the wavenumber difference between them (ν_I - ν_{II}), for control scaffolds and collagen scaffolds with HMW and LMW chitosan.

Samples	Amide I (ν_I)	Amide I (ν_{II})	ν_I-ν_{II}
Control	1631	1544	87
HMW	1636	1555	81
LMW	1635	1552	83

The differences in the relative intensity between FTIR bands, as well as band shifting, suggested physical interactions between collagen and chitosan, probably by hydrogen bonding among carboxyl, amino, and hydroxyl groups present in the components of the scaffold forming formulation.

6.2.3 X-ray diffraction (XRD)

X-ray diffraction (XRD) was carried out to investigate the structure of collagen with LMW and HMW chitosan. As can be seen in **Figure 6.3**, the peak around 7° indicated the intermolecular lateral packing distance between the collagen molecular chains, as collagen molecules generally assemble into fibrils by the Schmitt model within chitosan and then formed collagen fibers by intermolecular crosslinking (Hu et al., 2013). A second broad peak around 20° resulted from the diffuse scattering of collagen fibers, and the third one around 32° was ascribed to the helical rise per residue distance, related to the conformational integrity of collagen (Hu et al., 2013). When chitosan was added, samples showed the same peak pattern, indicating that the structural integrity of collagen was retained, in consistence with FTIR results.

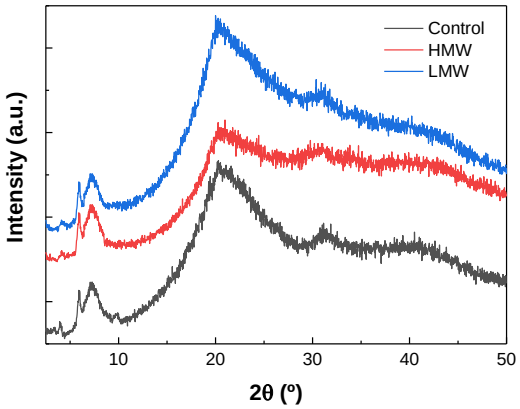

Figure 6.3. XRD patterns of control scaffolds and collagen scaffolds with HMW and LMW chitosan.

6.2.4 X-ray photoelectron spectroscopy (XPS)

XPS was performed to get a detailed insight into the corresponding elemental composition. As can be seen in **Figure 6.4A**, the predominant peaks identified were those related to C 1s (284.6 eV), N 1s (399.7 eV), and O 1s (531.9 eV) (Gao et al., 2020). Furthermore, the C 1s spectra could be fitted into three main separating peaks, at 284.6 eV, 288.1 eV and 285.9 eV. Generally, the peak at 284.6 eV was dominantly attributed to the aliphatic carbons (C-H and C-C), the peak at 285.9 eV was attributed to the carbons associated with oxygen or nitrogen atoms (C-O, C-N), and the peak at 288.1 eV was assigned to carbons in the collagen peptide chain (C=O) (Wu et al., 2011). These three relative peak areas of C1s spectra differed from control scaffolds (**Figure 6.4B**) and those with HMW (**Figure 6.4C**) and LMW (**Figure 6.4D**). In particular, the relative area of the peak at 284.6 eV decreased, while those of the peaks at 285.9 and 288.1 eV increased. The decrease of the relative area of the peak corresponding to C-H/C-C bonds indicated that the hydrophobic character of the surface decreased, while the increase of the relative areas associated to the presence of C-O, C-N, and O=C-NH_2 suggested that the presence of polar groups towards the surface increased. These facts indicated the increase of the surface hydrophilicity, which improves the bonding capacity of the surface.

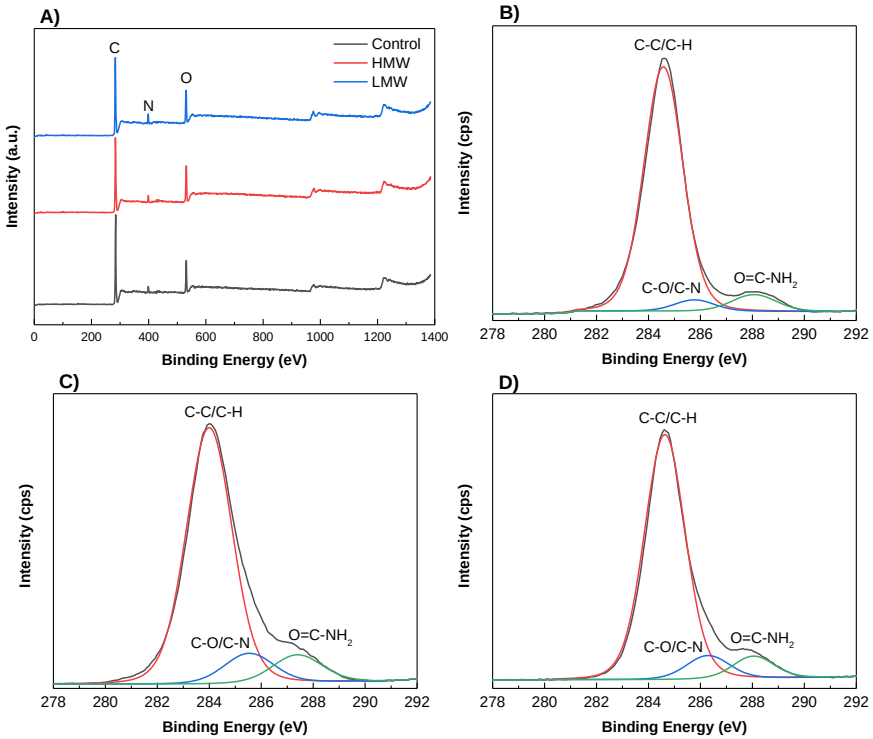

Figure 6.4. XPS survey spectra of A) all samples and XPS of C 1s features for B) control scaffolds and collagen scaffolds with C) HMW chitosan and D) LMW chitosan.

As can be seen in **Table 6.3**, the peak corresponding to C-O and C-N increased from 3.59% to 6.93% for LMW samples and to 8.18% for HMW samples, may be attributed to the interactions between hydroxyl and amino groups in collagen and chitosan. Additionally, the relative area of the peak associated to the peptide bond increased from 5.89 % to 6.21 % for scaffolds with LMW and to 7.51 % for those with HMW chitosan, probably due to hydrogen bonding among polar groups of collagen and chitosan. Furthermore, the relative areas of O 1s and N 1s were assessed. The weak peak of N 1s appeared at 399.7 eV, and the signal was 1.81% for control scaffolds and increased close to 4% for the scaffolds with chitosan. Additionally, the O 1s spectra was fitted to one peak at 531.9 eV, attributed to O-C=O/O=C-N. This signal represented 12.73% for the control scaffold and increased up to 13.79% and 15.84% for LMW and HMW samples, respectively. This percentage is of great importance since oxygen influences the stability in biological media (Wang et al., 2016b).

Table 6.3. Area (%) of the XPS spectra peaks for control scaffolds and collagen scaffolds with HMW and LMW chitosan.

Samples	C-C/C-H 284.6 (eV)	C-O/C-N 285.9 (eV)	O=C-NH2 288.1 (eV)	C=N/C-N 399.7 (eV)	O-C=O/O=C-N 531.9 (eV)
Control	75.98	3.59	5.89	1.81	12.73
HMW	69.11	6.93	6.21	3.96	13.79
LMW	64.93	8.18	7.51	3.54	15.84

6.2.5 Scanning electron microscopy (SEM)

Since homogenous microporosity is an essential attribute for scaffolds in tissue engineering applications, SEM analysis was carried out to analyze the scaffolds morphology. As can be observed in **Figure 6.5**, collagen scaffolds had an evenly distributed three-dimensional reticular pore structure. The LMW group presented a more homogeneous distribution and greater regularity of the pore size as compared to the HMW group. These results would be indicative of the fact that lower molecular weight facilitated the interactions of chitosan with collagen chains, leading to smaller pores. These findings suggest that chitosan-collagen scaffolds have an ideal pore distribution and uniform density for cellular growth in tissue engineering applications (Las Heras et al., 2020).

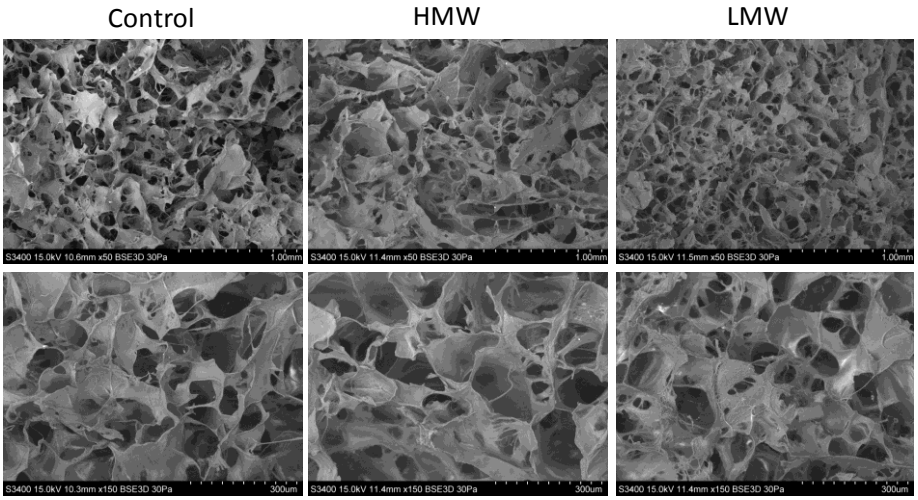

Figure 6.5. SEM images of control scaffolds and collagen scaffolds with HMW chitosan and LMW chitosan at a magnification of x50 (top) and x150 (bottom).

6.2.6 Compression test

The required mechanical properties of scaffolds include stretchability, flexibility, and tensile strength in order to provide the ideal 3D growth directing structure to mimic native tissues. Since scaffolds are hydrated in the *in vivo* environment, compressive properties in the hydrated state are likely to be more relevant and, thus, strength and moduli values were also reported for hydrated collagen scaffolds. As can be seen in **Figure 6.6A**, stress-strain curves match the typical compression curves and show elastic and plastic regions. In particular, there were three stages in the stress-strain curves of both dry and hydrated scaffolds: a linear elastic stage (strain < 5%), a steady collapse plateau stage (15% < strain < 50%), and a sharply increasing densification stage (strain > 55%). For biomedical applications, the stress-strain region of larger interest is between 0 and 10% strain and, thus, this was the selected section for determining the elastic modulus.

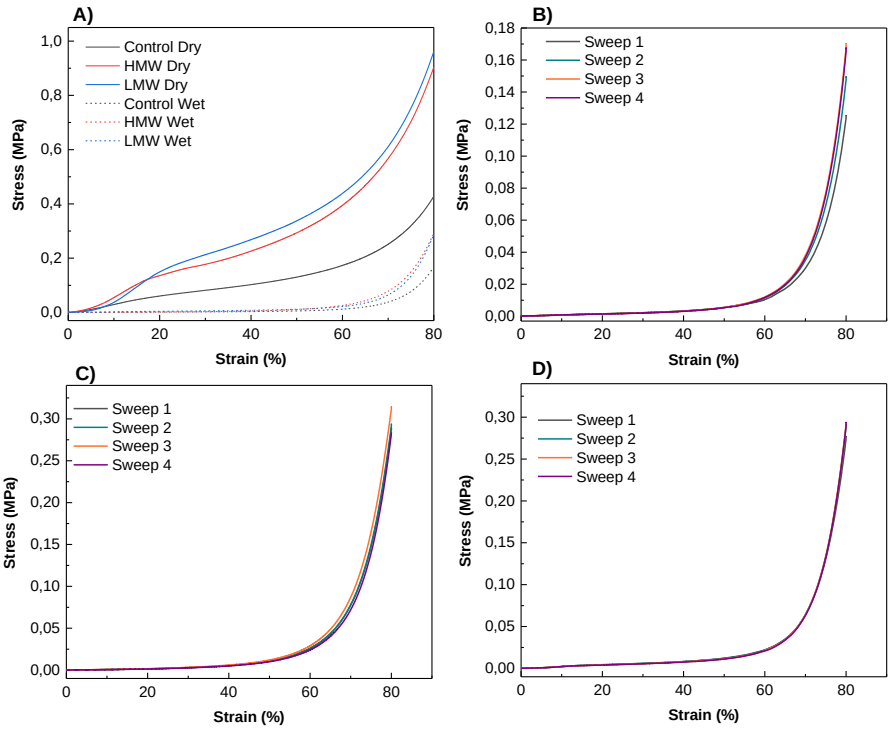

Figure 6.6. Compression stress - strain curves for A) dry scaffolds, B) hydrated control scaffolds, C) hydrated collagen scaffolds with HMW chitosan, and D) hydrated collagen scaffolds with LMW chitosan.

As expected, there was a notable difference in compressive moduli values between dry and hydrated scaffolds, but in both cases the moduli increased with the addition of chitosan, as shown in **Table 6.4**. In the same manner, compressive strength showed a remarkable increase when chitosan was incorporated into the scaffold formulation. In this sense, it is worth noting that dry scaffolds did not recover their size after the compression test, while hydrated scaffolds preserved their size under compression. In this regard, the scaffolds with chitosan showed no difference after the four sweeps carried out (**Figure 6.6C and D**), while the control scaffolds showed an increase of the stress after each sweep (**Figure 6.6B**). This mechanical behavior of collagen scaffolds with chitosan under compression may be explained by the interactions between both biopolymers, as shown by FTIR results.

Table 6.4. Elastic modulus (E) and compression strength of control scaffolds and scaffolds with HMW and LMW chitosan.

	E (MPa)		σ (MPa)	
Samples	**dry**	**hydrated**	**dry**	**hydrated**
Control	0.122±0.002	0.006±0.001	0.430±0.03	0.170±0.021
HMW	0.563±0.011	0.013±0.003	0.951±0.041	0.294±0.012
LMW	0.423±0.013	0.018±0.004	0.965±0.049	0.291±0.008

6.2.7 Degradation studies

Degradation studies were carried out to evaluate the biomaterial behavior exposed to PBS and collagenase solution (**Table 6.5**). Regarding hydrolytic degradation, control scaffolds did not suffer degradation. However, collagen scaffolds with chitosan underwent a degradation of over 10% after 4 days of immersion. The highest HDD value for collagen scaffolds with LMW chitosan may be related to the highest hydrophilicity of these samples, as shown by XPS analysis.

Table 6.5. Hydrolytic (HDD) and enzymatic (EDD) degree of degradation for control scaffolds and collagen scaffolds with HMW and LMW chitosan after 4 days.

Samples	HDD (%)	EDD (%)
Control	0	100
HMW	10.6±1.8	55.8±1.6
LMW	15.1±0.4	44.4±4.4

Under the collagenase effect, control scaffolds showed complete degradation, while collagen scaffolds with chitosan showed a degradation around 50% after 4 days of immersion. This may be explained by the fact that collagenase degrades native collagen by targeting the polar zone of the molecule with a (Gly-Pro-y)n sequence, whereas chitosan can only be degraded by enzymes that hydrolyze glucosamine-glucosamine, glucosamine-N-acetyl-glucosamine and N-acetyl-glucosamine-N-acetyl-glucosamine bonds, such as chitinases and lysozymes (Kean & Thanou, 2010). Therefore, chitosan improved the ability to resist collagenase degradation, preventing the action of the enzyme (Ma et al., 2019). The lowest EDD value observed for collagen scaffolds with LMW chitosan may be related to the crosslinking between collagen and chitosan. In this regard, a lower molecular weight facilitates the interactions between collagen and chitosan, leading to a higher crosslinking degree and to a smaller pore size, as observed by SEM; thus, enzymatic degradation is hindered. This study shows the advantages of including chitosan into the scaffold formulation to enhance scaffold biostability, prolonging its biodegradation and reaffirming its potential use for biomedical applications.

6.3 CONCLUSIONS

The environmental assessment carried out with the aim of evaluating the environmental impact associated to the main processes involved in the development of collagen scaffolds showed that mechanical stirring and freeze-drying were the processes with a higher environmental load. Although scaling up the production of collagen

biomaterials could notably reduce those impacts, further research is needed in order to optimize the conditions used, reducing the energy consumed in those processes. Regarding the physicochemical properties of the scaffolds, FTIR results showed that the interactions between collagen and chitosan were physical interactions by hydrogen bonding, which contributed to stabilize the triple helix structure of native collagen. Additionally, the hydrophilic character of the scaffold surface was enhanced, which is considered a beneficial property in biomaterials in order to promote cell adhesion and proliferation. In this regard, the scaffold morphology presented smaller and more homogenously distributed pores for the scaffolds with LMW chitosan. Also these scaffolds showed a more controlled degradation rate under the effect of collagenase, enhancing their biostability.

Chapter 7

TETRAHYDROCURCUMIN CONTAINING COLLAGEN SCAFFOLDS

3D-printed mucoadhesive collagen scaffolds as a local tetrahydrocurcumin delivery system

.

7.1 SUMMARY

Native collagen doughs were processed using a syringe-based extrusion 3D printer to obtain collagen scaffolds. Before processing, the rheological properties of the doughs were analyzed to determine the optimal 3D printing conditions. Samples showed a high shear-thinning behavior, reported beneficial in the 3D printing process. In addition, tetrahydrocurcumin (THC) was incorporated into the dough formulation and its effect on collagen structure, as well as the resulting scaffold's suitability for wound healing applications, were assessed. The denaturation peak observed by differential scanning calorimetry (DSC), along with the images of the scaffold surfaces assessed using scanning electron microscopy (SEM), showed that the fibrillar structure of collagen was maintained. These outcomes were correlated with X-ray diffraction (XRD) results, which showed that an increase of the lateral packaging of collagen chains was observed in the samples with a THC content up to 4%, while a higher content of THC considerably decreased the structural order of collagen. Furthermore, physical interactions between collagen and THC molecules were observed using Fourier transform infrared (FTIR) spectroscopy. Additionally, all samples showed swelling and a controlled release of THC. These results along with the mucoadhesive properties of collagen suggested the potential of these THC–collagen scaffolds as sustained THC delivery systems.

7.2 RESULTS AND DISCUSSION

7.2.1 Rheological properties

The knowledge and control of rheological properties are of great relevance to analyze and design the 3D printing process (Corker et al., 2019). Hence, stress sweep, frequency sweep, and flow tests were performed to analyze rheological properties before 3D printing. First, stress sweep tests were performed to determine the linear viscoelastic range (LVR) of THC–collagen doughs and then, frequency sweet tests were carried out within the LVR. The results are shown in **Figure 7.1**. A predominant elastic behavior was

observed in all samples since the storage modulus (G') was greater than the loss modulus (G") in the studied interval (Zuidem et al., 2013). Additionally, small dependence on frequency was observed in the loss modulus, while the storage modulus remained nearly constant, demonstrating the system stability. It is worth noting that the collagen network structure did not collapse, since no crossover point between G' and G" was observed. This behavior followed the typical response of protein-based hydrogels observed in several studies (Machado, Martins & Plepis 2002; Yang et al., 2018). Furthermore, the hydrogel behavior did not show noteworthy differences with the addition of THC, since similar tan δ (G"/G´) values were obtained for all the formulations. Likewise, the dough printability can be assessed in terms of the minimum pressure required and modelled using the loss tangent. The loss tangent values found in this study ranged from 0.15 to 0.40, in accordance with other studies that suggested good printability within loss tangent values from 0.25 to 0.45 (Lee et al., 2021).

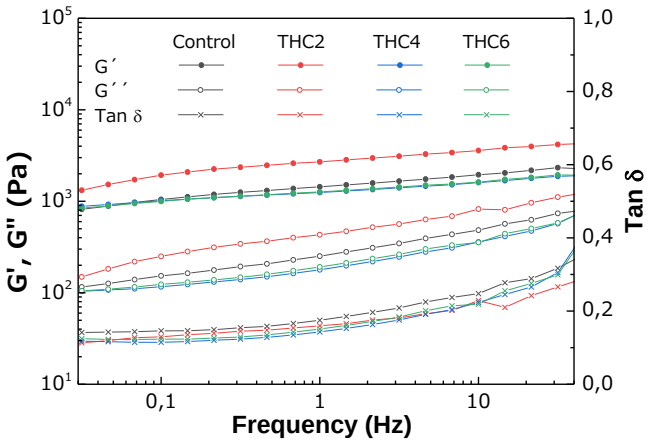

Figure 7.1. Storage moduli (G'), loss moduli (G''), and loss tangent (tanδ) obtained through frequency sweep test of the samples.

The viscosity suitable for 3D printing must be low enough to permit easy extrusion through the nozzle and high enough to be cohesive with the previously deposited layer while maintaining the shape (Lille et al., 2018). Therefore, the flow behavior of THC–collagen samples was analyzed and the dependence of apparent viscosities on shear rate is shown in **Figure 7.2A**. All samples displayed similar steady-state viscosity (η)

pattern of non-Newtonian fluids with a shear-thinning behavior and a tendency to reach a Newtonian region at a low shear rate (Newtonian plateau zone); thus, zero-shear viscosity (η_0) was estimated (Wu, Gray & Chen, 2018). Zero-shear viscosity is the viscosity when the material is at rest; this is a limiting value that cannot be measured directly and must be estimated by extrapolation, fitting the data to the model. The experimental flow data obtained were satisfactorily fitted (R^2> 0.996) to the Williamson model (**2.5 section**), and the resulting fit parameters are shown in **Table 7.1**. The shear-thinning performance indicated that collagen chains were affected by the shear stress between the layers when the flow rate increased, thereby reducing the force between them (Peralta, Meza & Zorrilla, 2017). This behavior was reported beneficial in the 3D-printing process for solid-like materials to be extruded through the nozzle (Alvarez-Castillo et al., 2021; Guo, Zhang & Devahastin, 2020). As can be seen in **Table 7.1**, all samples showed relatively low flow index values (n < 0.42), corroborating the shear-thinning behavior of the samples (Moreira, Chenlo & Torres, 2012). Furthermore, the decrease of η_0 with the increase of THC concentration denoted the establishment of a lower number of links between collagen and THC molecules (Torres, Hallmark & Wilson, 2014).

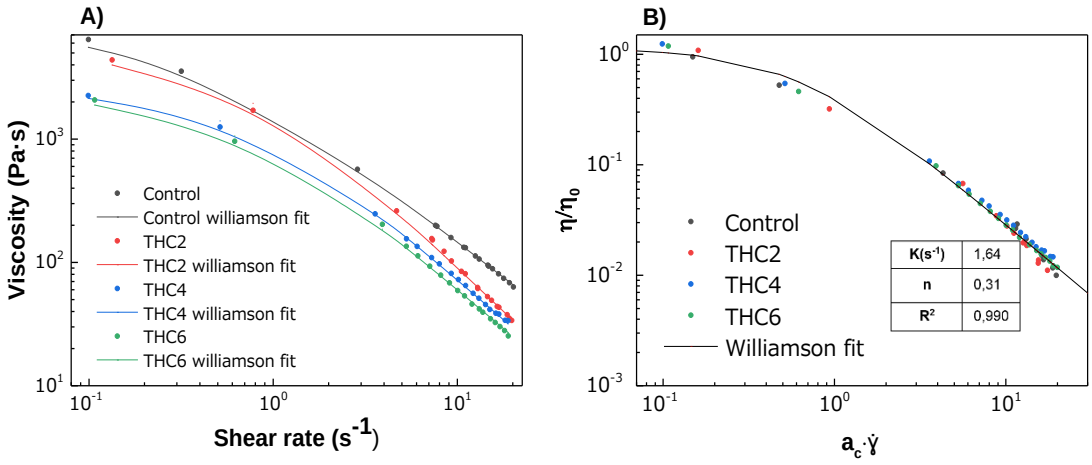

Figure 7.2. A) Flow curves of collagen-THC doughs fitted by Williamson model. B) Master flow curve for collagen doughs fitted by Williamson model, after performing a THC concentration-dependent shift (η_0, a_c) using the control sample as reference.

As all samples showed a similar shear-thinning tendency, curves could be fitted to a single master curve (**Figure 7.2B**). The shift factor (a_c) was calculated and included in **Table 7.1**, where $a_c = 1$ was assigned to the control sample. A decrease of a_c from 1 to 0.67 in THC4 and THC6 doughs indicated a higher consistency when the THC content increased (Alvarez-Castillo et al., 2021). The relatively small tan δ and the low viscosity observed at high shear rates suggested that the THC–collagen doughs would be easily extruded by the syringe with a high shear rate at the nozzle tip (Yang et al., 2019).

Table 7.1. Parameters of Williamson model, master curve shift factors, and shear rate values for collagen doughs.

Samples	η_0 (Pa·s^{-1})	k (s^{-1})	n	R^2	a_c	γ_w
Control	6764	2.71	0.15	0.996	1	69.05
THC2	4402	1.51	0.42	0.989	0.80	38.43
THC4	2298	1.37	0.31	0.996	0.67	44.47
THC6	2083	1.57	0.28	0.997	0.67	46.94

For a further assessment of the flow behavior of collagen doughs, the shear rate in the nozzle tip was calculated (2.5 section) and the values are shown in **Table 7.1**. Once shear-thinning behavior of doughs was observed, high shear rate values were selected since, under these conditions, the material offers less resistance (lower viscosity) and flows better. As the flow index (n) of the master curve was obtained, the printing velocity could be obtained using the equation of Weissenberg-Rabinowitsch (2.5 section). 3D printed scaffolds are shown in **Figure 7.3.**

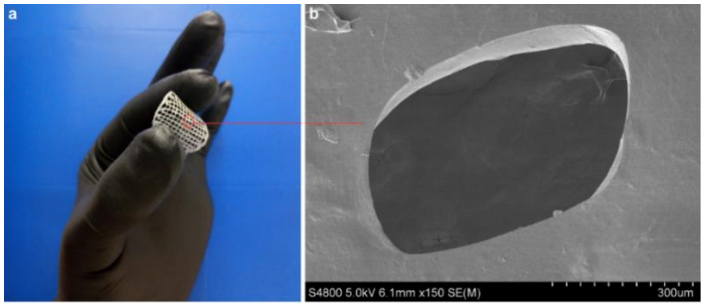

Figure 7.3. 3D printed scaffold and SEM image of the surface.

7.2.2 Physicochemical and thermal properties

To assess the interactions among the components of the scaffold formulation, FTIR analysis was carried out and FTIR spectra are shown in **Figure 7.4**.

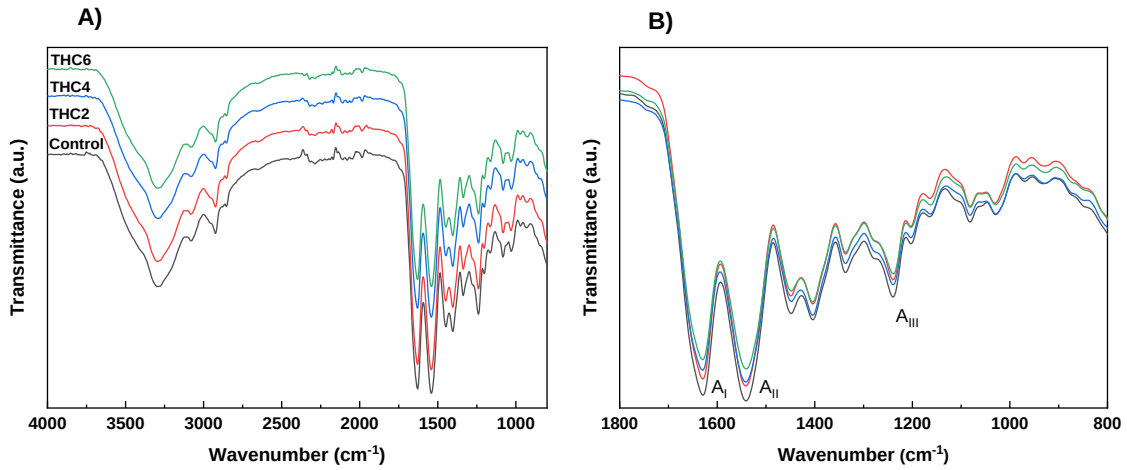

Figure 7.4. FTIR spectra of 3D printed collagen scaffolds: A) from 4000 to 800 cm^{-1} and B) from 1800 to 800 cm^{-1}.

All the spectra showed the main absorption bands assigned to the peptide bonds in collagen: N–H stretching vibration of amide A at 3287 cm^{-1}, C=O stretching of amide I at 1630 cm^{-1}, N–H bending of amide II at 1540 cm^{-1}, and C–N stretching of amide III at 1240 cm^{-1} (Riaz et al., 2018). The amide A band is commonly observed in the wavenumber range of 3400–3440 cm^{-1} but, when the band position is shifted to a lower frequency, this shift indicates that N–H groups in collagen are involved in hydrogen bonding (**Figure 7.5**), leading to stability in the collagen triple-helical structure (Liao et al., 2018). Additionally, a change in the intensity of the amide bands was observed with the incorporation of THC, indicative of physical crosslinking. No more obvious changes were observed in FTIR spectra, suggesting the prevalence of collagen secondary structure after the mixture preparation and 3D printing processes (de Campos Vidal & Mello, 2011).

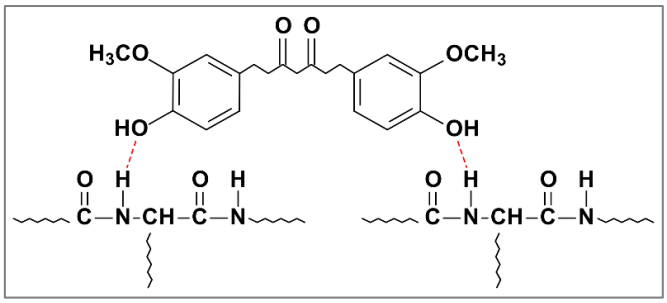

Figure 7.5. Schematic diagram of the interactions between collagen and THC by hydrogen bonding.

The thermal behavior of collagen scaffolds was studied using DSC analysis. As can be seen in **Figure 7.6**, all samples exhibited two endothermic peaks: the first peak, around 82 °C, is related to the free and bound water release (Kaczmarek, Sionkowska & Skopiska-Wisniewska, 2018); and the second peak, around 210 °C, is associated with collagen thermal denaturation process (Bozec & Odkyha, 2011). During this transition, collagen experienced conformational changes from triple helix to random coil and the structural water was released (Gauza-Wlodarczyk et al., 2017; Schroepfer & Meyer, 2017; Shi et al., 2019). Therefore, it is worth noting that these values confirmed the prevalence of the triple helix structure of collagen after THC addition and 3D printing, as also observed by FTIR analysis. Additionally, samples with THC showed a small peak around 95 °C, related to THC melting (Kakkar et al., 2018), and the enthalpy value increased with THC content.

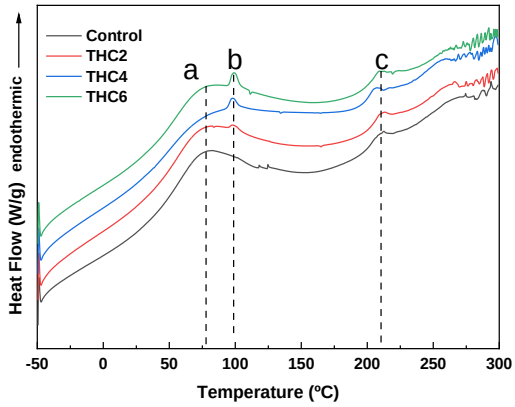

Figure 7.6. DSC thermograms of collagen scaffolds: a) free and bond water release, b) THC melting, and c) collagen denaturation.

7.2.3 Morphological and barrier properties

For a further analysis of the effect of THC addition on collagen structure, XRD and SEM analyses were carried out. As for XRD analysis (**Figure 7.7**), all samples showed XRD patterns of nearly amorphous materials. The peak around 7°, related to the triple helix structure of collagen, represents the lateral packing distance between collagen chains (Valencia et al., 2019) and the broad peak around 20°, associated with the diffuse scattering of collagen fibers, represents the amorphous structure of the samples (Zou et al., 2017). Furthermore, the samples with THC showed the characteristic peaks of THC at 18° and 24° (Rramaswamy et al., 2018). As can be seen, all samples showed similar XRD patterns, indicating the prevalence of the collagen structural order. When a higher THC content was added (THC6), the peak intensity at 7° and 20° decreased, suggesting the decrease of the structural order in collagen scaffolds.

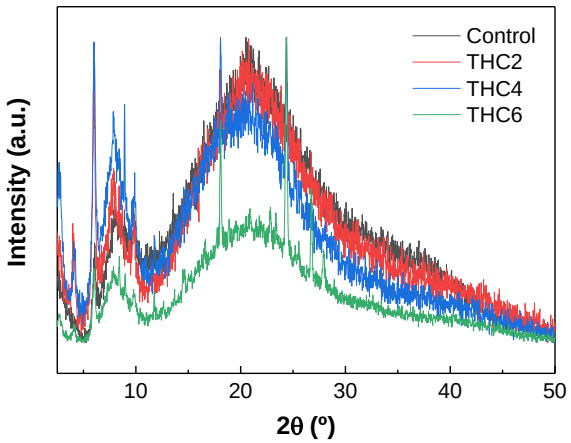

Figure 7.7.XRD patterns of collagen scaffolds.

To assess the morphology of 3D printed scaffolds and ensure a good comprehension of the microstructure of the scaffold, SEM analysis was carried out and cross-section images are shown in **Figure 7.8.** SEM micrographs showed that all samples had a similar compact amorphous structure. When THC content increased from 4 to 6 wt %, a less organized structure was observed, in accordance with XRD results. It is worth noting that 3D printed layers cannot be differentiated, indicating their good adhesion.

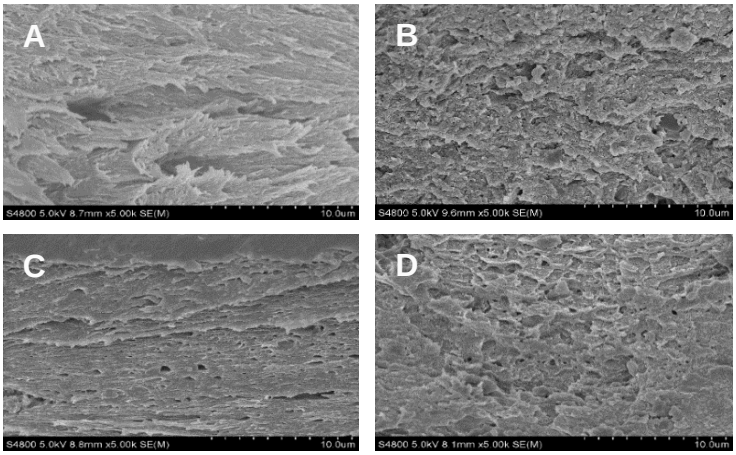

Figure 7.8.SEM images of the cross-section of collagen scaffolds: A) control, B) THC2, C) THC4, and D) THC6.

Considering wound dressing as a feasible application of these scaffolds, UV–vis spectroscopy was carried out. As can be seen in **Figure 7.9**, control samples showed the characteristic UV light barrier of collagen with an absorbance maximum from 200 to 250 nm, associated with carbonyl, carboxyl and amide groups, and a small peak between 250 and 280 nm, related to chromophores groups of tyrosine and phenylalanine amino acids (Kezwón et al., 2016; Trivedi et al., 2017). The addition of THC showed a slight increase of the absorbance in the visible light range (400–800 nm) and a strong increase in the UV range (200–400 nm) due to the absorption peak of THC around 280 nm with a shoulder at 310 nm (Adriani, Rahayu & Saepudin, 2020). Furthermore, the increase of the absorbance around 210 nm may be related to the photo-oxidized THC (Castellan et al., 2007). Nevertheless, no relevant difference was observed when THC was added.

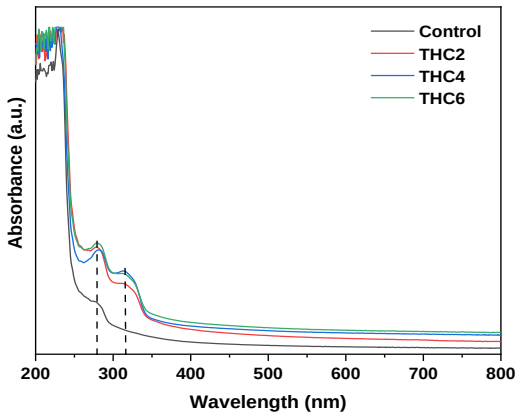

Figure 7.9. UV-vis spectra of collagen scaffolds.

7.2.4 Water uptake (WU) and THC release

WU measurements were performed to determine the effect of THC on the water absorption capacity of the scaffolds. WU results showed the capacity of collagen scaffolds to hold a large number of water molecules. As can be observed in **Figure 7.10A**, THC concentration had no relevant effect on the WU capacity, which was around 600%. The continuous growth of WU values occurred until 1880 min, when the equilibrium was achieved. It is worth noting that scaffolds were stable and maintained integrity during the immersion period analyzed in this study.

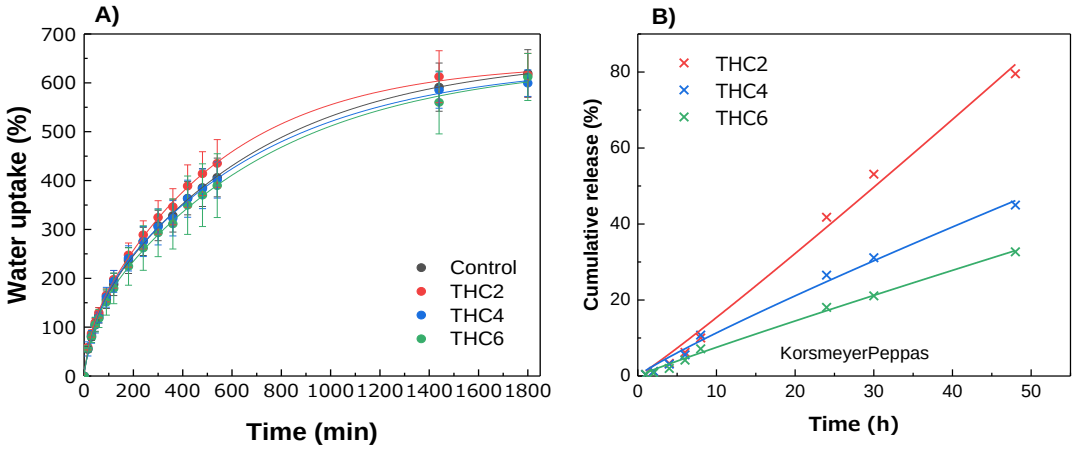

Figure 7.10. A) Water uptake and B) THC release from THC–collagen scaffolds (data fitted to Korsmeyer–Peppas model).

The release of THC from collagen scaffolds was assessed to determine the delivery trend. As can be observed in **Figure 7.10B**, all samples showed a sustained drug release, in which 82%, 45%, and 33% of THC was released from THC2, THC4, and THC6, respectively. It is worth noting that no initial burst of drug release was observed, probably due to collagen–THC interactions by hydrogen bonding (**Figure 7.5**), as suggested by FTIR analysis, and due to the compact structure observed by SEM. In order to provide a more sustained release, THC6 scaffold could be preferred.

For a better understanding of the release mechanism, experimental THC release data were fitted to the Korsmeyer–Peppas model and the estimated kinetic parameters are summarized in **Table 7.2**. As can be seen, the release data were well-fitted to the

Korsmeyer–Peppas model, with R^2 values higher than 0.9900. The value of *n* indicates the mechanism that describes how the active compound is released from the matrix. In this study, *n* values were higher than 0.89, indicating that the case II release mechanism controls the THC release (Abubakr, Lin & Chin, 2009). These results are particularly interesting since case II release is purely controlled by the swelling of the hydrophilic glassy polymeric system through the relaxation of collagen chains, indicating that the drug transport mechanism is independent of time (Supramaniam et al., 2018; Vigata et al., 2020).

Table 7.2. Parameters of Korsmeyer–Peppas model for THC release from collagen scaffolds.

Samples	THC2	THC4	THC6
K	1.3227	1.4457	0.8651
N	1.0660	0.8947	0.9406
R^2	0.9913	0.9900	0.9944

7.2.5 Mucoadhesive properties

Considering the potential application of these collagen scaffolds as a local treatment of wounds, a good adhesiveness is essential to immobilize the scaffold, which is the drug-delivery device, on a specific site for targeted release and optimal drug delivery. Mucoadhesion is defined as the adhesion between the polymer and the mucus and intimate contact between them must be formed for the occurrence of mucoadhesion (Boddupalli et al., 2010). In this study, mucoadhesive properties of wet collagen scaffolds in contact with type II mucin from porcine stomach were measured. The height of the peak is the maximum force (F_{max}) required to separate the probe from the mucin, while the total amount of forces involved in the probe withdrawal from the mucin is the work of adhesion (W_{adh}), calculated from the area under the force versus distance curve (Thirawong et al., 2007). All the scaffolds investigated in this study showed positive adhesive forces and, therefore, some form of adhesion occurred between mucus and

collagen. Representative load versus deformation curves for THC–collagen scaffolds are displayed in **Figure 7.11**. All the recordings from the mucoadhesion experiments showed a similar shape.

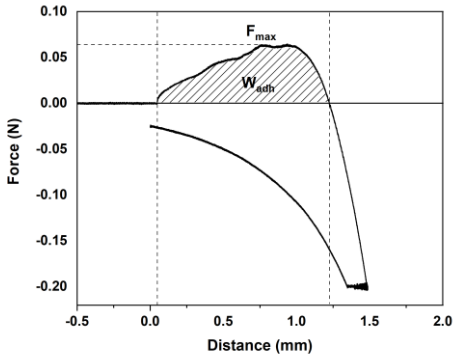

Figure 7.11. Characteristic load versus deformation curve for the collagen scaffolds analyzed in this study. THC2 scaffold.

The good mucoadhesive properties observed on all the samples is the result of the physical interactions among the mucin and collagen, mainly by hydrogen bonding and Van der Waals attraction. These forces are related to the amino acid residues in collagen that form hydrogen bonds with the glycoproteins in mucin (Soe et al., 2020). Due to these weak interactions between collagen and mucus, fracture strengths were moderate. The forces produced were mainly due to either mechanical engulfment of the collagen by the mucus or by mechanical penetration of the mucus into collagen crevices. When fracture occurred, collagen almost “popped” out of the mucus layer, as if mucin was not bound to collagen. A failure occurred nearly at the same stage position as the point of initial contact.

As can be seen in **Table 7.3**, similar ($P > 0.05$) F_{max} and W_{adh} values were found. The incorporation of THC did not affect F_{max} and W_{adh} values of collagen scaffolds. It is worth noting that different responses can be obtained depending on the analysis type used and the testing conditions employed (Bassi da Silva et al., 2018). Additionally, the mucoadhesive behavior of pure collagen has not been widely studied and, thus, data for comparison have not been found. Therefore, the results of this report should open new

avenues of thought regarding the properties of bioadhesive candidates, although further work is needed to promote their application for wound healing.

Table 7.3. Mucoadhesive properties of collagen scaffolds in terms of the detachment force (F_{max}) and the work of adhesion (W_{adh}).

Samples	F_{max} (N)	W_{adh} (N·mm)
Control	0.0652±0.0035[a]	0.0492±0.00304[a]
THC2	0.0672±0.0020[a]	0.0475±0.00203[a]
THC4	0.0681±0.0020[a]	0.0494±0.00303[a]
THC6	0.0699±0.0030[a]	0.0485±0.00233[a]

[a]Means followed by the same letter in the same column do not differ statistically among themselves by Tukey test ($P < 0.05$).

7.3 CONCLUSIONS

Collagen scaffolds with controlled THC delivery and potential for local wound healing were developed by 3D printing. The samples were prepared with high collagen concentration (200 mg/mL) and rheological analysis showed suitable flow behavior to be 3D printed. Neither the addition of THC nor the 3D printing conditions affected the triple helix structure of native collagen, as observed by SEM and XRD analyses, although physical interactions between collagen and THC were suggested by FTIR analysis. Furthermore, the high water holding capacity of THC–collagen scaffolds, together with the sustained THC release and mucoadhesive properties, make these scaffolds potential candidates for wound healing application. In this sense, the sample with 6 wt % THC could be preferred for a more sustained release of the bioactive. In future works, in vitro assays will be carried out to assess the scaffold stability in cell culture conditions as well as cell viability, adhesion, and spreading. Additionally, *in vivo* tests will be performed to show the therapeutic effect of these scaffolds and their potential in promoting wound healing processes.

Chapter 8

ZnO NANOPARTICLES CONTAINING COLLAGEN FILMS

ZnO nanoparticle-incorporated collagen films by solution casting with electro-conductive properties

.

8.1 SUMMARY

Collagen obtained from bovine skin was mechanically pre-treated with the aim of preserving the triple helix structure of native collagen. Furthermore, zinc oxide nanoparticles were incorporated into film forming formulations due to their inherent biological properties, which are of great relevance for biomedical applications. All the films showed good mechanical properties with a predominant elastic behavior, as shown by dynamic mechanical analysis (DMA) curves, and collagen films were easy to handle in both dry and wet states. It is worth noting that the integrity in the wet state was achieved without incorporating chemical crosslinkers, in contrast to chemically treated collagen that must be crosslinked chemically due to collagen denaturation after the pre-treatment. As shown by Fourier Transform Infrared (FTIR) spectroscopy analysis, collagen preserved the triple helix structure, although a slight decrease was observed with the increase of zinc oxide nanoparticles (ZnO NPs) content, which slightly increased the equilibrium water uptake values and also caused some changes in the denaturation collagen peak observed above 200 ºC by Differential Scanning Calorimetry (DSC) measurements. Additionally, collagen films showed good barrier properties, protection again Ultraviolet (UV) light and optimal Water Vapor Permeability (WVP) values (occlusivity) for biomedical purposes such as wound healing, since the WVP values measured would allow exudate absorption. Regarding electrical conductivity, collagen films presented a semiconductor behavior and memory properties and, thus, these films could be used as biosensors.

8.2 RESULTS AND DISCUSSION

8.2.1 Amino acid composition

In order to identify the amino acids composition in bovine skin native collagen and treated collagen, elemental analysis was performed and the amount of each amino acid residue is shown in **Table 8.1**. Glycine is the major amino acid in both collagens,

followed by proline and alanine. The content of both proline and hydroxyproline is 22.1 % in native collagen and 22.6 % in treated collagen. Furthermore, histidine, lysine and hydroxylysine residues were around 3.7 % in both collagens, and no cysteine was found indicating that there were no thiol groups present in collagen.

Amino acid analysis showed that glycine was the most abundant residue in native and treated collagen. Since glycine is the smallest amino acid, its repetition throughout the protein sequence allows close packing of the chains (Piez, 1984). Furthermore, the high content of both proline and hydroxyproline plays an important role in the structural integrity of collagen, forming hydrogen bonds between collagen α-chains and limiting rotation (Ramachandran, 1988). Moreover, proline and hydroxyproline contain the pyrrolidine ring, which helps to strengthen the triple helix structure of the collagen (Minh et al., 2014; Pal & Suresh, 2017). Therefore, the amino acid analysis suggests that the stability of the triple helix remains practically intact after the treatment performed. In fact, hydrogen bonding is known to play a significant role in the formation and stabilization of protein secondary structure.

Table 8.1. Amino acid composition of bovine skin native collagen and treated collagen (expressed as residues/1000 residues).

Amino acid	Native collagen	Treated collagen
Aspartic acid	45.3	44.8
Threonine	16.1	15.9
Serine	37.0	36.8
Glutamic acid	72.5	73.0
Glycine	330.9	331.2
Alanine	109.7	108.9
Valine	18.7	17.8
Methionine	6.0	6.2
Isoleucine	10.3	9.8
Leucine	28.8	33.8
Tyrosine	5.7	6.5
Phenylalanine	15.6	15.9
Hydroxylysine	6.7	6.8
Lysine	25.7	26.4
Histidine	4.5	4.3
Arginine	45.4	45.4
Hydroxyproline	98.1	93.6
Proline	122.9	122.8

8.2.2 Physicochemical properties

The interactions among the components of the films and the integrity of collagen structure were assessed by FTIR analysis and FTIR spectra are exhibited in **Figure 8.1**. All the spectra showed the characteristic absorption bands assigned to the peptide bonds in collagen. Specifically, the absorptions related to the amide A, amide I, amide II and amide III bands appeared at 3300, 1634, 1544, and 1238 cm^{-1}, respectively (Riaz et al., 2018). The amide A band, corresponding to O-H and N-H stretching vibrations, which typically appears at 3400 cm^{-1} in collagen, shifted to 3300 cm^{-1}, indicating hydrogen bonding between collagen, glycerol and ZnO (Duan et al., 2009; Liao et al., 2018).

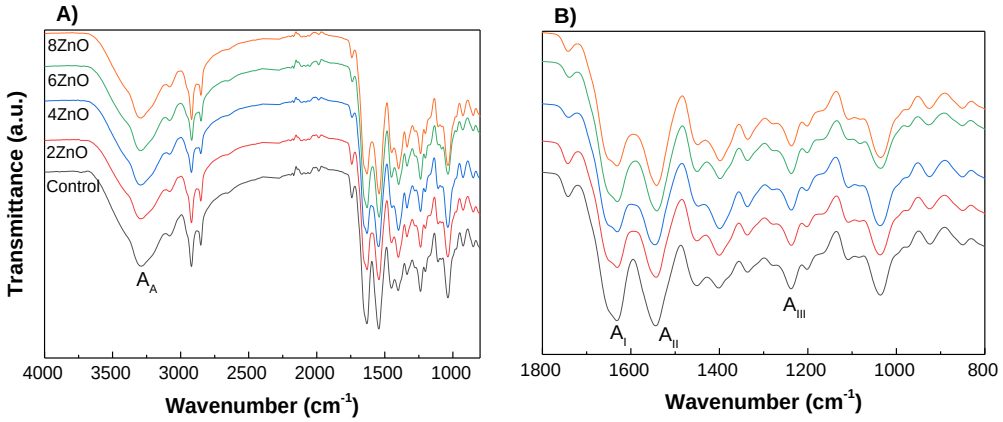

Figure 8.1. FTIR spectra of collagen sheets with different ZnO NPs contents: A) from 4000 to 800 cm^{-1} and B) from 1800 to 800 cm^{-1}.

In particular, interpeptide hydrogen bonding stabilizes secondary structures such as the α-helix and β-sheet conformations; therefore, the amide I profile was analyzed with the aim of assessing the effect of ZnO NPs on the secondary structure of collagen. Amide I contains three major components: a band at 1650 cm^{-1}, associated to the α-helix/random coil conformation, and two bands corresponding to the β-sheet conformation, which appear at 1615 – 1630 cm^{-1} and 1680 – 1700 cm^{-1} (Etxabide et al., 2016). As shown in **Table 8.2**, the addition of ZnO NPs, decreased the content of α-helix conformation. Additionally, the preservation of the integrity of the triple helix structure of collagen was estimated from the absorption ratio between the Amide III band and the

band at 1452 cm^{-1} (A_{III}/A_{1452}) (Shi et al., 2019). As shown in **Table 8.2**, the A_{III}/A_{1452} ratio slightly decreased, indicating that ZnO NPs slightly modified the triple helical structure of collagen.

Table 8.2. Area (%) of the curve fitting of amide I and absorption ratio between amide III band and the band at 1452 cm^{-1} (A_{III}/A_{1452}) for ZnO NPs-collagen films.

Samples	β- Sheet (%)	α- helix/random coil (%)	A_{III}/A_{1452}
Control	36.28	63.72	1.00
2ZnO	36.38	63.62	0.99
4ZnO	38.63	61.37	0.97
6ZnO	40.84	59.16	0.95
8ZnO	42.94	57.06	0.93

The moisture content (MC) and the mass loss (ML) of the films were also analyzed and values are shown in **Table 8.3**. On the one hand, all films showed low MC values, decreasing ($P < 0.05$) from 2.0 to 0.6 % when ZnO NPs content increased. This slight variation in moisture content may be associated with the hydrophobicity of ZnO NPs (Ni et al., 2018). On the other hand, mass loss values increased ($P < 0.05$) from 12.9% in control samples to 22.8% in 8ZnO samples. The mass loss of control sample can be attributed to the partial dissolution of glycerol. Moreover, the increase in mass loss values can be associated with the slight loss of the triple helix structure, as shown by A_{III}/A_{1450} ratio (**Table 8.2**), which would allow an easier diffusion of glycerol into PBS.

Table 8.3. Moisture content (MC) and mass loss (ML) of ZnO NPs-collagen films.

Samples	MC (%)	ML (%)
Control	2.0 ± 0.3^{a}	12.9 ± 1.8^{a}
2ZnO	1.0 ± 0.1^{b}	16.7 ± 1.1^{b}
4ZnO	0.9 ± 0.1^{bc}	17.3 ± 1.3^{b}
6ZnO	0.7 ± 0.1^{bc}	22.4 ± 0.9^{c}
8ZnO	0.6 ± 0.2^{c}	22.8 ± 0.8^{c}

$^{a-c}$Two means followed by the same letter in the same column are not significantly ($P > 0.05$) different through the Tukey's multiple range test.

Considering that one potential application of collagen films can be as wound dressings, water uptake tests were carried out and results are shown in **Figure 8.2**. It is worth noting that all samples maintained their structural integrity after immersion in PBS. Water uptake increased rapidly in the first 30 min and the equilibrium, around 100% for control sample and around 130% for samples with ZnO NPs, was achieved after 150 min of immersion in PBS. In accordance with FTIR and ML results, water uptake behavior suggested the existence of physical interactions between ZnO NPs and collagen, which would increase the space between collagen chains and facilitate the film swelling. Collagen films showed the characteristic properties of hydrogels, allowing the permeation of bioactive compounds into the system effectively.

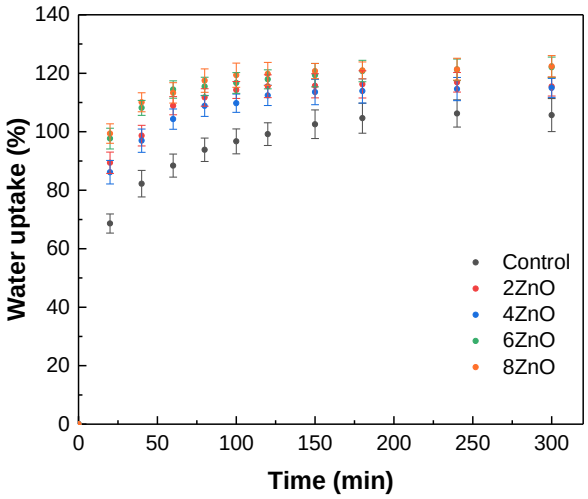

Figure 8.2. Water uptake curves of collagen films with different ZnO NPs contents.

8.2.3 Thermal properties

Thermal denaturation of collagen induces modifications in the collagen structure that can be followed by DSC. All samples exhibited two endothermic peaks, as shown in **Figure 8.3**. The first peak, situated around 100 ºC, was related to free water release (Miles & Gelashvili, 1999). This peak temperature increased with the addition of ZnO NPs due to the decrease of moisture content (Rochdi, Foucat & Renou, 1999), as shown in **Table 8.3**. The second endothermic peak appeared between 210 and 250 ºC and it

was associated to the denaturation of collagen (Bozec & Odlyha, 2011). The denaturation peak of collagen changed with the addition of ZnO NPs, specifically, the height of this denaturation peak decreased and its width increased, which may be associated to the conformational changes from a triple helix to a random coil structure observed by FTIR analysis.

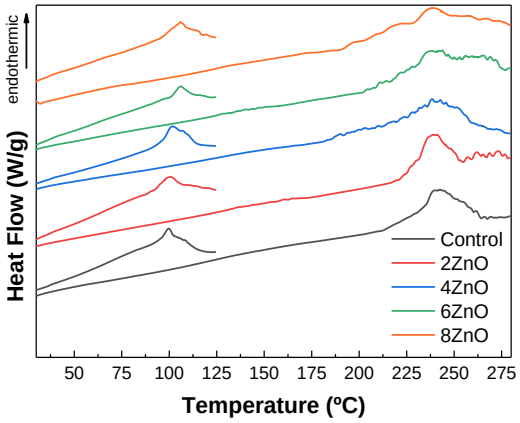

Figure 8.3. DSC thermograms of collagen films with different ZnO NPs contents.

In order to study the effect of ZnO NPs in the viscoelastic behavior of collagen films, DMA was carried out and the temperature dependence of storage modulus (E') and loss modulus (E'') of collagen films is shown in **Figure 8.4A**. The storage modulus (E') is generally related to the stored energy, representing the elastic behavior of the material, while the loss modulus (E'') is used to indicate the energy dissipated as heat (Guerrero et al., 2019). The films showed higher E' values than E'' values, in the whole temperature range, which determined the predominantly elastic character of the films. As the temperature increased, the samples moduli decreased. The moduli decreased slowly until -10 ºC and then, they dropped sharply up to 20 ºC for the control samples and 30 ºC for the films with ZnO NPs. This sharp reduction of storage modulus involved the transition of the material from the glassy to the rubbery state (Guerrero et al, 2019). Afterwards, and up to 80 ºC, an increase was observed, related to the triple helix structure of collagen. This increase in the temperature at which the minimum values of storage and loss moduli are found with the addition of ZnO NPs may corroborate the

interactions observed by FTIR and DSC analyses. Additionally, the subsequent increase of storage and loss moduli after the achievement of the minimum value was smaller for 6ZnO and 8ZnO films, in accordance with the decrease in the content of triple helix structure shown by FTIR results (**Table 8.2**).

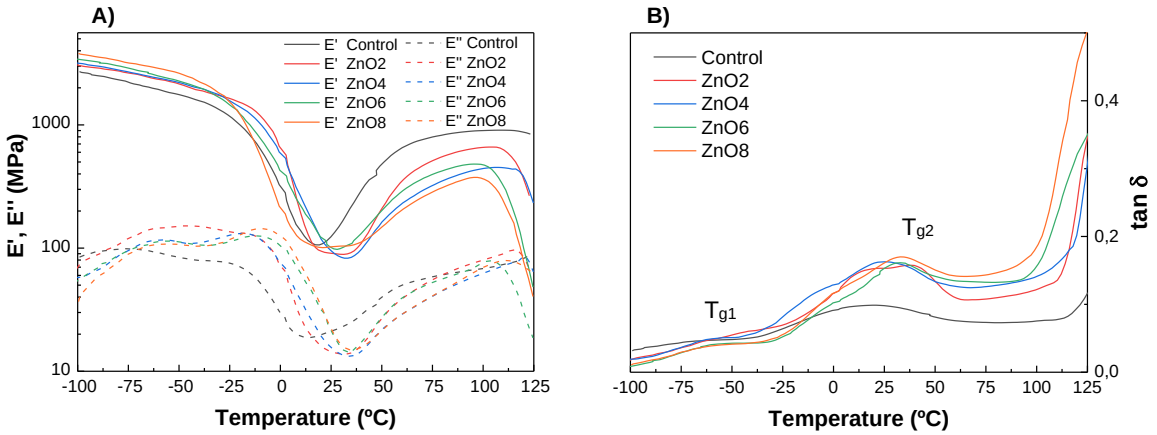

Figure 8.4. Temperature dependence of A) the storage modulus (E'), loss modulus (E") and B) loss tangent (tan δ) curves for collagen films with different ZnO NPs contents.

The loss factor (tan δ), defined as the ratio between loss modulus and storage modulus (tan δ = E''/E'), is represented in **Figure 4B**. The temperature at which the loss factor is maximum is defined as the glass transition temperature (T_g). The first glass transition (T_{g1}), at around -60 ºC, was attributed to the glass transition of glycerol. The second glass transition (T_{g2}), at around 20 ºC for control film and 30 ºC for ZnO NPs-collagen films, was attributed to the glass transition of collagen. This increase in T_{g2} could be related to the decrease of film moisture content (Rochdi, Foucat & Renou, 1999), as shown in **Table 8.3**.

8.2.4 Barrier, mechanical and electrical properties

Light barrier properties were analyzed and UV-vis spectra are shown in **Figure 8.5**. As can be seen, the films exhibited a maximum absorbance peak from 200 to 240 nm, associated with C=O, COOH, and $CONH_2$ groups in collagen chains (Pal, Nidheesh & Suresh, 2015; Veeruraj, Arumugam & Balasubramanian, 2013), and a small absorption

peak at 250-280 nm, associated to tyrosine and phenylalanine amino acid residues in collagen (Duan et al., 2009; Huang et al., 2011). The addition of ZnO NPs influenced the films UV-vis absorbance, increasing slightly the absorbance in the visible light range (400-800 nm) and strongly in the UV range, concretely in the 250-280 nm range. Moreover, there was no ZnO NPs characteristic absorption peak near 360 nm, suggesting that there were not ZnO NPs with a size larger than the visible wavelength (Ni et al., 2018).

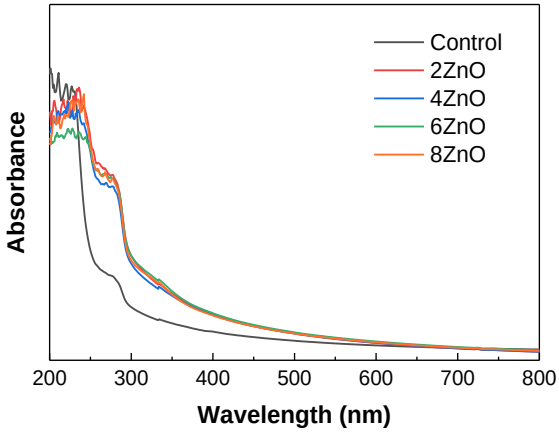

Figure 8.5. UV-vis spectra of the collagen films with different ZnO NPs contents.

In order to assess if collagen films could maintain an acceptable level of moisture in the wound when applied as wound dressings, the occlusivity of the films was evaluated measuring water vapor permeability. Water vapor permeability is a two-step process: water vapor sorption and water vapor diffusion (Uranga et al., 2019) and it depends on the collagen structure, organization and interactions of collagen molecules in the film (Ma et al., 2018). As can be seen in **Table 8.4**, there was no difference ($P > 0.05$) with the increase of ZnO NPs content and all samples showed a high occlusive character, with WVP values within the range of commercial wound dressings. Thus, they presented an adequate control of moisture, allowing exudate to evaporate, while maintaining some moisture into the wound to prevent tissue dehydration and help in re-epithelization.

In addition to barrier properties, mechanical properties are of great importance to assure that the films are easy to handle. In order to assess the mechanical behavior of

collagen films, elastic modulus (EM), tensile strength (TS) and elongation at break (EB) were measured. As shown in **Table 8.4**, EM and TS increased ($P < 0.05$) when ZnO NPs were incorporated into the collagen formulation; however, these values did not change when ZnO NPs increased, as also observed for EB values.

Table 8.4. Water vapor permeability (WVP), elastic modulus (EM), tensile strength (TS), and elongation at break (EB) of collagen films prepared with different ZnO NPs contents.

Samples	WVP 10^{12} ($g \cdot cm^{-1} \cdot s^{-1} \cdot Pa^{-1}$)	EM (MPa)	TS (MPa)	EB (%)
Control	4.9 ± 0.3^{a}	382.8 ± 19.8^{a}	15.9 ± 1.7^{a}	14.4 ± 0.8^{a}
2ZnO	5.6 ± 0.2^{b}	430.7 ± 19.3^{b}	17.7 ± 1.6^{ab}	13.7 ± 0.7^{ab}
4ZnO	5.8 ± 0.4^{b}	445.8 ± 12.3^{b}	18.3 ± 0.7^{b}	13.2 ± 0.2^{b}
6ZnO	5.9 ± 0.4^{b}	452.4 ± 12.1^{b}	18.9 ± 0.4^{b}	13.1 ± 0.5^{b}
8ZnO	5.9 ± 0.6^{b}	455.8 ± 7.2^{b}	19.6 ± 1.3^{b}	12.9 ± 0.6^{b}

$^{a-b}$Two means followed by the same letter in the same column are not significantly ($P > 0.05$) different through the Tukey's multiple range test.

Considering the special attention acquired by electro-conductive biocompatible materials for tissue engineering applications, the electrical properties of the films were analyzed from the intensity-voltage (I-V) curves shown in **Figure 8.6**. It is well known that the electrical conductivity of proteins increases enormously with increasing content of adsorbed water, but the conductivity of both wet protein and dry proteins is almost purely electronic. The adsorbed water decreases the semiconduction activation energy, which is lower than 3.0 eV, but does not change the number of states available for releasing mobile charge or the mobility of the charge carriers (Rosenberg, 1962).

As can be seen in **Figure 8.6A**, collagen films showed electrical conductivity from negative to positive voltage and also from negative to positive voltage. When a positive current passed through the films and operated in the top right quadrant, the curve increased gradually in an extremely small current and voltage. The voltage was swept first from −20 V up to +20 V and then backwards, from +20V to −20 V. When the forward voltage exceeded 20 V, which was the film internal barrier voltage, avalanche occurred

and the forward current increased rapidly for a small increase in voltage producing a non-linear curve, called the “Knee” point. Likewise, when a negative current passed and operated in the bottom left quadrant of the curve, a small gradual decrease of the film electrical resistance was observed, until the reverse voltage across the film became greater than its breakdown voltage point, resulting in a sudden increase in reverse current, producing a fairly straight line downward curve as the voltage losses control. This procedure was repeated several times and **Figure 8.6B** shows the successive sweeps, and it presents the electrical behavior of a collagen film when a current sweep is applied and it shows the reproducibility of the semiconductor electrical behavior. As can be seen, the initial pinched hysteresis was shifted towards higher currents in the consecutive sweeps, but preserved its shape, illustrating clearly another property of the memristor: memory. Furthermore, all collagen films showed the characteristic semiconductor electrical behavior and similar resistance values were observed for all films regardless of ZnO NPs contents, as shown in **Figure 8.6C.**

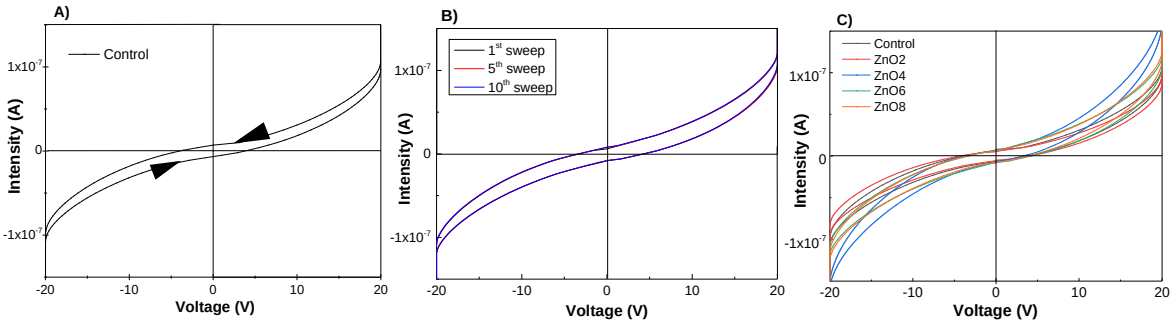

Figure 8.6. Intensity-voltage curves of collagen films with different ZnO NPs contents.

8.2.5 Morphological properties

In order to determine the film microstructure and relate it to the properties measured, XRD and SEM analyses were carried out. All the films exhibited XRD patterns of amorphous materials (**Figure 8.7**). The peak around 7º indicated the intermolecular lateral packing distance between the molecular collagen chains (Valencia et al., 2019), which is related to the triple helix structure of collagen and, thus, its presence indicated

the maintenance of this structure after the addition of ZnO NPs. The broad band centered at 20º is associated to the diffuse scattering of collagen fibers, indicating the amorphous structure of the films. It is worth noting that the characteristic peaks of ZnO at ~31.5º, ~34.4º, and ~36.2º could not be observed due to the interactions between collagen and ZnO NPs, as shown by FTIR analysis.

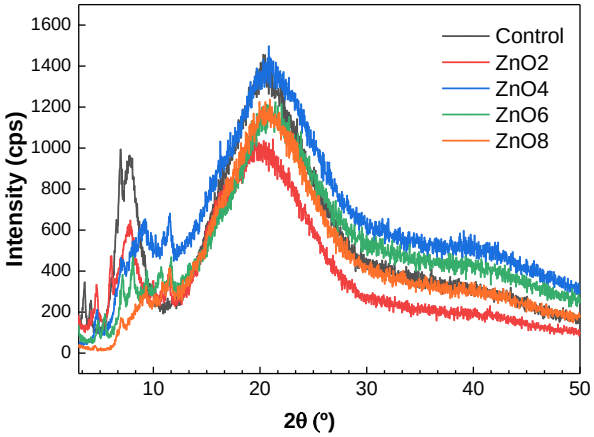

Figure 8.7. XRD patterns of collagen films prepared with different ZnO NPs contents.

To further assess the changes caused by the addition of ZnO NPs in the collagen films, SEM analysis was carried out and the images of cross-sections are shown in **Figure 8.8**. SEM micrographs exhibit the dense network of fibers in control films (**Figure 8.8A**). With the addition of ZnO NPs (**Figure 8.8B** and **8.8C**) the fibers were not further shown, indicating a structural change to a more compact network, in accordance with the gradual decrease shown in the lateral packaging of collagen chains observed by XRD analysis. Therefore, considering the preservation of the collagen triple helix shown by FTIR results (**Table 8.2**), this difference might be related to the decrease of the lateral packing among chains observed by XRD (**Figure 8.7**).

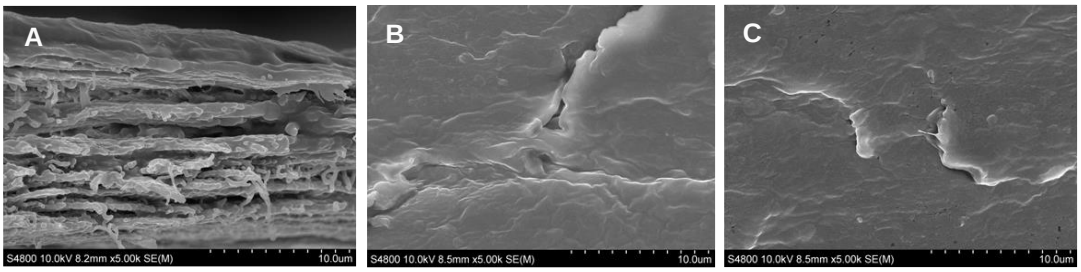

Figure 8.8. SEM images of the cross-sections for A) control, B) 4ZnO, and C) 8ZnO films.

8.3 CONCLUSIONS

Collagen was mechanically pretreated, maintaining its native structure, and subsequently processed to obtain films with induced electro-conductive properties, which could be used to promote cell growth and make these collagen films suitable for biomedical applications. With this in mind, zinc oxide nanoparticles (ZnO NPs) were incorporated into film forming formulations and the effect of ZnO NPs content was assessed. The obtained films showed good mechanical properties and were easy to handle, preserving their physical integrity after immersion into PBS and indicating the maintenance of the triple helix structure, as observed by FTIR analysis and corroborated by XRD results. This fact is of great relevance since the preservation of the triple helix structure allows to avoid the use of chemical crosslinkers, necessary when collagen is chemically treated due to collagen denaturation during the chemical treatment. Furthermore, collagen films showed good occlusivity values for the absorption of fluids, highlighting the potential use of these films as wound dressings. Additionally, collagen films showed a semiconductor behavior, which was maintained after current sweeps and with the incorporation of ZnO NPs.

Chapter 9

IONIC LIQUIDS AND WOOL CONTAINING COLLAGEN FILMS

Ionic liquids and wool containing collagen films processed by solution casting for advanced applications

9.1 SUMMARY

In order to develop next generation advanced functional materials based on natural polymers for sustainable electronics, wool and choline dihydrogen phosphate ([Ch][DHP]) or choline serinate ([Ch][Seri) ionic liquids (ILs) were incorporated into native collagen formulations. Films were prepared by compression molding and their mechanical and electrical properties were analyzed and related to film structure. The denaturation peak observed by differential scanning calorimetry (DSC), along with infrared spectroscopy (FTIR) results, showed that the fibrillary structure of collagen was preserved in all samples. These outcomes were correlated with X-Ray spectroscopy (XRD) patterns, in which slight differences in lateral packaging and structural order were observed. Furthermore, scanning electron microscopy (SEM) images showed a more compact structure when ILs or wool were added, explaining the detected lower water uptake capacity. It is worth noting that no agglomeration was observed in the films with ILs or wool, indicating the good dispersion of these additives in the films. Regarding mechanical properties, the addition of wool led to a significant increase in tensile strength (TS), while lLs caused a significant increase in both tensile strength (TS) and elongation at break (EB) values. Finally, the addition of ILs and wool improved the electrical conductivity of collagen and all films showed antistatic behavior in the range of $1.87\ 10^{-8}$ S/cm. It must be highlighted that no significant differences were observed between ILs containing films. The samples showed dielectric constant above 69 and tan δ values above 4.6, mainly determined by the mobile charge contributions. This work shows the potential of native collagen films with tunable physicochemical characteristics for a new generation of sustainable materials for a wide variety of applications.

9.2 RESULTS AND DISCUSSION

9.2.1 Rheological behavior

Compression molding is a processing method in which the raw material is summited to a determined pressure and temperature for a specific period by using a metal mold, in order to obtain the final product with a specific shape (Verma et al., 2021). In this sense, it is of great relevance to determine the minimum processing temperature at which collagen flows while preserving its native structure (Bozec & Odlyha, 2011). Therefore, the thermo-rheological behavior of the control sample was analyzed by performing temperature sweep tests in oscillatory shear. As can be observed in **Figure 9.1**, G´ was greater than G´´ at room temperature and, thus, the sample showed a predominant elastic behavior due to the limited molecular free motion (Tran-Ba et al., 2017). As the temperature increased, the storage and loss moduli, as well as the complex viscosity (η*), decreased down to a minimum value of 50 ºC, demonstrating a large influence of temperature on the collagen structure. This decrease of η* with temperature was related to the motion of collagen chains caused by the breakage of hydrogen bonds of free and bound water, as can be observed by the first endothermic peak of the DSC curves (**Figure 9.2**). In this regard, it has been analyzed the effect of temperature on the rheological properties of collagen solutions and defined the transition observed at 25-39 ºC as collagen denaturation temperature (Tian et al., 2016; Yoshimura, Chonan, & Shirai, 1999). However, taking into consideration that the thermal denaturation depends strongly on the degree of hydration (Bozec & Odlyha, 2011), collagen was minimally hydrated in this work to be processed at low temperature and avoid collagen denaturation. Furthermore, it is worth nothing that the viscous behavior predominated within the temperature range of 47-53 ºC, since G´´ was slightly higher than G´ and, thus, this represented the optimum temperature range to process collagen by compression molding.

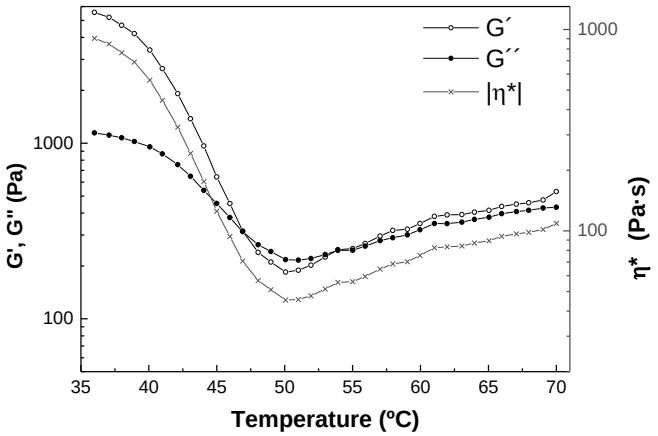

Figure 9.1. Storage moduli (G´), loss moduli (G´´), and complex viscosity (η*) of the control film as a function of temperature.

9.2.2 Thermal and physicochemical properties

While rheological properties provide information about the sample processability, thermal properties provide information about the effective temperature limits at processing conditions and the effect of manufacturing processes on collagen structure (Abeykoon et al., 2021). Therefore, DSC analysis was carried out and results are shown in **Figure 9.2**.

It can be observed that all samples exhibited the characteristic endothermic peaks of collagen: the first peak, around 75-80 ºC, was related to free and bound water release (Kaczmarek, Sionkowska, & Skopinska-Wisniewska, 2018); and the second phase transition, around 125 ºC, was associated to the denaturation of native collagen triple helix and, simultaneously, to the structural water release (Chakrapani et al., 2012). This denaturation peak also appeared when the additives were incorporated, indicating the maintenance of the triple helix structure after compression molding, even if the peak appeared at lower temperatures. It can be noted that the height of the first peak decreased when the additives were incorporated, probably due to the difference on moisture content of the samples (Rochdi, Foucat & Renou, 1999).

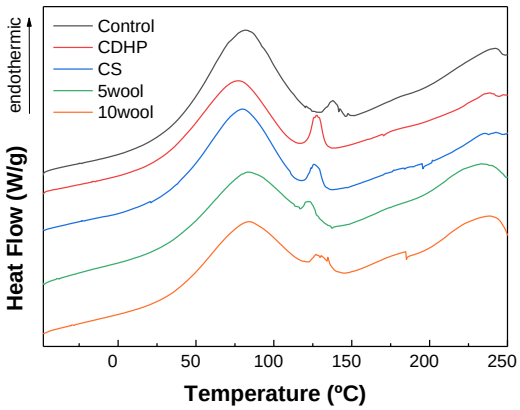

Figure 9.2. DSC thermograms of all collagen-based films.

In order to assess the interactions among the components of the films, FTIR analysis was carried out and the spectra are exhibited in **Figure 9.3A**. All the spectra showed the characteristic absorption bands assigned to the peptide bonds in collagen: amide I (C=O stretching), amide II (N-H bending) and amide III (C-N stretching) observed at 1632, 1540, and 1239 cm^{-1}, respectively (Barth & Zscherp, 2002; Riaz et al., 2018). No significant differences were observed when ILs or wool were added. Although the hydrocarboxylic radical of choline cation in ILs and phosphorus dioxide group in CDHP should be perceived at 1065 and 946 cm^{-1} (Reizabal et al., 2019), these bands were overlapped by the characteristic bands of glycerol in the region of 850-1000 cm^{-1}. Similarly, the disulphide linkages of keratin in wool should appear in the region of 998-1100 cm^{-1} (Cardamone et al., 2009).

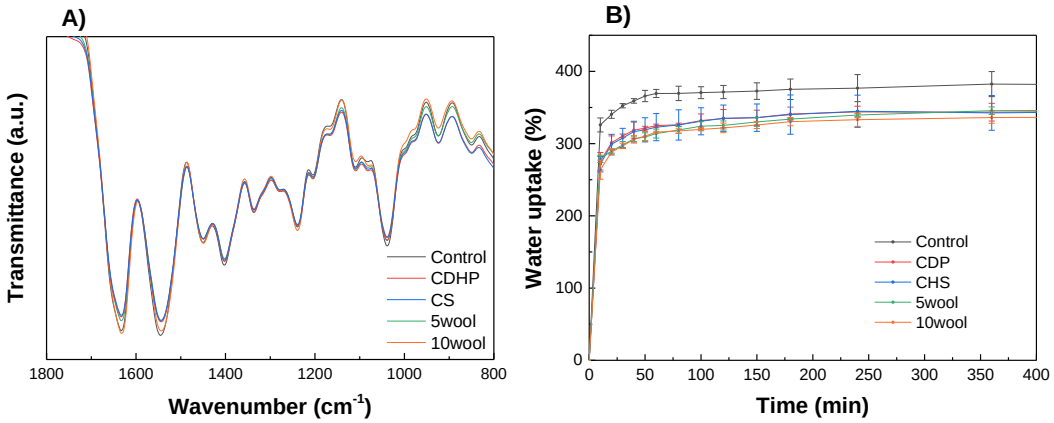

Figure 9.3. Physicochemical properties of collagen-based films: A) FTIR spectra from 1800 to 800 cm^{-1} and B) water uptake curves.

Additionally, water uptake tests were carried out and the results are shown in **Figure 9.3B**. In the first 10 min of immersion, the water uptake values increased rapidly due to the low thickness of the samples. After 60 min of immersion, the equilibrium values were achieved at around 375 % for control films and 325 % for the films with ILs or wool. These different water uptake values suggested that the incorporation of both ILs types or wool promoted the interactions with the polar groups of collagen and glycerol. As a consequence, polar groups were less accessible to interact with water molecules and, thereby, a lower water uptake degree was achieved. Furthermore, the more compact structure of the samples with ILs or wool, observed by SEM analysis (**Figure 9.4**), may decrease the water uptake values as well. It is also worth noting that no significant differences were observed between the water uptake values of the films with ILs or wool.

9.2.3 Morphological properties

The effect of ILs or wool on collagen structure was assessed by SEM and XRD analyses (**Figure 9.4**). Concerning SEM analysis, the micrograph of the cross-section in control films -pristine collagen- **(Figure 9.4A**) exhibited the dense network of collagen fibers. With the addition of ILs or wool (**Figure 9.4B-E**), fibers could not be observed, and a more compact structure was achieved, which could explain the lower water uptake capacity observed in the samples containing ILs or wool (**Figure 9.3B**). It is worth noting that no agglomeration was observed in the samples with ILs or wool, indicating the good dispersion of both ILs and wool within the films.

Regarding XRD analysis (**Figure 9.4F**), all samples showed the characteristic collagen amorphous structure, with a broad peak around 20º, associated with the diffuse scattering of collagen fibers (Zou et al., 2017). The first peak around 7º represents the triple helix structure of collagen and the lateral packing distance between collagen chains (Valencia et al., 2019). All samples showed similar XRD patterns, with a slight decrease in the intensity of the peak at 7º with the addition of wool, indicating a decrease in the

structural order of the samples when wool was incorporated. Additionally, a shoulder around 10º can be appreciated in 5wool and 10wool that may represent the α-helix structure of keratin in wool (Wang et al., 2016c). Furthermore, the incorporation of ILs or wool caused a decrease in the intensity of the peak at 20º, suggesting the decrease of the structural order in collagen films.

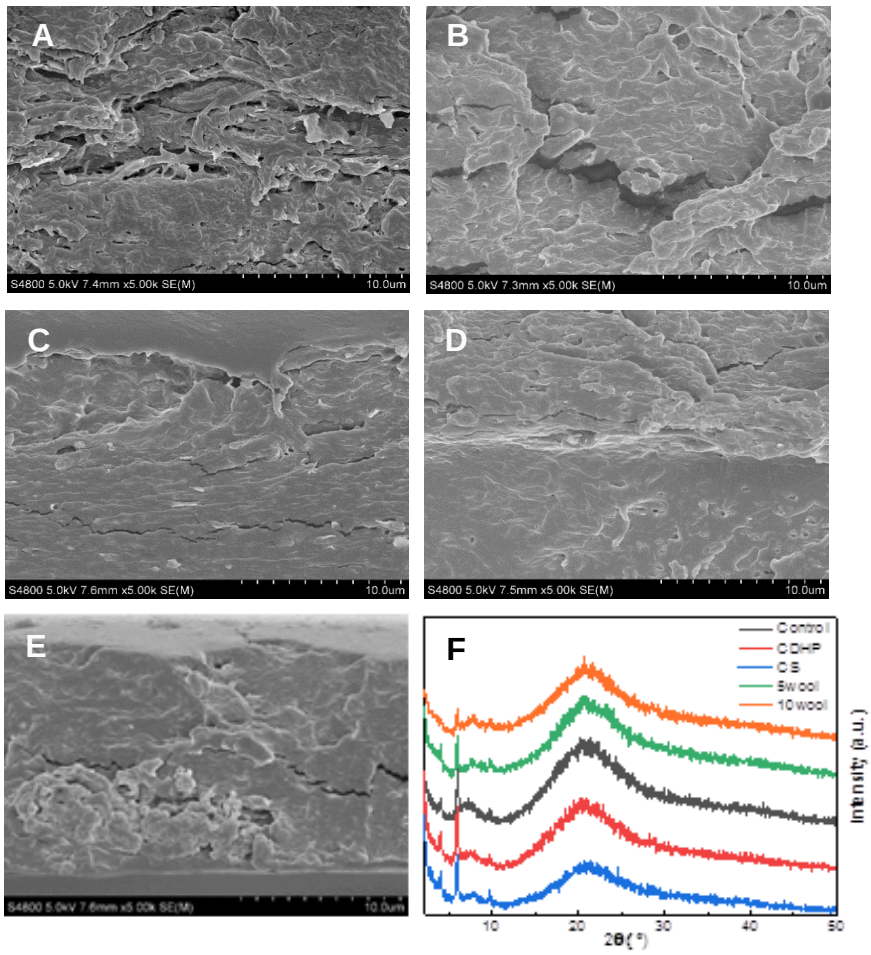

Figure 9.4. Morphological and structural properties of collagen films: SEM images of cross-sections for A) control B) CDHP, C) CS, D) 5wool, and E) 10wool films; and F) XRD patterns.

9.2.4 Mechanical properties

Tensile tests were performed in order to evaluate the effect of ILs or wool addition on tensile strength (TS) and elongation at break (EB) (**Table 9.1**). Furthermore, in Figure 9.5 the fibril structure of collagen and the effect of the ILs and wool addition can be observed. This behavior is associated to the fibril structure of collagen. As the elongation

increased, the fibers of collagen were orientated, increasing tensile resistance up to the point of break (Sherman, Yang & Meyers, 2015).

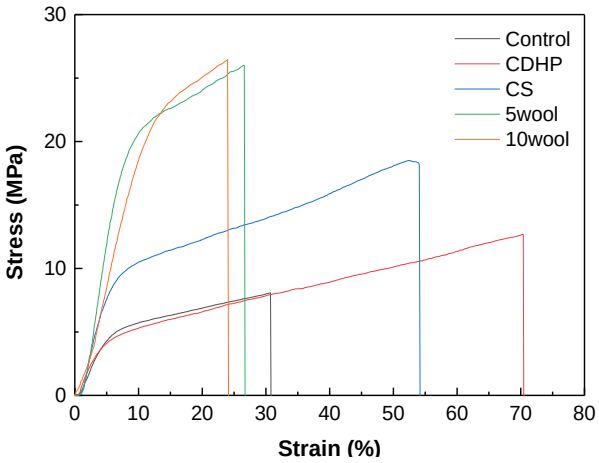

Figure 9.5. Stress-strain curves of collagen based films.

On the one hand, the addition of ILs caused a significant ($P < 0.05$) increase in both TS and EB values, attributed to the chemical structure of ILs and their role as plasticizers, respectively (Rahman & Brazel, 2006). On the other hand, when wool was added, TS significantly ($P < 0.05$) increased and EB decreased ($P < 0.05$). Although different collagen treatments and processing methods used in the works reported in the literature make comparisons difficult, a similar effect was shown for collagen films with casein (Wu et al., 2018), where TS values increased from 17.24 MPa to 24.87 MPa and, simultaneously, EB values decreased from 13.88 to 2.87 %.

Table 9.1. Tensile strength (TS) and elongation at break (EB) of the collagen-based films.

Samples	TS (MPa)	EB (%)
Control	7.36 ± 1.13^{a}	31.99 ± 4.68^{a}
CDHP	13.30 ± 0.33^{b}	$68.00 \pm 4.57^{a,b}$
CS	18.07 ± 1.16^{c}	57.72 ± 4.57^{b}
5wool	24.39 ± 3.64^{d}	27.25 ± 3.21^{c}
10wool	28.31 ± 2.85^{d}	23.30 ± 1.87^{d}

$^{a\text{-}d}$Two means followed by the same letter in the same column are not significantly ($P > 0.05$) different through the Turkey's multiple range test. N = 5 was the minimum number of replications.

9.2.5 Electrical and dielectric properties

Figure 9.6A shows the I-V curves obtained for the collagen pristine film and the ones reinforced with ILs or wool. The addition of ILs or wool improved the electrical conductivity of collagen.

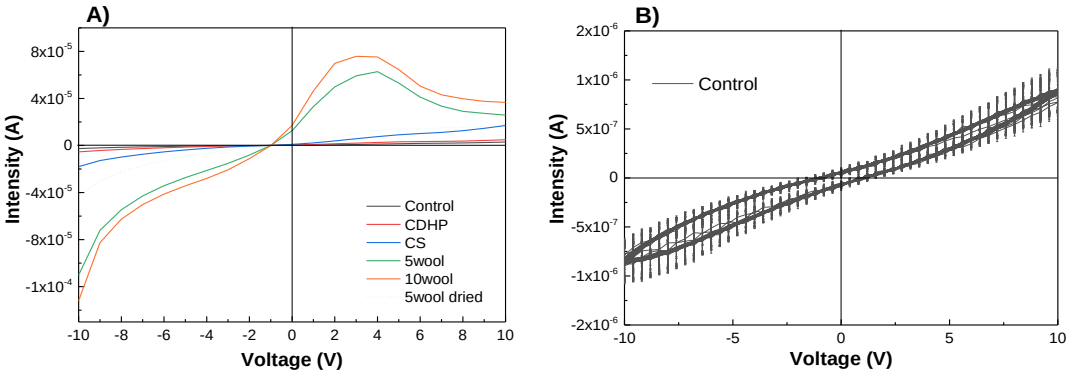

Figure 9.6. A) Current-voltage (I-V) curves and B) cycling current-voltage (I-V) curves.

As can be seen in **Figure 9.6A**, the collagen-based films show electrical conductivity values compatible with an antistatic behavior (Jachowicz, 2013). DC conductivity of pristine collagen films was 2.34×10^{-9} S/cm, and increases with the addition of IL, being 1.03×10^{-9} S/cm for CDHP and 1.87×10^{-8} S/cm for CS films. This increase is related to the increase of ionic mobile species associated to the IL. When wool is introduced in the films, the DC electrical conductivity increases with wool addition and with increasing wool content, due to the proton conduction of the hydroxyl groups present in the wool. In this case, it is interesting the nonlinear behavior and, in particular, the peak detected around 3 V, indicative of a variation of the conduction regime - decrease of the electrical conductivity-, related to the effect of absorbed water in wool, as demonstrated in the 5wool films (dot line in **Figure 9.5A**) in which the effect is reduced after drying, demonstrating the effect on proton conduction of the hydroxyl groups. Additionally, **Figure 9.6B** shows the I-V cycling curves for 20 cycles for the pristine collagen films, demonstrating a low hysteresis in the electrical conductivity, which is representative for the rest of the samples.

Figures 9.7A and **B** show the dielectric constant (ε') and the loss factor (tan δ), respectively. As the frequency increased, ε' and tan δ decreased indicating a slow dynamic of the contributions to the dielectric response, mainly attributed to mobile charge carriers. Furthermore, ε' and tan δ increased with the addition of ILs and 5 wt % wool due to the fact that these fillers increased the number of charge carriers. Further, the high values of ε' and, in particular, of tan δ demonstrate conductivity contributions to the dielectric response by the different charge carriers from collagen, wool and IL.

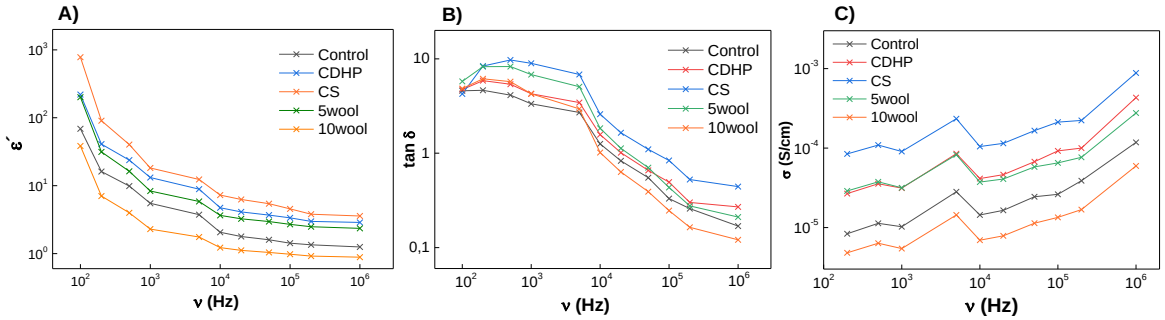

Figure 9.7. A) variation of ε', B) tan δ and C) AC electrical conductivity values as a function of frequency in a log–log plot.

As can be seen in **Figure 9.7C**, the conductivity increased with frequency, indicating strong contributions from localized charge carrier mobility. Two regimes in the conductivity behavior were observed in all films: one regime for medium frequencies up to 10^4 Hz, dominated by the DC conductivity; the second, at higher frequencies, assigned to the AC conductivity. Furthermore, the presence of ILs and 5 wt % wool increased the AC conductivity values compared to the control film due to the increased presence of localized charge carriers, contributing to the electrical response.

9.3 CONCLUSIONS

Advanced functional materials based on native collagen with ILs or wool were successfully prepared by compression molding, resulting in homogeneous and easy to handle films. The results found by DSC, FTIR, and XRD showed the prevalence of the collagen fibrillar structure in all films after the compression molding process. Regarding

physicochemical properties, lower water uptake capacity was observed with the incorporation of ILs or wool into the formulations, probably due to the formation of a more compact structure, as shown by the SEM images of film cross-sections. Furthermore, the addition of ILs or wool caused a significant increase in tensile strength and improved the electrical conductivity and dielectric response. The dielectric response of the samples demonstrated the mobile contributions, highlighting the potential of these collagen films for an antistatic application with a focus on sustainability.

Chapter 10

GENERAL CONCLUSIONS

The general conclusions of this doctoral thesis are summarized as follows:

- Collagen sheets and films were successfully prepared by compression molding, maintaining the triple helix structure of collagen.
- Functional properties of collagen for biomedical applications were enhanced by incorporating 20 wt % aloe vera.
- Chitosan-collagen films with enhanced functional properties for wound healing were developed. No significant differences were found as a function of the molecular weight of chitosan.
- The high water holding capacity, the sustained THC release, and mucoadhesive properties of THC–collagen scaffolds make them potential candidates for wound healing applications.
- The good occlusivity values for the absorption of fluids, together with the induced electro-conductive properties, highlight the potential of collagen films with ZnO NPs as wound dressings.
- Advanced functional materials based on native collagen with ILs or wool, which could be potentially used in antistatic applications, were successfully prepared.
- Mechanical stirring and freeze-drying were the processes with a higher environmental load. Although scaling up the production of collagen biomaterials could notably reduce those impacts, further research is needed in order to optimize processes.

Chapter 11

REFERENCES

Abdollahi, M., Rezai, M., Jafarpour, A. & Undeland, I. (2018). Sequential extraction of gel-forming proteins, collagen and collagen hydrolysate from gutted silver carp (*Hypophthalmichthys molitrix*), a biorefinery approach. *Food Chemistry, 242,* 568-578. http://dx.doi.org/10.1016/j.foodchem.2017.09.045

Abeykoon, C., McMillan, A., Dasannayaka, C.H., Huang, X. & Xu, P. (2021). Remanufacturing using end-of life vehicles and electrical and electronic equipment polymer recyclates – a paradigm for assessing the value proposition. *International Journal of Lightweight Materials and Manufacture, 4,* 4344-448. https://doi.org/10.1016/j.ijlmm.2021.06.005

Abubakr, N., Lin, S. X. & Chin, X. D. (2009). Effects of drying methods on the release kinetics of vitamin B12 in calcium alginate beads. *Drying Technology, 27,* 1258-1265. https://doi.org/10.1080/07373930903267732

Abuine, R., Rathnayake, A. U. & Byun, H.-G. (2019). Biological activity of peptides purified from fish skin hydrolysates. *Fisheries and Aquatic Sciences, 22,* 10. https://doi.org/10.1186/s41240-019-0125-4

Adriani, N.H., Rahayu, D.U.C. & Saepudin, E. (2020). Activity of hydrogenated curcuminoid on Pd/C catalyst and its antibacterial activity against *Staphylococcus aureus* and *Streptococcus mutans*. *IOP Conference Series: Materials Science and Engineering, 902*, 012068. https://doi.org/10.1088/1757-899X/902/1/012068

Agrawal, C. M., & Ray, R. B. (2001). Biodegradable polymeric scaffolds for musculoskeletal tissue engineering. *Journal of Biomedical Materials Research, 55*, 141–150. https://doi.org/10.1002/1097-4636(200105)55:2<141::AID-JBM1000>3.0.CO;2-J

Ahlawat, K.S. & Khatkar, B.S. (2011). Processing, food applications and safety of aloe vera product indicating the interactions of collagen with the additives incorporated in the formulations: a review. *Journal of Food Sciency and Technology, 48,* 525-533. https://doi.org/10.1007/s13197-011-0229-z

Ahmad, T., Ismail, A., Ahmad, S. A., Khalil, K. A., Kumar, Y., Adeyemi, K. D., & Sazili, A. Q. (2017). Recent advances on the role of process variables affecting gelatin yield and characteristics with special reference to enzymatic extraction: A review. *Food Hydrocolloids, 63*, 85-96. https://doi.org/10.1016/j.foodhyd.2016.08.007

Ahmed, R., Getachew, A. T., Cho, Y. & Chun, B. (2018). Application of bacterial collagenolytic proteases for the extraction of type I collagen from the skin of bigeye tuna (*Thunnus obesus*). *LWT-Food Science and Technology, 89*, 44-51. https://doi.org/10.1016/j.lwt.2017.10.024

Álvarez-Castillo, E., Oliveira, S., Bengoechea, C., Sousa, I., Raymundo, A. & Guerrero, A. (2021). A rheological approach to 3D printing of plasma protein based doughs. *Journal of Food Engineering, 288,* 110255. https://doi.org/10.1016/j.jfoodeng.2020.110255

Alves, A., Marques, A., Martins, E., Silva, T. & Reis, R.L. (2017). Cosmetic Potential of Marine Fish Skin Collagen. *Cosmetics*, *4*, 39. https://doi.org/10.3390/cosmetics4040039

An, B., Lin, Y. & Brodsky, B. (2016). Collagen interactions: drug design and delivery, *Advanced Drug Delivery Reviews, 97,* 69–84, https://doi.org/10.1016/j.addr.2015.11.013

Andonegi, M., de la Caba, K. & Guerrero, P. (2020). Effect of citric acid on collagen sheets processed by compression. *Food Hydrocolloids, 100*, 105427. https://doi.org/10.1016/j.foodhyd.2019.105427.

Andonegi, M., Peñalba, M., de la Caba, K. & Guerrero, P. (2020). ZnO nanoparticle-incorporated native collagen films with electro-conductive properties. *Materials Science and Engineering C, 108,* 110394. http://doi.org/10.1016/j.msec.2019.110394

Aspevik, T., Oterhals, Å., Rønning, S.B., Altintzoglou, T., Wubshet, S.G., Gildberg, A., Afseth, N.K., Dragøy, R. & Lindberg, D. (2017). Valorization of proteins from co- and by-products from fish and meat industry. *Topics in current chemistry, 375,* 53. https://doi.org/10.1007/s41061-017-0143-6

ASTM D638-03 (2003). Standard test method for tensile properties of plastics. In: Annual Book of ASTM Standards, American Society for testing and materials, Philadelphia.

ASTM E96-00 (2000) Standard test methods for water vapour transmission of material, Annual Book of ASTM Standards, American Society for Testing and Materials, Philadelphia.

Astre, G., Deleruyelle, S., Dortignac, A., Bonnet, C., Valet, P. & Dray, C. (2018). Diet-induced obesity and associated disorders are prevented by natural bioactive type 1 fish collagen peptides (Naticol®) treatment. *Journal of Physiology and Biochemistry, 74,* 647–654. https://doi.org/10.1007/s13105-018-0650-0

Avila Rodríguez, M. I., Rodríguez Barroso, M. G. & Sánchez, M. L. (2018). Collagen: A review on its sources and potential cosmetic applications. *Journal of Cosmetic Dermatology, 17*, 20–26. https://doi.org/10.1111/jocd.12450

Bajer, D., Janczak, K. & Bajer K. (2020). Novel starch/chitosan/aloe vera composites as promising biopackaging materials. *Journal of Polymers and the Environment, 28*, 1021-1039. https://doi.org/10.1007/s10924-020-01661-7

Balaure, P.C., Holban, A.M., Grumezescu, A.M., Mogoşanu, G.D., Bălşeanu, T.A., Stan, M.S., Dinischiotu, A, Volceanov, A. & Mogoantă, L. (2019). *In vitro* and *in vivo* studies of novel fabricated

bioactive dressings based on collagen and zinc oxide 3D scaffolds. *International Journal of Pharmaceutics, 557*, 199-207. https://doi.org/10.1016/j.ijpharm.2018.12.063

Barrientos, S., Brem, H., Stojadinovic, O. & Tomic-Canic, M. (2014). Clinical application of growth factors and cytokines in wound healing. *Wound Repair and Regeneration, 22,* 569-578. https://doi.org/10.1111/wrr.12205

Barth, A. & Zscherp, C. (2002). What vibrations tell about proteins. *Quarterly Reviews of Biophysics, 35*, 369-430. https://doi.org/10.1017/S0033583502003815

Bassi da Silva, J., Ferreira, S.B.D.S., Reis, A.V., Cook, M.T., Bruschi, M.L. (2018). Assessing mucoadhesion in polymer gels: the effect of method type and instrument variables. *Polymers* 10, 254. https://doi.org/10.3390/polym10030254

Beghetto, V., Gatto, V., Conca, S., Bardella, N. & Scrivanti, A. (2019). Polyamidoamide dendrimers and cross-linking agents for stabilized bioenzymatic resistant metal-free bovine collagen. *Molecules, 24,* 3611. https://doi.org/10.3390/molecules24193611

Bello, A.B., Kim, D., Kim, D., Park, H. & Lee S.-H. (2020). Engineering and Functionalization of Gelatin Biomaterials: From Cell Culture to Medical Applications. *Tissue Engineering Part B: Reviews*, *26*, 2. https://doi.org/10.1089/ten.TEB.2019.0256

Benayahu, D., Pomeraniec, L., Shemesh, S., Heller, S., Rosenthal, Y., Rath-Wolfson, L. & Benayahu, Y. (2020). Biocompatibility of a Marine Collagen Based Scaffold in Vitro and in Vivo. *Marine Drugs, 18,* 420. https://doi.org/10.3390/MD18080420

Benayahu, D., Sharabi, M., Pomeraniec, L., Awad, L., Haj-Ali, R. & Benayahu, Y. (2018). Unique Collagen Fibers for Biomedical Applications. *Marine Drugs, 16,* 102. https://doi.org/10.3390/md16040102

Bhuimbar, M. V., Bhagwat, P. K. & Dandge, P. B. (2019). Extraction and characterization of acid soluble collagen from fish waste: Development of collagen-chitosan blend as food packaging films. *Journal of Environmental Chemical Engineering, 7,* 102983. https://doi.org/10.1016/j.jece.2019.102983

Bilek, S.E. & Bayram, S.K. (2015). Fruit juice drink production containing hydrolyzed collagen. *Journal of Functional Foods, 14*, 562–569. https://doi.org/10.1016/j.jff.2015.02.024

Boddupalli, B.M., Mohammed, Z.N.K., Nath, R.A. & Banji, D. (2010). Mucoadhesive drug delivery system: An overview. *Journal of Advanced Pharmaceutical Technology & Research, 1,* 381-387. https://doi.org/10.4103/0110-5558.76436

Bolognesi, V. J., Spier, M. R. & Rocha Garcia, C. E. (2020). Brine solution with hydrocolloids used to enhance the properties of sterilized meat. *Food Technology and Biotechnology, 58,* 2. https://doi.org/10.17113/ftb.58.02.20.6336

Bozec, L. & Odlyha, M. (2011). Thermal denaturation studies of collagen by microthermal analysis and atomic force microscopy. *Biophysical Journal, 101,* 228-236. https://doi.org/10.1016/j.bpj.2011.04.033

Brodsky, B. & Ramshaw, J.A.M. (1997). The collagen triple-helix structure. *Matrix Biology, 15,* 545-554. https://doi.org/10.1016/S0945-053X(97)90030-5

Bryan, M.A., Brauner, J.W., Anderie, G., Flach, C.R., Brodsky, B. & Mendelsohn, R. (2007). FTIR studies of collagen model peptides: complementary experimental and simulation approaches to conformation and unfolding. *Journal of the American Chemical Society, 129*, 7877-7884. https://doi.org/10.1021/ja071154i

Campos, Y., Sola, F.J., Almirall, A., Fuentes, G., Eich, C., Que, I., Chan, A., Kaijzel, E., Tabata, Y., Quintanilla, L., Rodriguez-Cabello, J.C. & Cruz, L.J. (2020). Design, Construction, and Biological Testing of an Implantable Porous Trilayer Scaffold for Repairing Osteoarthritic Cartilage. *Journal of Tissue Engineering and Regenerative Medicine, 14*, 355-368. https://doi.org/10.1002/term.3001

Cardamone, J. M., Nuñez, A., Garcia, R. A. & Aldema-Ramos, M. (2009). Characterizing woll keratin. *Research Letters in Materials Science*, 147175. https://doi.org/10.1155/2009/147175

Castellan, A., Ruggiero, R., da Silva, L.G., Portes, E., Grelier, S. & Gardrat, C. (2007). Photophysics and photochemistry of tetrahydrocurcuminoids. *Journal of Photochemistry and Photobiology A: Chemistry, 190,* 110-120. https://doi.org/10.1016/j.jphotochem.2007.03.019

Chakrapani, V.I., Gnanamani, A., Giridev, V.R., Madhusoothanan, M. & Sekaran, G. (2012). Electrospinning of type I collagen and PCL nanofibers using acetic acid. *Journal of Applied Polymer Science, 125,* 3221-3227. https://doi.org/10.1002/app.36504

Chen, J., Li, L., Yi, R., Xu, N., Gao, R. & Hong, B. (2016a). Extraction and characterization of acid-soluble collagen from scales and skin of tilapia (*Oreachromis niloticus*). *LWT-Food Science and Technology, 66*, 453-459. https://doi.org/10.1016/j.lwt.2015.10.070

Chen, S., Chen, H., Xie, Q., Hong, B., Chen, J., Hua, F., Bai, K., He, J., Yi, R. & Wu, H. (2016b). Rapid isolation of high purity pepsin-soluble type I collagen from scales of red drum fish (*Sciaenops ocellatus*). *Food Hydrocolloids, 52*, 468-477. https://doi.org/10.1016/j.foodhyd.2015.07.027

Chen, S., Tang, L., Hao, G., Weng, W., Osako, K. & Tanaka, M. (2016c). Effects of α1/α2 ratios and drying temperatures on the properties of gelatin films prepared from tilapia (*Tilapia zillii*) skins. *Food Hydrocolloids, 52,* 573-580. https://doi.org/10.1016/j.foodhyd.2015.07.026

Chen, X., Zhou, L., Xu, H., Yamamoto, M., Shinoda, M., Tada, I., Minami, S., Urayama, K. & Yamane, H. (2019). The structure and properties of natural sheep casing and artificial films prepared from natural collagen with various crosslinking treatments. *International Journal of Biological Macromolecules, 135,* 959-968. https://doi.org/10.1016/j.ijbiomac.2019.05.182

Chhabra, R.P. & Richardson, J.F. (1999). Chapter 2- Rheometry for non-newtonian fluids. Non-newtonian flow in the process industries. Fundamentals and Engineering Applications. *Materials Science*. https://doi.org/10.1016/B978-0-7506-3770-1.X5000-3

Chuaychan, S., Benjakul, S. & Kishimura, H. (2015). Characteristics of acid- and pepsin-soluble collagens from scale of seabass (Lates calcarifer). *LWT-Food Science and Technology, 63,* 71-76. https://doi.org/10.1016/j.lwt.2015.03.002

Chuaychan, S., Benjakul, S. & Nuthong, P. (2016). Element distribution and morphology of spotted Golden goatfish fish scales as affected by demineralisation. *Food Chemistry, 197,* 814-820. https://doi.org/10.1016/j.foodchem.2015.11.044

Clark, J. H., Farmer, T. J., Herrero-Davila, L. & Sherwood, J. R. (2016). Circular economy design considerations for research and process development in the chemical sciences. *Green Chemistry, 18*, 3914–3934. https://doi.org/10.1039/C6GC00501B

Cockerham, K. & Hsu, V. (2009). Collagen-based dermal fillers: past, present, future. *Facial Plastic Surgery, 25,* 106-113. https://doi.org/10.1055/s-0029-1220650

Coppola, D., Oliviero, M., Vitale, G. A., Lauritano, C., D'Ambra, I., Iannace, S. & de Pascale, D. (2020). Marine collagen from alternative and sustainable sources: Extraction, processing and applications. *Marine Drugs, 18*, 214. https://doi.org/10.3390/md18040214

Corker, A., Ng, H.C.H., Poole, R.J. & García-Tuñón, E. (2019). 3D printing with 2D colloids: Designing rheology protocols to predict "printability" of soft-materials. *Soft Matter 15*, 1444–1456. https://doi.org/10.1039/C8SM01936C

Costa, P. & Lobo, J.M. (2001). Modeling and comparison of dissolution profiles. European Journal of Pharmaceutical Sciences*, 13,* 123-133. https://doi.org/10.1016/S0928-0987(01)00095-1

de Campos Vidal, B., & Mello, M. L. S. (2011). Collagen type I amide I band infrared spectroscopy. Micron, 42, 283–289. https://doi.org/10.1016/j.micron.2010.09.010.

Deepthi, S., Sundaram, M.N., Karaavan, J.D. & Jayakumar, R. (2016). Layered chitosan-collagen hydrogel/aligned PLLA nanofiber construct for flexor tendon regeneration. *Carbohydrates Polymers, 153,* 492-500. https://doi.org/10.1016/j.carbpol.2016.07.124

Dey, A., Bera, R. & Chakrabarty, D. (2015). Influence of *Aloe vera* on the properties of N-vinylpyrrolidone-Acrylamide copolymer hydrogel. *Materials Chemistry and Physics, 168,* 168-179. https://doi.org/10.1016/j.matchemphys.2015.11.017

Di Summa, P. G., Kingham, P. J., Campisi, C. C., Raffoul, W. & Kalbermatten, D. F. (2014). Collagen (NeuraGen®) nerve conduits and stem cells for peripheral nerve gap repair. *Neuroscience Letters, 572*, 26-31. https://doi.org/10.1016/j.neulet.2014.04.029

Ding, C., Zhang, M. & Li, G. (2014). The response of collagen molecules in acid solution to temperature. *Polymers, 55*, 5751-5759. https://doi.org/10.1016/j.polymer.2014.09.011

Drury, J.L. & Mooney, D.J. (2003). Hydrogels for tissue engineering: scaffold design variables and applications. *Biomaterials, 24,* 4337-4351. https://doi.org/10.1016/S0142-9612(03)00340-5

Duan, R., Zhang, J., Du, X., Yao, X. & Konno, K. (2009). Properties of collagen from skin, scale and bone of carp (Cyprinus carpio). *Food Chemistry, 112*, 702-706. https://doi.org/10.1016/j.foodchem.2008.06.020

El-Azazy, M., Dimassi S.N., El-Shafie, A.S. & Issa, A.A. (2019). Bio-Waste *Aloe vera* leaves as an efficient adsorbent for titan yellow from wastewater. *Applied Sciences*, *9*, 4856. https://doi.org/10.3390/app9224856

Etemadian, Y., Ghaemi, V. Shaviklo, A. R., Pourashouri, P., Mahoonak, A.R.S. & Rafipour, F. (2021). Development of animal/plant-based protein hydrolysate and its application in food, feed and nutraceutical industries: State of the art. *Journal of Cleaner Production, 278,* 123219. https://doi.org/10.1016/j.jclepro.2020.123219

Etxabide, A., Leceta, I., Cabezudo, S., Guerrero, P. & de la Caba, K. (2016). Sustainable fish gelatin films: From food processing waste to compost. *ACS Sustainable Chemistry & Engineering, 4,* 4626-4634. https://doi.org/10.1021/acssuschemeng.6b00750

Etxabide, A., Vairo, C., Santos-Vizcaino, E., Guerrero, P., Pedraz, J.L., Igartua, M., de la Caba, K. & Hernandez, R.M. (2017). Ultra thin hydro-films based on lactose-crosslinked fish gelatin for wound healing applications. *International Journal of Pharmaceutics, 530,* 455-467. https://doi.org/10.1016/j.ijpharm.2017.08.001

European Commission. (2020). COM(2020) 98 final A new Circular Economy Action Plan For a cleaner and more competitive Europe. https://eur-

lex.europa.eu/resource.html?uri=cellar:9903b325-6388-11ea-b735-01aa75ed71a1.0017.02/DOC_1&format=PDF. (Accessed 19 December 2021)

Exposito, J.Y., Cluzel, C., Garrone, R. & Lethias, C. (2002). Evolution of collagens. *The Anatomical Record, 268,* 302-316. https://doi.org/10.1002/ar.10162

Ferraro, V., Gaillard-Martinie, B., Sayd, T., Chambon, C., Anton, M. & Santé-Lhoutellier, V. (2017). Collagen type I from bovine bone. Effect of animal age, bone anatomy and drying methodology on extraction yield, self-assembly, thermal behaviour and electrokinetic potential. *International Journal of Biological Macromolecules, 97*, 55-66. https://doi.org/10.1016/j.ijbiomac.2016.12.068

Ferreira, A.M., Gentile, P., Chiono, V. & Ciardelli, G. (2012). Collagen for bone tissue regeneration. *Acta Biomaterialia, 8*, 3191-3200. https://doi.org/10.1016/j.actbio.2012.06.014

Figueroa-Lopez, K.J., Castro-Mayorga, J.L., Andrade-Mahecha, M.M., Cabedo, L. & Lagaron, J.M. (2018). Antibacterial and barrier properties of gelatin coated by electrospun polycaprolactone ultrathin fibers containing black pepper oleoresin of interest in active food biopackaging applications. *Nanomaterials*, *8*, 199. https://doi.org/10.3390/nano8040199

Food and Agriculture Organization of the United States (FAO). The state of world fisheries and aquaculture 2018.

Fratzl, P., Misof, K., Zizak, I., Rapp, G., Amenitsch, H. & Bernstorff, S. (1998). Fibrillar structure and mechanical properties of collagen. *Journal of Structural Biology, 122*, 119-122. https://doi.org/10.1006/jsbi.1998.3966

Fu, F., Zhu, X., Qin, Z., Wang, J.J., Xu, C., Wang, L.N., Tu, Y. Zhang, S., Li, R.X., Li, X.H. & Zhao, M.L. (2018). Differential degradation rate and underlying mechanism of a collagen/chitosan complex in subcutis, spinal cord and brain tissues of rat. *Journal of Materials Science: Materials in Medicine, 29*, 35. https://doi.org/10.1007/s10856-018-6033-9.

Fustier, P., Achouri, A., Taherian, A.R., Britten, M., Pelletier, M., Sabik, H., Villenueve, S. & Mondor, M. (2015). Protein-protein multilayer oil-in-water emulsions for the microencapsulation of flaxseed oil: Effect of whey and fish gelatin concentration. *Journal of Agricultural and Food Chemistry*, *63*, 9239-9250. https://doi.org/10.1021/acs.jafc.5b00858

Ganceviciene, R., Liakou, A.I., Theodoridis, A., Makrantonaki, E. & Zouboulis, C.C. (2012). Skin anti-aging strategies. *Dermato-Endocrinology 4:3*, 308-319. http://dx.doi.org/10.4161/derm.22804

Gandini, A., Lacerda, T. M., Carvalho, A. J. F. & Trovatt, E. (2016). Progress of polymers from renewable resources: Furans, vegetable oils, and polysaccharides. *Chemical Reviews, 116*, 1637–1669. https://doi.org/10.1021/acs.chemrev.5b00264

Gao, D., Cheng, Y., Wang, P., Li, F., Wu, Y., Lyu, B., Ma, J. & Qin, J. (2020). An eco-friendly approach for leather manufacture based on P(POSS-MAA)-aluminum tanning agent combination tannage. *Journal of Cleaner Production, 257,* 120546. https://doi.org/10.1016/j.jclepro.2020.120546

Gauza-Włodarczyk, M., Kubisz, L., Mielcarek, S. & Włodarczyk D. (2017). Comparison of thermal properties of fish collagen and bovine collagen in the temperature range 298-670 K. *Materials Science and Engineering: C, 80*, 468-471. https://doi.org/10.1016/j.msec.2017.06.012

Gelse, K., Pöschl, E. & Aigner, T. (2003). Collagens-structure, function, and biosynthesis. *Advanced Drug Delivery Reviews, 55*, 1531-1546. https://doi.org/10.1016/j.addr.2003.08.002

Genovese, L., Corbo, A. & Sibilla, S. (2017). An insight into the changes in skin texture and properties following dietary intervention with a nutricosmeceutical containing a blend of collagen bioactive peptides and antioxidants. *Skin Pharmacology and Physiology*, *30*, 146-158. https://doi.org/10.1159/000464470

Georgopoulou, A., Papadogiannis, F., Batsali, A., Marakis, J., Alpantaki, K., Eliopoulos, A. G., Pontikpglou, C. & Chatzinikolaidou, M. (2018). Chitosan/gelatin scaffolds support bone regeneration. *Journal of Materials Science: Materials in Medicine, 29*, 59. https://doi.org/10.1007/s10856-018-6064-2

Ghodbane, S.A. & Dunn, M.G. (2016). Physical and mechanical properties of cross-linked type I collagen scaffolds derived from bovine, porcine, and ovine tendons. *Journal of Biomedical Materials Research Part A 104,* 2685–2692, https://doi.org/10.1002/jbm.a.35813

Gomez, A. V. A., Gomez, G., Chamorro, E., Bustillo, S. & Leiva, L. C. (2018). Digestive aspartic protease from sábalo (*Prochilodus lineatus*): Characterization and application for collagen extraction. *Food Chemistry, 269*, 610-617. https://doi.org/10.1016/j.foodchem.2018.07.043

Guan, X., Avci-Adali, M., Alarçin, E., Cheng, H., Kashaf, S.S., Li, Y., Chawla, A., Jang, H.L. & Khademhosseini, A. (2017). Development of Hydrogels for Regenerative Engineering. *Biotechnology Journal*, *12,* 1600394. https://doi.org/10.1002/biot.201600394

Guerrero, P., Kerry, J. P. & de la Caba, K. (2014). FTIR characterization of protein-polysaccharide interactions in extruded blends. *Carbohydrate Polymers, 111,* 598-605. https://doi.org/10.1016/j.carbpol.2014.05.005

Guerrero, P., Muxika, A., Zarandona, I. & de la Caba, K. (2019). Crosslinking of chitosan films processed by compression molding. *Carbohydrate Polymers, 206,* 820-826. https://doi.org/10.1016/j.carbpol.2018.11.064

Guo, C., Zhang, M. & Devahastin, S. (2020). 3D extrusion-based printability evaluation of selected ceral grains by computational fluid dynamic simulation. Journal of Food Engineering, 286, 110113. https://doi.org/10.1016/j.jfoodeng.2020.110113

Guo, L., Harnedy, P.A., Zhang, L., Li, B., Zhang, Z., Hou, H., Zhao, X. & FitzGerald, R.J. (2015). *In vitro* assessment of the multifunctional bioactive potential of Alaska pollock skin collagen following simulated gastrointestinal digestion. *Journal of the Science of Food and Agriculture*, *95*, 1514–1520. https://doi.org/10.1002/jsfa.6854

Guo, S., He, L., Yang, R., Chen, B., Xie, X., Jiang, B., Weidong, T. & Ding, Y. (2020). Enhanced Effects of Electrospun Collagen-Chitosan Nanofiber Membranes on Guided Bone Regeneration. *Journal of Biomaterials Science, 31,* 155-168. https://doi.org/10.1080/09205063.2019.1680927

Gustavsson, J., Cederberg, C., Sonesson, U. & Emanuelsson, A. (2013) The methodology of the FAO study: ‘‘Global Food Losses and Food Waste-extent, causes and prevention’’. FAO, 2011. SIK report No. 857

Haifei, S., Xingang, W., Shoucheng, W., Zhengwei, M., Chuangang, Y. & Chunmao, H. (2014). The Effect of Collagen-Chitosan Porous Scaffold Thickness on Dermal Regeneration in a One-Stage Grafting Procedure. *Journal of the Mechanical Behavior of Biomedical Materials, 29,* 114-125. https://doi.org/10.1016/j.jmbbm.2013.08.031

Hanjabam, M. D., Kannaiyan, S. K., Kamei, G., Jakhar, J. K., Chouksey, M. K. & Gudipati, V. (2015). Optimisation of gelatin extraction from Unicorn leatherjacket (*Aluterus Monoceros*) skin waste: response surface approach. *Journal of Food Science and Technology, 52,* 976-983. https://doi.org/10.1007/s13197-013-1075-y

Hayashi, Y., Yamada, S., Guchi, K.Y., Koyama, Z. & Ikeda, T. (2012). Chitosan and Fish Collagen as Biomaterials for Regenerative Medicine. *Advances in Food and Nutrition Research*, *65*, 107-120. https://doi.org/10.1016/B978-0-12-416003-3.00006-8

Heino, J. (2007). The collagen family members as cell adhesion proteins. *Bioessays, 29,* 1001–1010. https://doi.org/10.1002/bies.20636

Hennink, W. E. & van Nostrum, C. F. (2012). Novel Crosslinking Methods to Design Hydrogels. *Advanced Drug Delivery Reviews, 64,* 223-236. https://doi.org/10.1016/j.addr.2012.09.009

Hernández-Nava, R., López-Malo, A., Palou, E., Ramírez-Corona, N. & Jiménez-Munguía, M.T. (2020). Encapsulation of oregano essential oil (*Origanum vulgare*) by complex coacervation

between gelatin and chia mucilage and its properties after spray drying. *Food Hydrocolloids, 109,* 106077. https://doi.org/10.1016/j.foodhyd.2020.106077

Hollister, S. J. (2009). Scaffold Design and Manufacturing: From Concept to Clinic. *Advanced Materials, 21,* 3330-3342. https://doi.org/10.1002/adma.200802977

Hou, C., Gao, L., Wang, Z., Rao, W., Du, M. & Zhang, D. (2020). Mechanical properties, thermal stability and solubility of sheep bone collagen-chitosan films. *Journal of Food Process Engineering, 43,* e13086. https://doi.org/10.1111/jfpe.13086

Hu, K., Cui, F., Lv, Q., Ma, J., Feng, Q., Xu, L. & Fan, D. (2008). Preparation of fibroin/recombinant human-like collagen scaffold to promote fibroblasts compatibility. *Journal of Biomedical Materials Research A*, *84*, 483-490. https://doi.org/10.1002/jbm.a.31440

Hu, Y., Liu, L., Dan, W.H., Dan, N.H. & Gu, Z.P. (2013). Evaluation of 1-ethyl-3-methylimidazolium acetate based ionic liquid systems as a suitable solvent for collagen. *Journal of Applied Polymer Science., 130*, 2245-2256. https://doi.org/10.1002/app.39298

Huang, C. Y., Kuo, J.M., Wu, S.J., & Tsai, H.T. (2016). Isolation and characterization of fish scale collagen from tilapia (*Oreochromis sp*.) by a novel extrusion-hydroextraction process. *Food Chemistry, 190*, 997-1006. https://doi.org/10.1016/j.foodchem.2015.06.066

Huang, T., Tu, Z.C., Zou, Z.Z., Shangguan, X., Wang, H. & Bansal, N. (2020). Gycosylated fish gelatin emulsion: Rheological, tribological properties and its application as model coffee creamers. *Food Hydrocolloids*, 102, 105552. https://doi.org/10.1016/j.foodhyd.2019.105552

Huang, C. Y., Kuo, C. H., Wu, C. H., Ku, M. W. & Chen, P. W. (2018). Extraction of crude chitosans from squid (*Illex argentinus*) pen by a compressional puffing-pretreatment process and evaluation of their antibacterial activity. *Food Chemistry, 254*, 217-223. https://doi.org/10.1016/j.foodchem.2018.02.018

Huang, T., Tu, Z.C., Zou, Z.Z., Shangguan, X., Sha, X. Wang, H. Zhang, L. & Bansal, N. (2019). Fish gelatin modifications: A comprehensive review. *Trends in Food Science & Technology*, 86, 260-269. https://doi.org/10.1016/j.tifs.2019.02.048

Huang, Y.R, Shiau, C.Y., Chen, H.H. & Huang, B.C. (2011). Isolation and characterization of acid and pepsin-solubilized collagens from the skin of balloon fish (*Diodoon holocanthus*). *Food Hydrocolloids, 25,* 1507-1513. https://doi.org/10.1016/j.foodhyd.2011.02.011

Hulmes, D.J.S. (2002). Building collagen molecules fibrils and suprafibrillar structures. *Journal of Structural Biology, 137,* 2-10. https://doi.org/10.1006/jsbi.2002.4450

Hwang, E., Thiagarajan, G., Parmar, A.S. & Brodsky, B. (2010). Interruptions in the collagen repeating tripeptide pattern can promote supramolecular association. *Protein Science, 19,* 1053-1064. https://doi.org/10.1002/pro.383

Ishak, N. & Sarbon, N. A. (2018). A review of protein hydrolysates and bioactive peptides deriving from wastes generated by fish processing. *Food Bioprocess Technology, 11*, 2–16. https://doi.org/10.1007/s11947-017-1940-1

ISO 10993-5 (2009). Biological evaluation of medical devices-Part 5: Tests for in vitro cytotoxicity. https://www.iso.org/standard/36406.html

ISO 14040, 2006. Environmental Management - Life Cycle Assessment - Principals and Framework. https://www.iso.org/standard/37456.html

Ito, N., Seki S. & Ueda, F. (2019). Effects of composite supplement containing collagen peptide and ornithine on skin conditions and plasma IGF-1 levels-a randomized, double-blind, placebo-controlled trial. *Marine Drugs*, *16,* 482. https://doi.org/10.3390/md16120482

Jachowicz, M. (2013). Electrostatic properties of selected personal protective equipment regarding explosion hazard. *Journal of sustainable mining, 12,* 27-33. https://doi.org/10.7424/jsm130106

Jakab, K., Marga, F., Kaesser, R., Chuang, T.H., Varadarajau, H., Cassingham, D., Lee, S., Forgacs, A. & Forgacs, G. (2019). Non-medical applications of tissue engineering: biofabrication of a leather-like material. *Materials Today Sustainability, in press*. https://doi.org/10.1016/j.mtsust.2019.100018

Jeevithan, E., Qingbo, Z., Bao, B. & Wu, W. (2013). Biomedical and pharmaceutical application of fish collagen and gelatin: a review. *Journal of Nutritional Therapeutics, 2*, 218-227. http://dx.doi.org/10.6000/1929-5634.2013.02.04.6

Jiang, Y. Lan, W., Sameen, D. E., Ahmed, S., Qin, W., Zhang, Q., Chen, H., Dai, J., He, L. & Liu, Y. (2020). Preparation and characterization of grass carp collagen-chitosan-lemon essential oil composite films for application as food packaging. *International Journal of Biological Macromolecules*, *160,* 340-351. https://doi.org/10.1016/j.ijbiomac.2020.05.202

Jridi, M., Nasri, R., Salem, R. B. S. B., Lassoued, I., Barkia, A., Nasri, M. & Souissi, N. (2015). Chemical and biophysical properties of gelatins extracted from the skin of octopus (*Octopus vulgaris*). *LWT-Food Science and Technology, 60,* 881-889. https://doi.org/10.1016/j.lwt.2014.10.057

Kaczmarek, B., Sionkowska, A. & Skopinska-Wisniewska, J. (2018). Influence of glycosaminoglycans on the properties of thin films based on chitosan-collagen blends. *Journal of*

the Mechanical Behavior of Biomedical Materials 80, 189-193. https://doi.org/10.1016/j.jmbbm.2018.02.006

Kakkar, V., Kaur, I. P., Kaur, A. P., Saini, K. & Singh, K. K. (2018). Topical delivery of tetrahydrocurcumin lipid nanoparticles effectively inhibits skin inflammation: in vitro and in vivo study. Drug Development and Industrial Pharmacy. https://doi.org/10.1080/03639045.2018.1492607

Kapashi, E., Kapnisti, M., Dafnomili, A. & Noli, F. (2019). Aloe Vera as an effective biosorbent for the removal of thorium and barium from aqueous solutions. *Journal of Radioanalytical and Nuclear Chemistry, 321*, 217-226. https://doi.org/10.1007/s10967-019-06558-x

Kean, T. & Thanou, M. (2010). Biodegradation, biodistribution and toxicity of chitosan. *Advanced Drug Delivery Reviews, 62,* 3-11. https://doi.org/10.1016/j.addr.2009.09.004

Kezwoń, A., Góral, I., Fraczyk, T., & Wojciechowski, K. (2016). Effect of surfactants on surface active and rheological properties of type I collagen at air/water interface. *Colloids and Surfaces B: Biointerfaces, 148,* 238-248. https://doi.org/10.1016/j.colsurfb.2016.08.058

Kim, D.U., Chung, H.C., Choi, J., Sakai, Y. & Lee, B.Y. (2018). Oral intake of low-molecular weight collagen peptide improves hydration, elasticity, and wrinkling in human skin: a randomized, double-blind, placebo-controlled study. *Nutrients, 10,* 826. https://doi.org/10.3390/nu10070826

Kiran, P. & Rao, P.S. (2016). Development and characterization of reconstituted hydrogel from Aloe vera (*Aloe barbadensis* Miler) powder. *Journal of Food Measurement and Characteization, 10*, 411-424. https://doi.org/10.1007/s11694-016-9320-5

Kittiphattanabawon, P., Benjakul, S., Sinthusamran, S. & Kishimura, H. (2016). Gelatin from clown featherback skin: Extraction conditions*. LWT-Food Science and Technology, 66,* 186-192. https://doi.org/10.1016/j.lwt.2015.10.029

Knupp, C. & Squire, J.M. (2005). Molecular packing in network-forming collagens. *Advances in Protein Chemistry, 70*, 375–403. https://doi.org/10.1016/S0065-3233(05)70011-5

Koch, M., Foley, J. E., Hahn, R., Zhou, P., Burgeson, R. E., Gerecke, D. R. & Gordon, M.K. (2001). α1 (XX) collagen, a new member of the collagen subfamily, fibril-associated collagens with interrupter triple helices. *Journal of Biological Chemistry, 276*, 23120–23126. https://doi.org/10.1074/jbc.M009912200

Kuai, L., Liu, F., Ma, Y., Goff, H.D. & Zhong, F. (2020). Regulation of nano-encapsulated tea polyphenol release from gelatin films with different Bloom values. *Food Hydrocolloids, 108,* 106045. https://doi.org/10.1016/j.foodhyd.2020.106045

Labastida-Pólito, A., Piña-Barba, C., Romero-Valdovinos, M.G. & Tello-Solís, S.R. (2009). Physicochemical properties of collagen sheet from bovine femur. *Journal of Applied Biomaterials & Biomechanics, 7,* 200-204.

Lamke, L.O., Nilsson, G.E. & Reithner, H.L. (1977). The evaporative water loss from burns and the water-vapour permeabililty of grafts and artificial membranes used in the treatments of burns. *Burns, 3,* 159-165. https://doi.org/10.1016/0305-4179(77)90004-3

Langer, R. S. & Vacanti, J. P. (1999). Tissue Engineering: The Challenges Ahead. *Scientific American, 280,* 86-89. https://doi.org/10.1038/scientificamerican0499-86

Las Heras, K., Santos-Vizcaíno, E., Garrido, T., Gutierrez, F.B., Aguirre, J.J., de la Caba, K., Guerrero, P., Igartua, M. & Hernandez, R.M. (2020). Soy protein and chitin sponge-like scaffolds: from natural by-products to cell delivery systems for biomedical applications. *Green Chemistry, 22*, 3445. https://doi.org/10.1039/d0gc00089b.

Lauritano, C. & Ianora, A. (2016). Marine organisms with anti-diabetes properties. *Marine Drugs*, *14*, 220. https://doi.org/10.3390/md14120220

Leceta, I. Guerrero, P., Ibarburu, I., Dueñas, M.T. & de la Caba, K. (2013). Characterization and antimicrobial analysis of chitosan-based films. *Journal of Food Engineering, 116,* 889-899. https://doi.org/10.1016/j.jfoodeng.2013.01.022

Leceta, I., Peñalba, M., Arana, P., Guerrero, P. & de la Caba, K. (2015). Ageing of chitosan films: Effect of storage time on structure and optical, barrier and mechanical properties. *European Polymer Journal, 66,* 170-179. https://doi.org/10.1016/j.eurpolymj.2015.02.015

Lee, J. K., Patel, S. K. S., Sung, B. H. & Kalia, V. C. (2020). Biomolecules from municipal and food industry wastes: An overview. *Bioresource Technology, 298*, 122346. https://doi.org/10.1016/j.biortech.2019.122346

Lee, J. M., Suen, S. K. Q., Ng, W.L., Ma, W. C. & Yeong, W. Y. (2021). Bioprinting of collagen: considerations, potentials and application. *Macromolecular Bioscience, 21,* 2000280. https://doi.org/10.1002/mabi.202000280

León-López, A., Fuentes-Jiménez, L., Hernández-Fuentes, A. D., Camps-Montiel, R. G. & Aguirre-Álvarez, G. (2019). Hydrolysed Collagen from Sheepskins as a Source of Functional Petides with Antioxidant Activity. *International Journal of Molecular Science*, *20,* 3931. https://doi.org/10.3390/ijms20163931

Li J., Yu, X., Tang, W., Wan, C., Lu, Y., Dong, N., Chen, Z., Lei, Z. Ren, T., Wang, Z. & Liu, J. (2021). Characterization of food gels prepared from the water extract of fish (Cyprinus carpio L.). scales: From molecular components to sensory attributes. *Food Hydrocolloids, 112,* 106263. https://doi.org/10.1016/j.foodhyd.2020.106263

Li, H., Liu, B.L., Gao, L.Z. & Chen, H.L. (2004). Studies on bullfrog skin collagen. *Food Chemistry 84,* 65-69. https://doi.org/10.1016/S0308-8146(03)00167-5

Liang, Q., Wang, L., He, Y., Wang, Z., Xu, J., & Ma, H. (2014b). Hydrolysis kinetics and antioxidant activity of collagen under simulated gastrointestinal digestion. *Journal of Functional Foods, 11,* 493-499. https://doi.org/10.1016/j.jff.2014.08.004

Liang, Q., Wang, L., Sun, W., Wang, Z., Xu, J. & Ma, H. (2014a). Isolation and characterization of collagen from the cartilage of Amur sturgeon (*Acipenser schrenckii*). *Process Biochemistry, 49*, 318-323. https://doi.org/10.1016/j.procbio.2013.12.003

Liao, W., Guanghua, X., Li, Y., Shen, X.R. & Li, C. (2018). Comparison of characteristics and fibril-forming ability of skin collagen from barramundi (*Lates calcarifer*) and tilapia (*Oreochromis niloticus*). *International Journal of Biological Macromolecules, 107*, 549-559. https://doi.org/10.1016/j.ijbiomac.2017.09.022

Lille, M., Nurmela, A., Nordlund, E., Metsä-Kortelainen, S., & Sozer, N. (2018). Applicability of protein and fiber-rich food materials in extrusion-based 3D printing. *Journal of Food Engineering, 220,* 20-27. https://doi.org/10.1016/j.jfoodeng.2017.04.034

Liu, B., Huang, W., Yang, G., An, Y., Yin, Y., Wang, N. & Jiang, B. (2020). Preparation of gelatin/poly(γ-glutamic acid) hydrogels with stimulated response by hot-pressing preassembly and radiation crosslinking. *Materials Science and Engineering: C, 116*, 111259. https://doi.org/10.1016/j.msec.2020.111259

Liu, D., Wei, G., Li, T., Hu, J., Lu, N., Regenstein, J. M. & Zhou, P. (2015). Effects of alkaline pretreatments and acid extraction conditions on the acid-soluble collagen from grass carp (*Ctenopharyngodon idella*) skin. *Food Chemistry, 172*, 836-843. https://doi.org/10.1016/j.foodchem.2014.09.147

Liu, L., Hu, D. & Han, X. (2018). A three-dimensional unit cell model with controllable crimped structure for investigating strain response of collagen fiber reinforced biological composites. *Composites Science and Technology, 164*, 178–186. https://doi.org/10.1016/j.compscitech.2018.05.050

Liu, Y., Ma, L. & Gao, C. (2012). Facile Fabrication of the Glutaraldehyde Cross-Linked Collagen/Chitosan Porous Scaffold for Skin Tissue Engineering. *Materials Science and Engineering: C, 32*, 2361-2366. https://doi.org/10.1016/j.msec.2012.07.008

Lodish H., Berk, A., Zipursky, SL, et al. (2000). Molecular Cell Biology. 4TH edition. New York: W. H. Freeman; 2000. Section 22.3, Collagen: The Fibrous Proteins of the Matrix. Available from: https://www.ncbi.nlm.nih.gov/books/NBK21582

Lotfi, G., Shokrgozar, M. A., Mofid R., Abbas, F. M., Ghanavati, F., Baghban, A.A., Yavari, S.K. & Pajoumshariati, S. (2016). Biological Evaluation (*In Vitro* and *In Vivo*) of Bilayered Collagenous Coated (Nano Electrospun and Solid Wall) Chitosan Membrane for Periodontal Guided Bone Regeneration. *Annals of Biomedical Engineering, 44*, 2132-2144. https://doi.org/10.1007/s10439-015-1516-z

Lui, Y. S., Sow, W.T., Tan, L.P., Wu, Y., Lai, Y. & Li, H. (2019). 4D Printing and Stimuli-Responsive Materials in Biomedical Aspects. *Acta Biomaterialia, 92,* 19-36. https://doi.org/10.1016/j.actbio.2019.05.005

Lynn, A.K., Yannas, I.V. & Bonfield, W. (2004). Antigenicity and immunogenicity of collagen. *Journal of Biomedical Materials Research Part B, 71B*, 343–354, https://doi.org/10.1002/jbm.b.30096

Ma, D., Jiang, Y., Ahmed, S., Qin, W. & Liu, Y. (2020). Antilisterial and physical properties of polysaccharide-collagen films embedded with cell-free supernatant of *Lactococcus lactis*. *International Journal of Biological Macromolecules, 145,* 1031-1038. https://doi.org/10.1016/j.ijbiomac.2019.09.195

Ma, L., Gao, C., Mao, Z., Zhou, J., Shen, J., Hu, X. & Han, C. (2003). Collagen/chitosan porous scaffolds with improved biostability for skin tissue engineering. *Biomaterials*, *24,* 4833-4841. https://doi.org/10.1016/S0142-9612(03)00374-0

Ma, Y., Wang, W., Wang, Y., Guo, Y., Duan, S., Zhao, K. & Li, S. (2018). Metal ions increase mechanical strength and barrier properties of collagen-sodium polyacrylate composite films. *International Journal of Biological Macromolecules*, *119*, 15-22. https://doi.org/10.1016/j.ijbiomac.2018.07.092

Ma, Y., Zeng, X., Ma, X., Yang, R. & Zhao, W. (2019). A simple and eco - friendly method of gelatin production from bone: One-step biocatalysis. *Journal of Cleaner Production, 209,* 916-926 https://doi.org/10.1016/j.jclepro.2018.10.313

Machado, A.A.S., Martins, V.C.A. & Plepis, A.M.G (2002). Thermal and rheological behavior of collage. Chitosan blends. *Journal of Thermal Analysis and Calorimetry, 67,* 491-498. https://doi.org/10.1023/A:1013953316829

MacNeeil, S. (2007). Progress and opportunities for tissue-engineered skin. *Nature, 445*, 874–880. https://doi.org/10.1038/nature05664

Mantha, S., Pillai, S., Khayambashi, P., Upadhyay, A., Zhang, Y., Tao, O., Pham, H.M. & Tran, S. D. (2019). Smart Hydrogels in Tissue Engineering and Regenerative *Medicine. Materials, 12*, 3323. https://doi.org/10.3390/ma12203323

Mardani, M., Yeganehzad, S., Ptichkina N., Kodatsky, Y., Kliukina, O., Nepovinnykh, N. & Naji-Tabasi, S. (2019). Stud on foaming, rheological and thermal properties of gelatin –free marshmallow. *Food Hydrocolloids, 93,* 335-341. https://doi.org/10.1016/j.foodhyd.2019.02.033

Martínez, A., Blanco, M. D., Davidenko, N. & Cameron, R. E. (2015). Tailoring Chitosan/Collagen Scaffolds for Tissue Engineering: Effect of Composition and Different Crosslinking Agents on Scaffold Properties. *Carbohydrate Polymers, 132,* 606-619. https://doi.org/10.1016/j.carbpol.2015.06.084

Martínez-Alvarez, O., Chamorro, S. & Brenes, A. (2015). Protein hydrolysates from animal processing by-products as a source of bioactive molecules with interest in animal feeding: A review. *Food Research International, 73,* 204-212. https://doi.org/10.1016/j.foodres.2015.04.005

Martínez-Ortiz, M. A., Hernandez-Fuentes, A. D., Pimentel-Gonzalez, D. J., Campos- Montiel, R. G., Vargas-Torres, A. & Aguirre-Alvarez, G. (2015). Extraction and characterization of collagen from rabbit skin: Partial characterization. *CyTA- J. Food*, *13,* 253-258. https://doi.org/10.1080/19476337.2014.946451

McBane, J. E., Vulesevic, B., Padavan, D.T., McEwan, K.A., Korbutt, G.S. & Suuronen, E.J. (2013). Evaluation of a Collagen-Chitosan Hydrogel for Potential Use as a Pro-Angiogenic Site for Islet Transplantation. *PLoS ONE*, 8(10), e77538. https://doi.org/10.1371/journal.pone.0077538

Meena, R. A. A., Banu, J. R., Kannah, R. Y., Yogalakshmi, K. N. & Kumar, G. (2020). Biohythane production from food processing wastes - challenges and perspectives. *Bioresource Technology, 298,* 122449. https://doi.org/10.1016/j.biortech.2019.122449

Miles, C.A. & Ghelashvili, M. (1999). Polymer-in-a-Box mechanism for the thermal stabilization of collagen molecules in fibers. *Biophysical Journal, 76*, 3243-3252. https://doi.org/10.1016/S0006-3495(99)77476-X

Miles, C.A., Avery, N.C., Rodin, V.V. & Bailey, A.J. (2005). The increase in denaturation temperature following cross-linking of collagen is caused by dehydration of the fibres. *Journal of Molecular Biology, 346*, 551-556. https://doi.org/10.1016/j.jmb.2004.12.001

Miller, E.J. (1984). Biomedical and industrial application of collagen; In: Extracellular Matrix Biochemistry, K. A. Piez and A. H. Reddi, eds. Elsevier, New York. pp. 41-81.

Minh Thuy, L.T., Okazaki, E. & Osako, K. (2014). Isolation and characterization of acid-soluble collagen from the scales of marine fishes from Japan and Vietnam. *Food Chemistry, 149,* 264-270. https://doi.org/10.1016/j.foodchem.2013.10.094

Mohseni, F. & Goli, S.A.H. (2019). Encapsulation of flaxseed oil in the tertiary conjugate of oxidized tannic acid-gelatin and flaxseed (*Linum usitatissimum*) mucilage. *International Journal of Biological Macromolecules, 140,* 959-964. https://doi.org/10.1016/j.ijbiomac.2019.08.197

Molino, S., Casanova, N.A., Rufián Henares, J.Á. & Fernandez Miyakawa, M.E. (2020). Natural Tannin Wood Extracts as a Potential Food Ingredient in the Food Industry. *Journal of Agricultural and Food Chemistry, 68,* 2836-2848. https://doi.org/10.1021/acs.jafc.9b00590

Moreira, R., Chenlo, F. & Torres, M.D. (2012). Effect of shortenings on the rheology of gluten-free doughs: study of chestnut flour with chia flour, olive and sunflower oils. Journal of Texture Studies. https://doi.org/10.1111/j.1745-4603.2012.00348.x

Moreno, O., Atarés, L., Chiralt, A., Cruz-Romero, M.C. & Kerry, J. (2018). Starch-gelatin antimicrobial packaging materials to extend the shelf life of chicken breast fillets. *LWT, 97*, 483-490. https://doi.org/10.1016/j.lwt.2018.07.005

Muthukumar, T., Sreekumar, G., Sastry, T. P. & Chamundeeswari, M. (2018). Collagen as a potential biomaterial in biomedical applications. *Reviews on Advanced Materials Science, 53*, 29–39. https://doi.org/10.1515/rams-2018-0002

Myllyharju, J. & Kivirikko, K. (2001). Collagens and collagen-related diseases. *Annals of Medicine, 33*, 7–21. https://doi.org/10.3109/07853890109002055

Nguyen, T. T., Heimann, K. & Zhang W. (2020). Protein Recovery from Underutilised Marine Bioresources for Product Development with Nutraceutical and Pharmaceutical Bioactivities. *Marine Drugs, 18,* 391. https://doi.org/10.3390/md18080391

Ni, S., Zhang, H., Godwin, P.M., Dai, H. & Xiao, H. (2018). ZnO nanoparticles enhanced hydrophobicity for starch film and paper. *Materials Letters, 230,* 207-210. https://doi.org/10.1016/j.matlet.2018.07.075

Nilsuwan, K., Guerrero, P., de la Caba, K., Benjakul, S. & Prodpran, T. (2020). Properties and application of bilayer films based on poly (lactic acid) and fish gelatin containing epigallocatechin gallate fabricated by thermo-compression molding. *Food Hydrocolloids*, 105, 105792. https://doi.org/10.1016/j.foodhyd.2020.105792

Noorzai, S., Verbeek, C.J.R., Lay, M.C. & Swan, J. (2020). Collagen Extraction from Various Waste Bovine Hide Sources. *Waste and Biomass Valorization*, 11, 5687-5698. https://doi.org/10.1007/s12649-019-00843-2

O'Brien, F. J. (2011). Biomaterials & Scaffolds for Tissue Engineering. *Materials Today, 14*, 88-95. https://doi.org/10.1016/S1369-7021(11)70058-X

Oertzen-Hagemann, V., Kirmse, M., Eggers, B., Pfeiffer, K., Marcus, K., de Marées, M. & Platen, P. (2019). Effects of 12 Weeks of Hypertrophy Resistance Exercise Training Combined with Collagen Peptide Supplementation on the Skeletal Muscle Proteome in Recreationally Active Men. *Nutrients, 11,* 1072. https://doi.org/10.3390/nu11051072

Oliveira, V.D.M., Assis, C.R.D., Costa, B.D.A.M., Neri, R.C.D.A., Monte, F.T., Freitas, H.M.S.D.C.V., França, R.C.P., Santos, J., Bezerra, R.D.S. & Porto, A.L.F. (2021). Physical, biochemical, densitometric and spectroscopic techniques for characterization collagen from alternative sources: A review based on the sustainable valorization of aquatic by-products. *Journal of Molecular Structure, 1224,* 129023. https://doi.org/10.1016/j.molstruc.2020.129023

Ong, K. L., Kaur, G., Pensupa, N., Uisan, K. & Lin, C. S. K. (2018). Trends in food waste valorization for the production of chemicals, materials and fuels: Case study South and Southeast Asia. *Bioresource Technology, 248*, 100-112. https://doi.org/10.1016/j.biortech.2017.06.076

Pal, G. K., Nidheesh, T. & Suresh, P. V. (2015). Comparative study on characteristics and *in vitro* fibril formation ability of acid and pepsin soluble collagen from the skin of catla (*Catla catla*) and rohu (*Labeo rohita*). *Food Research International, 76,* 804-812. https://doi.org/10.1016/j.foodres.2015.07.018

Pal, G.K. & Suresh, P.V. (2016). Sustainable valorisation of seafood by-products: Recovery of collagen and development of collagen-based novel functional food ingredients. *Innovative Food Science and Emerging Technologies, 37*, 201-215. https://doi.org/10.1016/j.ifset.2016.03.015

Pal, G.K. & Suresh, P.V. (2017). Comparative assessment of physicochemical characteristics and fibril formation capacity of thermostable carp scales collagen. *Materials Science and Engineering: C, 70,* 32-40. https://doi.org/10.1016/j.msec.2016.08.047

Pal, G.K., Nidheesh, T. & Suresh, P.V. (2015). Comparative study on characteristics and *in vitro* fibril formation ability of acid and pepsin soluble collagen from the skom pf catla (*Catla catla*) and rohu (*Labeo rohita*). *Food Research International, 76,* 804-812. https://doi.org/10.1016/j.foodres.2015.07.018

Pan, M., Liu, K., Yang, J., Liu, S., Wang, S. & Wang S. (2020). Advances on food-derived peptidic antioxidants- a review. *Antioxidants, 9,* 700. https://doi.org/10.3390/antiox9090799

Patino, M.G., Neiders, M.E., Andreana, S., Noble, B. & Cohen, R.E. (2002). Collagen: an overview. *Implant Dentistry, 11,* 280-285. https://doi.org/10.1097/00008505-200207000-00014

Paula, D.D.A., Martins, E.M.F., Costa, N.D.A., de Oliveira, P.M., de Oliveira, E.B. & Ramos, A.M. (2019). Use of gelatin and gum arabic for microencapsulation of probiotic cells from Lactobacillus plantarum by a dual process combining double emulsification followed by complex coacervation.

International Journal of Biological Macromolecules, *133*, 722-731. https://doi.org/10.1016/j.ijbiomac.2019.04.110

Pawelec, K. M., Best, S. M. & Cameron, R. E. (2016). Collagen: A Network for Regenerative Medicine. *Journal of Materials Chemistry B, 4,* 6484-6496. https://doi.org/10.1039/c6tb00807k

Pellá, M.C.G., Silva, O.A., Pellá, M.G., Beneton, A.G., Caetano, J., Simões, M.R. & Dragunski, D.C. (2020). Effect of gelatin and casein additions on starch edible biodegradable films for fruit surface coating. *Food Chemistry, 309*, 125764. https://doi.org/10.1016/j.foodchem.2019.125764

Peralta, J.M., Meza, B.E., Zorrilla, S. E. (2017). Analytical solutions for the free-draining flow of a Carreau-Yasuda fluid on a vertical plate. Chemical Engineering Science, 168, 391-402. https://doi.org/10.1016/j.ces.2017.05.002

Perez-Puyana, V., Jiménez-Rosado, M., Romero, A. & Guerrero, A. (2019). Crosslinking of Hybrid Scaffolds Produced from Collagen and Chitosan. *International Journal of Biological Macromolecules*, *139,* 262-269. https://doi.org/10.1016/j.ijbiomac.2019.07.198

Perumal, R.K., Perumal, S., Thangam, R., Gopinath, A., Ramadass, S.K., Madhan, A. & Sivasubramanian, S. (2018). Collagen-fucoidan blend film with the potential to induce fibroblast proliferation for regenerative applications. *International Journal of Biological Macromolecules, 106,* 1032-1040. http://dx.doi.org/10.1016/j.ijbiomac.2017.08.111

Pezeshki-Modaress, M., Zandi, M. & Rajabi, S. (2018). Tailoring the Gelatin/Chitosan Electrospun Scaffold for Application in Skin Tissue Engineering: An in Vitro Study. *Progress in Biomaterials, 7,* 207-218. https://doi.org/10.1007/s40204-018-0094-1

Piedade, A. P. (2019). 4D Printing: The Shape-Morphing in Additive Manufacturing. *Journal of Functional Biomaterials, 10*, 9. https://doi.org/10.3390/jfb10010009

Piez, K.A., (1984). Molecular and aggregate structures of the collagens. *In "Extracellular Matrix Biochemistry" (K.A. Piez and A.H. Reddi, eds.), 1-39. Elsevier,* New York.

Plepis, A. M. D. G., Goissis, G. & Das-Gupta, D. K. (1996). Dielectric and pyroelectric characterization of anionic and native collagen. *Polymer Engineering Science, 36,* 2932-2938. https://doi.org/10.1002/pen.10694

Plumb, D.A., Dhir, V., Mironov, A., Ferrara, L., Poulsom, R., Kadler, K.E., Thornton, D.J., Briggs, M.D. & Boot-Handford R.P. (2007). Collagen XXVII is developmentally regulated and forms thin fibrillary structures distinct from those of classical vertebrate fibrillar collagens. *Journal of Biological Chemistry, 282,* 12791–12795. https://doi.org/10.1074/jbc.C700021200

Rahman, M. & Brazel, C. S. (2006). Ionic liquids: New generation stable plasticizers for poly(vinyl chloride). *Polymer Degradation and Stability, 91*, 3371-3382. https://doi.org/10.1016/j.polymdegradstab.2006.05.012

Ramachandran, G.N. (1988). Stereochemistry of collagen. *Journal of Peptide Protein Research, 31,* 1-16. https://doi.org/10.1111/j.1399-3011.1988.tb00001.x

Reddy, N., Reddy, R. & Jiang, Q. (2015). Crosslinking Biopolymers for Biomedical Applications. *Trends in Biotechnology, 33*, 362-369. https://doi.org/10.1016/j.tibtech.2015.03.008

Regubalan B., Pandit P., Maiti S., Nadathur G.T. & Mallick A. (2018). Potential Bio-Based Edible Films, Foams, and Hydrogels for Food Packaging. In: Ahmed S. (eds) Bio-based Materials for Food Packaging. Springer, Singapore. https://doi.org/10.1007/978-981-13-1909-9_5

Reizabal, A., Correia, D. M., Costa, C. M., Perez-Alvarez, L., Vilas-Vilela, J. L. & Lanceros-Mendez, S. (2019). Silk fibroin bending actuators as an approach towards natural polymer based active materials. *ACS Applied Materials & Interfaces, 11,* 30197-30206. https://doi.org/10.1021/acsami.9b07533

Rethinam, S., Vihayan, S., Aruni, A.W., Basaran, B., Alagumuthu, T. & Ramamoorthy, R. (2020). Enhanced tissue regeneration using an nano-bioactive scaffold - A novel perspective. *Materials Chemistry and Physics*, *240*, 122303. https://doi.org/10.1016/j.matchemphys.2019.122303

Reyna-Urrutia, V. A., Mata-Haro, V., Cauich-Rodriguez, J.V., Herrera-Kao, W. A. & Cervantes-Uc, J.M. (2019). Effect of Two Crosslinking Methods on the Physicochemical and Biological Properties of the Collagen-Chitosan Scaffolds. *European Polymer Journal, 117,* 424-433. https://doi.org/10.1016/j.eurpolymj.2019.05.010

Rezaee, M., Askari, G., EmamDjomeh, Z. & Salami, M. (2018). Effect of organic additives on physiochemical properties and anti-oxidant release from chitosan-gelatin composite films to fatty food simulant. *International Journal of Biological Macromolecules, 114,* 844-850. https://doi.org/10.1016/j.ijbiomac.2018.03.122

Riaz, T., Zeeshan, R., Zarif, F., Ilyas, K., Muhammad, N., Safi, S.Z., Rahim, A., Rizvi, S.A.A. & Rehman, I.U (2018). FTIR analysis of natural and synthetic collagen. *Applied Spectroscopy Reviews, 53,* 703–746. https://doi.org/10.1080/05704928.2018.1426595

Ricard-Blum, S. (2011). The collagen family. Cold Spring Harbor Perspectives in Biology. https://doi.org/10.1101/cshperspect.a004978

Rochdi, A., Foucat, A. L. & Renou, J.P. (1999). Effect of thermal denaturation on water-collagen interactions: NMR relaxation and differential scanning calorimetry analysis. *Biopolymers, 50,* 690-696. https://doi.org/10.1002/(SICI)1097-0282(199912)50:7<690::AID-BIP2>3.0.CO;2-P

Rodrigues, M.Á.V., Bertolo, M.R.V., Marangon, C.A., Martins, V.D.C.A. & Plepis, A.M.D.G. (2020). Chitosan and gelatin materials incorporated with phenolic extracts of grape seed and jabuticaba peel: Rheological, physicochemical, antioxidant, antimicrobial and barrier properties. *International Journal of Biological Macromolecules*, *160*, 769-779. https://doi.org/10.1016/j.ijbiomac.2020.05.240

Rosenberg, B., Electrical conductivity of proteins. (1962). Nature 193, 364-365, https://doi.org/10.1038/193364a0

Rramaswamy, R., Mani, G., Venkatachalam, S., Yasam, R.V., Rajendran J.C.B., Tae, J.H. (2018). Preparation and characterization of tetrahydrocurcumin-loaded cellulose acetate phthalate/polyethylene glicol electrospun nanofibers. *AAPS PharmSciTech* 19, 3000-3008. https://doi.org/10.1208/s12249-018-1122-0

Sae-leaw, T., Benjakul, S. & O'Brien, N. M. (2016). Effects of defatting and tannic acid incorporation during extraction on properties and fishy odour of gelatin from seabass skin*. LWT-Food Science and Technology, 65,* 661-667. https://doi.org/10.1016/j.lwt.2015.08.060

Sarkar, S. D., Farrugia, B. L., Dargaville, T. R. & Dhara, S. (2013). Chitosan-Collagen Scaffolds with Nano/Microfibrous Architecture for Skin Tissue Engineering. *Journal of Biomedical Materials Research - Part A, 101,* 3482-3492. https://doi.org/10.1002/jbm.a.34660

Sato, K. (2017). The presence of food-derived collagen peptides in human boy-structure and biological activity. *Food & Function, 8,* 12. https://doi.org/10.1039/C7FO01275F

Schmidt, M.m., Dornelles, R.C.P., Mello, R.O., Kubota, E.H., Mazutti, M.A., Kempka, A.P. & Demiate, I.M. (2016). Collagen extraction process. *International Food Research Journal, 23,* 913-922

Schroepfer, M. & Meyer, M. (2017). DSC investigation of bovine hide collagen at varying degrees of crosslinking and humidities, *International Journal of Biological Macromolecules, 103,* 120-128. https://doi.org/10.1016/j.ijbiomac.2017.04.124

See, S. F., Ghassem, M., Mamot, S. & Babji, A. S. (2015). Effect of different pretreatments on functional properties of African catfish (*Clarias gariepinus*) skin gelatin. *Journal of Food Science and Technology, 52*, 753-762. https://doi.org/10.1007/s13197-013-1043-6

Senadheera, T. R. L., Dave, D. & Shahidi, F. (2020). Sea cucumber derived type I collagen: A comprehensive review. *Marine Drugs, 18*, 471. https://doi.org/10.3390/md18090471

Shadangi, K.P. & Mohanty, K. (2014). Kinetic study and thermal analysis of the pyrolysis of non-edible oilseed powders by thermogravimetric and differential scanning calorimetric analysis. *Renewable Energy*, *63,* 337-344. https://doi.org/10.1016/j.renene.2013.09.039

Shah, R., Stodulka,P., Skopalova, K. & Saha, P. (2019). “Dual Crosslinked Collagen/Chitosan Film for Potential Biomedical Applications”. *Polymers, 11,* 2094. https://doi.org/10.3390/polym11122094

Shekhter, A.B., Fayzullin, A.L., Vukolova, M.N., Rudenko, T.G., Osipycheva, V.D. & Litvitsky, P.F. (2019). Medical applications of collagen and collagen-based materials. *Current Medical Chemistry.*, *26*, 506-516. https://doi.org/10.2174/0929867325666171205170339

Sherman, V. R., Yang, W. & Meyers, M. A. (2015). The materials science of collagen. *Journal of the Mechanical Behavior of Biomedical Materials, 52*, 22-50. https://doi.org/10.1016/j.jmbbm.2015.05.023

Shi, D., Liu, F., Yu, Z., Chang, B., Goff, H.D. & Zhong, F. (2019). Effect of aging treatment on the physicochemical properties of collagen films. *Food Hydrocolloids, 87,* 436-447. https://doi.org/10.1016/j.foodhyd.2018.08.016

Shi, R., Bi, J., Zhang, Z., Zhu, A., Chen, D., Zhou, X., Zhang, L. & Tian, W. (2008). The effect of citric acid on the structural properties and cytotoxicity of the polyvinyl alcohol/starch films when molding at high temperatures. *Carbohydrate Polymers, 74,* 763-770. https://doi.org/10.1016/j.carbpol.2008.04.045

Shie, M. Y., Shen, Y. F., Astuti, S. D., Kai-Xing Lee, A., Lin, S. H., Dwijaksara, N.L.B. & Chen, Y.W. (2019). Review of Polymeric Materials in 4D Printing Biomedical Applications. *Polymers, 11,* 1864. https://doi.org/10.3390/polym11111864

Shoulders, M. D. & Raines, R. T. (2009). Collagen structure and stability. *Annual Review of Biochemistry, 78*, 929–958. https://doi.org/10.1146/annurev.biochem.77.032207.120833

Sila, A., Martinez-Alvarez, O., Haddar, A., Gómez-Guillén, M. C., Nasri, M., Montero, M. P. & Bougatef, A. (2015). Recovery, viscoelastic and functional properties of Barbel skin gelatine: Investigation of anti-DPP-IV and anti-prolyl endopeptidase activities of generated gelatine polypeptides. *Food Chemistry, 168*, 478-486. https://doi.org/10.1016/j.foodchem.2014.07.086

Silvipriya, K.S., Kumar, K.K., Bhat, A.R., Kumar, B.B., John A. & Lakshmanan, P. (2015). Collagen: Animal sources and biomedical application. *Journal of Applied Pharmaceutical Science, 5,* 123-127. https://doi.org/10.7324/JAPS.2015.50322

Singh, S., Gupta, A. & Gupta, B. (2018). Scar free healing mediated by the release of aloe vera and manuka honey from dextran bionanocomposite wound dressings. *International Journal of Biological Macromolecules, 120,* Part B, 1581-1590. https://doi.org/10.1016/j.ijbiomac.2018.09.124

Sinthusamran, S., Benjakul, S. & Kishimura, H. (2014). Characteristics and gel properties of gelatin from skin of seabass (*Lates calcarifer*) as influenced by extraction conditions. *Food Chemistry, 152*, 276-284. https://doi.org/10.1016/j.foodchem.2013.11.109

Sionkowska, A., Kaczmarek, B. & Lewandowska, K. (2014). Modification of Collagen and Chitosan Mixtures by the Addition of Tannic Acid. *Journal of Molecular Liquids, 199*, 318-323. https://doi.org/10.1016/j.molliq.2014.09.028

Six, L., Velghe, F., Verstichel, S. & De Meester, S. (2016). Sustainnability considerations on the valorization of organic waste. *Biotransformation of agricultural waste and by-products*, 287-307. http://dx.doi.org/10.1016/B978-0-12-803622-8.00011-2

Sizeland, K.H., Hofman, K.A., Hallett, I.C., Martin, D.E., Potgieter, J., Kirby, N.M., Hawley, A., Mudie, S.T., Ryan, T.M., Haverkamp, R.G. & Cumming, M.H. (2018). Nanostructure of electrospun collagen: Do electrospun collagen fibers form native structures? *Materialia, 3,* 90-96. https://doi.org/10.1016/j.mtla.2018.10.001

Skov, K., Oxfeldt, M., Thøgersen, R., Hansen, M. & Bertram, H.C. (2019). Enzymatic Hydrolysis of a Collagen Hydrolysate Enhances Postprandial Absorption Rate-A Randomized Controlled Trial. *Nutrients, 11,* 1064. https://doi.org/10.3390/nu11051064

Socrates, R., Prymak, O., Loza, K., Sakthivel, N., Rajaram, A., Epple, M. & Narayana Kalkura, S. (2019). Biomimetic fabrication of mineralized composite films of nanosilver loaded native fibrillar collagen and chitosan. *Materials Science and Engineering C, 99,* 357-366. https://doi.org/10.1016/j.msec.2019.01.101

Soe, M.T., Chitropas, P., Pongjanyakul, T., Limpongsa, E. & Jaipakdee, N. (2020). Thai glutinous rice starchh modified by ball milling and its application as a mucoadhesive polymer. Carbohydrate Polymers, 232, 115812. https://doi.org/10.1016/j.carbpol.2019.115812

Sun, Y., Yang, C., Zhu, X., Wang, J. J., Liu, X. Y., Yang, X. P., An, X. W., Liang, J., Dong, H.J., Jiang, W., Chen, C., Wanf, Z.G., Sun, H. T., Tu, Y., Zahng, S., Chen, F., & Li, X.H. (2019). 3D Printing Collagen/Chitosan Scaffold Ameliorated Axon Regeneration and Neurological Recovery after Spinal Cord Injury. *Journal of Biomedical Materials Research - Part A*, *107*,1898-1908. https://doi.org/10.1002/jbm.a.36675

Supramaniam, J., Adnan, R., Kaus, N. H. M. & Bushra, R. (2018). Magnetic nanocellulose alginate hydrogel beads as potential drug delivery system. *International Journal of Biological Macromolecules, 118,* 640-648. https://doi.org/10.1016/j.ijbiomac.2018.06.043

Suresh, K., Sugihara, F., Suzuki, K., Inoue, N.& Venkateswarathirukumara, S. (2015). A double-blind, placebo-controlled, randomized, clinical study on the effectiveness of collagen peptide on

osteoarthritis. *Journal of the Science of Food and Agriculture*, *94*, 4, 702-707. https://doi.org/10.1002/jsfa.6752

Sutmuller, M., Bruijn, J.A. & de Heer E. (1997). Collagen types VIII and X, two non-fibrillar, short-chain collagens. Structure homologies, functions and involvement in pathology. *Histol Histopathil, 12,* 557-566.

Tamay, D. G., Usal, T. D., Alagoz, A. S., Yucel, D., Hasirci, N. & Hasirci, V. (2019). 3D and 4D Printing of Polymers for Tissue Engineering Applications. *Frontiers in Bioengineering and Biotechnology, 7,* 164. https://doi.org/10.3389/fbioe.2019.00164

Tan, Y. & Chang, S. K. C., (2018) Isolation and characterization of collagen extracted from cannel catfish (*Ictalurus punctatus*) skin. *Food Chemistry, 242*, 147-155. https://doi.org/10.1016/j.foodchem.2017.09.013

Thirawong, N., Nunthanid, J., Puttipipatkhachorn, S. & Sriamornsak, P. (2007). Mucoadhesive properties of various pectins on gastrointestinal mucosa: An *in vitro* evaluation using texture analyzer. *European Journal of Pharmaceutics and Biopharmaceutics, 67,* 132-140. https://doi.org/10.1016/j.ejpb.2007.01.010

Thuy, L. T. M., Okazaki, E. & Osako, K. (2014). Isolation and characterization of acid-soluble collagen from the scales of marine fishes from Japan and Vietnam. *Food Chemistry, 149,* 264-270. https://doi.org/10.1016/j.foodchem.2013.10.094

Tian, Z., Duan, L., Wu, L., Shen, L. & Li, G. (2016). Rheological properties of glutaraldehyde-crosslinked collagen analysed quantitatively using mechanical models. *Materials Science and Engineering C, 63,* 10-17. http://dx.doi.org/10.1016/j.msec.2016.02.047

Tkaczewska, J., Morawska, M., Kulawik, P. & Zając, M. (2018). Characterization of carp *(Cyprinus carpio*) skin gelatin extracted using different pretreatments method. *Food Hydrocolloids, 81*, 169-179. https://doi.org/10.1016/j.foodhyd.2018.02.048

Tonndorf, R., Aibibu, D. & Cherif, C. (2020). Collagen multifilament spinning. *Materials Science and Engineering: C, 106,* 110105. https://doi.org/10.1016/j.msec.2019.110105

Torres, M.D., Hallmark, B. & Wilson, D.I. (2014). Effect of concentrqation on shear and extensional rheology of guar gum solutions. Food Hydrocolloids, 40, 85-95. https://doi.org/10.1016/j.foodhyd.2014.02.011

Tosati, J.V., Messias, V.C., Carvalho, P.I.N., Pollonio, M.A.R., Meireles, M.A.A. & Monteiro, A.R. (2017). Antimicrobial Effect of Edible Coating Blend Based on Turmeric Starch Residue and Gelatin Applied onto Fresh Frankfurter Sausage. *Food and Bioprocess Technology, 10,* 2165-2175. https://doi.org/10.1007/s11947-017-1985-1

Tran-Ba, K., Lee, D. J., Zhu, J., Paeng, K. & Kaufman, L. J. (2017). Confocal rheology probes the structure and mechanics of collagen through the sol-gel transition. *Biophysical Journal, 113*, 1882-1892. https://doi.org/10.1016/j.bpj.2017.08.025

Trivedi, M.K., Gangwar, M., Mondal, S. C. & Jana, S. (2017). Protective effects of tetrahydrocurcumin (THC) on fibroblast and melanoma cell lines in vitro: it´s implication for wound healing. *Journal of food science and Technology, 54,* 1137-1145. https://doi.org/10.1007/s13197-017-2525-8.

United Nations. (2015). A/RES/70/1 transforming our world: The 2030 agenda for sustainable development. https://www.un.org/ga/search/view_doc.asp?symbol=A/RES/70/1&Lang=E. (Accessed 19 December 2021).

Uranga, J., Leceta, I., Etxabide, A., Guerrero, P. & de la Caba K. (2016). Cross-linking of fish gelating to develop sustainable films with enhanced properties. *European Polymer Journal, 78*, 82-90. https://doi.org/10.1016/j.eurpolymj.2016.03.017

Uranga, J., Nguyen, B.T., Si, T.T., Guerrero, P. & de la Caba, K. (2020). The effect of cross-linking with citric acid on the properties of agar/fish gelatin films. *Polymers*, *12*, 291. https://doi.org/10.3390/polym12020291

Uranga, J., Puertas, A.I., Etxabide, A., Dueñas, M.T., Guerrero, P. & de la Caba, K. (2019). Citric acid-incorporated fish gelatin/chitosan composite films. *Food Hydrocolloids, 86,* 95-103. https://doi.org/10.1016/j.foodhyd.2018.02.018

Valencia, G. A., Luciano, C. G., Lourenço, R. V., Bittante, A. M. Q. B., & Sobral, P. J. A. (2019). Morphological and physical properties of nano-biocomposite films base on collagen loaded with laponite®. *Food Packaging and Shelf Life, 19,* 24–30. https://doi.org/10.1016/j.fpsl.2018.11.013.

Van der Rest, M. & Garrone, R. (1991). Collagen family of proteins. *The FASEB Journal, 5,* 2814-2823. https://doi.org/10.1096/fasebj.5.13.1916105

Veeruraj, A., Arumugam, M. & Balasubramanian, T. (2013). Isolation and characterization of thermostable collagen from marine eel-fish (*Evenchelys macrura*). *Process Biochemistry, 48,* 1592-1602. https://doi.org/10.1016/j.procbio.2013.07.011

Venkatesan, J., Anil, S., Kim, S. K. & Shim, M. S. (2017). Marine fish proteins and peptides for cosmeceuticals: A review. *Marine Drugs, 15,* 143. https://doi.org/10.3390/md15050143

Verma, N., Singh, M. K, Zafar, S. & Pathak, H. (2021). Comparative study of in-situ temperature measurement during microwave-assisted compression-molding and conventionally compression-molding process. *CIRRP Journal of Manufacturing Science and Technology, 35*, 336-345. https://doi.org/10.1016/j.cirpj.2021.07.005

Vidal, A.R., Duarte, L.P., Schmidt, M.M., Cansian, R.L., Fernandes, I.A., Mello, R.O., Demiate, I.M. & Dornelles, R.C.P. (20.20) Extraction and characterization of collagen from sheep slaughter by-products. *Waste Management, 102,* 838-846. https://doi.org/10.1016/j.wasman.2019.12.004

Vigata, M., Meinert, C., Hutmacher, D. W. & Bock, N. (2020). Hydrogels as drug delivery systems: a review of current characterization and evaluation techniques. *Pharmaceutics, 12,* 1188. https://doi.org/10.3390/pharmaceutics12121188

Wang, B.L., Han, Y.M., Lin, Q.K., Liu, H.H., Shen, C.H., Nan, K.H. & Chen, H. (2016b). *In vitro* and *in vivo* evaluation of xanthan gum-succinic anhydride hydrogels for the ionic strength-sensitive release of antibacterial agents. *Journal of Material Chemistry B*, 4, 1853-1861. https://doi.org/10.1039/C5TB02046H

Wang, K., Li, R., Ma, J. H., Jian, Y. K. & Che, J. N. (2016c). Extracting keratin from wool by using L-cysteine. *Green Chemistry*, 18, 476-481. https://doi.org/10.1039/c5gc01254f

Wang, L., Jiang, Y., Wang, X. Cui, H, Xu W., He, Y., Ma, H. & Gao R. (2018). Effect of oral administration of collagen hydrolysates from Nile tilapia on the chronologically aged skin. *Journal of Functional Foods*, *44*, 112-117. https://doi.org/10.1016/j.jff.2018.03.005

Wang, L., Liang, Q., Chen, T., Wang, Z., Xu, J., & Ma, H. (2014). Characterization of collagen from the skin of Amur sturgeon (*Acipenser schrenckii*). *Food Hydrocolloids, 38*, 104-109. https://doi.org/10.1016/j.foodhyd.2013.12.002

Wang, P., Li, Y., Zhang, C., Que, F., Weiss, J. & Zhang, H. (2020). Characterization and antioxidant activity of trilayer gelatin/dextran-propyl gallate/gelatin films: Electrospinning versus solvent casting. *LWT, 128,* 109536. https://doi.org/10.1016/j.lwt.2020.109536

Wang, X., Wang, G., Liu, L. & Zhang, D. (2016a). The mechanism of a chitosan-collagen composite film used as biomaterial support for MC3T3-E1 cell differentiation. *Scientific reports, 6,* 1-8. https://doi.org/10.1038/srep39322

Wei, Q., Lu, J., Wang, Q., Fan, H. & Zhang, X. (2015). Novel synthesis strategy for composite hydrogel of collagen/hydroxyapatite microsphere originating from conversion of CaCO3 templates. *Nanotechnology, 26,* 115605. https://doi.org/10.1088/0957-4484/26/11/115605

Whu, S. W., Hung, K. H., Hsieh, K. H., Chen, C. H., Tsai, C. L. & Hsu, S. H. (2013). In Vitro and in Vivo Evaluation of Chitosan-Gelatin Scaffolds for Cartilage Tissue Engineering. *Materials Science and Engineering: C, 33*, 2855-2863. https://doi.org/10.1016/j.msec.2013.03.003

Williamson, R.V. (1929). The Flow of Pseudoplastic Materials. *Industrial and Engineering Chemistry, 21*, 1108–1111. https://doi.org/10.1021/ie50239a035

Wu, H., Huang, X., Gao, M.M., Liao, X.P. & Shi, B. (2011). Polyphenol-grafted collagen fiber as reductant and stabilizer for one-step synthesis of size-controlled gold nanoparticles and their catalytic application to 4-nitrophenol reduction. *Green Chemistry 13,* 651-658. https://doi.org/10.1039/C0GC00843E

Wu, T., Gray, E. & Chen, B. (2018). A self-healing, adaptive and conductive polymer composite ink for 3D printing of gas sensors. *Journal of Materials Chemistry C*, 6, 6200. https://doi.org/10.1039/c8tc01092g.

Wu, X., Liu, A., Wang, W. & Ye, R. (2018). Improve mechanical properties and termal-stability of collagen fiber based film by crosslinking with casein, keratin or SPI: Effect of crosslinking processs and concentrations of proteins. *International Journal of Biological Macromolecules, 109,* 1319-1328. https://doi.org/10.1016/j.ijbiomac.2017.11.144

Wu, X., Liu, Y., Liu, A. & Wang, W. (2017). Improved thermal-stability and mechanical properties of type I collagen by crosslinking with casein, keratin and soy protein isolate using transglutaminase*. International Journal of Biological Macromolecules, 98,* 292-301. https://doi.org/10.1016/j.ijbiomac.2017.01.127

Wu, X., Luo, Y., Liu, Q., Jiang, S. & Mu, G. (2019). Improved structure-stability and packaging characters of crosslinked collagen fiber-based film with casein, keratin and SPI. *Journal of the Science of Food and Agriculture*, *99*, 4942-4951. https://doi.org/10.1002/jsfa.9726

Xiong, X., Yu, I.K.M., Tsang, D.C.W., Bolan, N.S., Ok, Y.S., Igalavithana, A.D., Kirkham, M.B., Kim K.-H. & Vikrant, K. (2019). Value-added chemicals from food supply chain wastes: State-of-the-art review and future prospects. *Chemical Engineering Journal, 375,* 121983. https://doi.org/10.1016/j.cej.2019.121983

Yan, L. P., Wang, Y. J., Ren, L., Wu, G., Caridade, S. G., Fan, J. B., Wang, L. Y., Ji, P. H., Oliveira, J. M., Oliveira, J. T., Mano, J. F., & Reis, R. L. (2010). Genipin-Cross-Linked Collagen/Chitosan Biomimetic Scaffolds for Articular Cartilage Tissue Engineering Applications. *Journal of Biomedical Materials Research, Part A, 95A*, 465-475. https://doi.org/10.1002/jbm.a.32869

Yang, F., Guo, C., Zhang, M., Bhandari, B. & Liu, Y. (2019). Improving 3D printing process of lemon juice gel based on fluid flow numerical simulation. *LWT*, 102, 89-99. https://doi.org/10.1016/j.lwt.2018.12.031

Yang, H., Duan, L., Li, Q., Tian, Z. & Li, G. (2018). Experimental and modeling investigation on the rheological behavior of collagen solution as a function of acetic acid concentration. *Journal of the Mechanical Behavior of Biomedical Materials, 77,* 125-134. https://doi.org/10.1016/j.jmbbm.2017.09.003

Yang, X., Li, A., Li, X., Sun, L. & Guoy. (2020). An overview of classifications, properties of food polysaccharides and their links to applications in improving food textures. *Trends in Food Science & Technology, 102*, 1-15. https://doi.org/10.1016/j.tifs.2020.05.020

Yeddes, W., Djebali, K., Aidi Wannes, W., Horchani.Naifer, K., Hammami, M., Younes, I. & Saidani Tounsi, M. (2020). Gelatin-chitosan-pectin films incorporated with rosemary essential oil: Optimized formulation using mixture design and response surface methodology. *International Journal of Biological Macromolecules, 154*, 92-103. https://doi.org/10.1016/j.ijbiomac.2020.03.092

Yoon, S.D., Chough, S.H. & Park, H.R. (2007). Preparation of resistant starch/poly(vinyl alcohol) blend films with added plasticizer and crosslinking agents. *Journal of Applied Polymer Science, 106*, 2485-2493. https://doi.org/10.1002/app.26755

Yoshimura, K., Chonan, Y. & Shirai, K. (1999). Preparation and dynamic viscoelastic characterization of pepsin-solubilized collagen from shark skin compared with pig skin. *Animal Science Journal, 70,* 227-234.

Yu, D., Chi, C.F., Wang, B., Ding, G.F. & Li, Z.R. (2014). Characterization of acid-and pepsin-soluble collagens from spines and skulls of skipjack tuna (*Katsuwonus pelamis*). *Chinese Journal of Natural Medicines, 12,* 712–720. https://doi.org/10.1016/S1875-5364(14)60110-2

Yüksel, A., Şahin-Yeşilçubuk, N. (2018). Encapsulation of structured lipids containing medium- and long chain fatty acids by complex coacervation of gelatin and gum arabic. *Journal of Food Process Engineering, 41,* e1290. https://doi.org/10.1111/jfpe.12907

Zamorano-Apodaca, J. C, García-Sifuentes, C. O., Carvajal-Millán, E., Vallejo-Galland, B., Scheuren-Acevedo, S. M. & Lugo-Sánchez, M. E. (2020). Biological and functional properties of peptide fractions obtained from collagen hydrolysate derived from mixed by-producst of different fish species. *Food Chemistry*, *331*, 127350 https://doi.org/10.1016/j.foodchem.2020.127350

Zhuang, C., Tao, F. & Cui, Y. (2017). Eco-friendly biorefractory films of gelatin and TEMPO-oxidized cellulose ester for food packaging applications. *Journal of the Science of Food and Agriculture, 97*, 3384-3395. https://doi.org/10.1002/jsfa.8189

Zou, Y., Wang, L., Cai, P., Li, P., Zhang, M., Sun, Z., Sun, C., Xu, W. & Wang, D. (2017). Effect of ultrasound assisted extraction on the physicochemical and functional properties of collagen from soft-shelled turtle calipash. *International Journal of Biological Macromolecules, 105,* 1602-1610. https://doi.org/10.1016/j.ijbiomac.2017.03.011

Zuidem, J.M., Rivet, C.J., Gilbert, R.J. & Morrison, F.A. (2013). A protocol for rheological characterization of hydrogels for tissue engineering strategies. *Journal of Biomedical Materials Research Part A, 102*, 1063–1073. https://doi.org/10.1002/jbm.b.33088